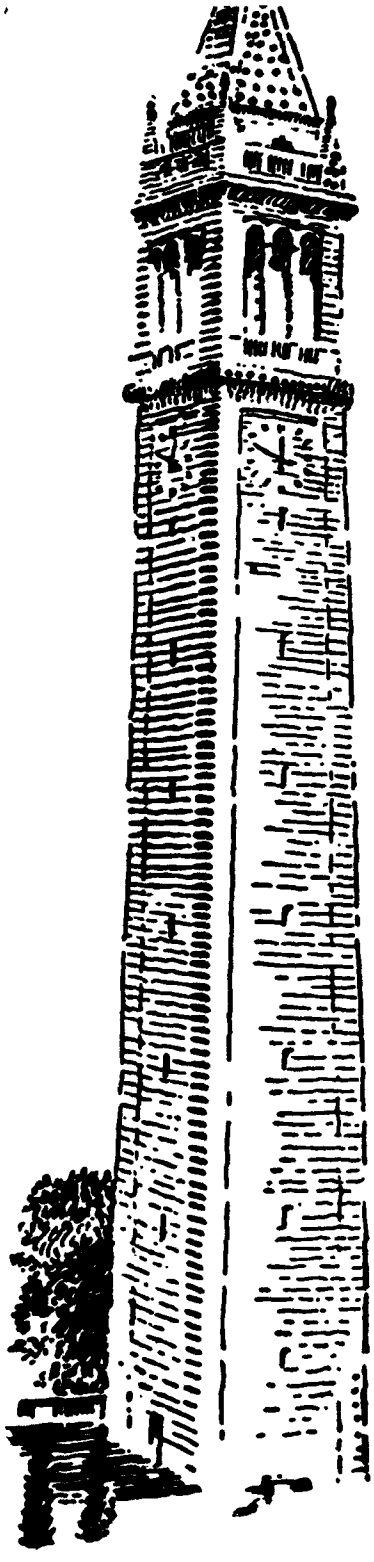

ANNUAL PROGRESS REPORT, FOR 1991
PLASMA THEORY AND SIMULATION GROUP

Professor C.K. Birdsall

January 1 to December 31, 1991

DOE Contract DE-FG03-90ER54079
ONR Contract FD-N00014-90-J-1198
State MICRO 90-018
University of Arizona 15546
Varian Associates

ELECTRONICS RESEARCH LABORATORY
College of Engineering
University of California, Berkeley, CA 94720

SECURITY CLASSIFICATION OF THIS PAGE (When Data Entered)

REPORT DOCUMENTATION PAGE		READ INSTRUCTIONS BEFORE COMPLETING FORM
1. REPORT NUMBER	2. GOVT ACCESSION NO.	3. RECIPIENT'S CATALOG NUMBER
4. TITLE (and Subtitle) Annual Progress Report Jan. 1, 1991–Dec. 31, 1991		5. TYPE OF REPORT & PERIOD COVERED Progress, 1/91–12/91
		6. PERFORMING ORG. REPORT NUMBER
7. AUTHOR(s) Professor Charles K. Birdsall		8. CONTRACT OR GRANT NUMBER(s) ONR FD–N00014–90–J–1198
9. PERFORMING ORGANIZATION NAME AND ADDRESS Electronics Research Laboratory University of California Berkeley, CA 94720		10. PROGRAM ELEMENT, PROJECT, TASK AREA & WORK UNIT NUMBERS Element No. 61153N, Project Task Area RRQ1–09–01, Work Unit No. NR 012–742
11. CONTROLLING OFFICE NAME AND ADDRESS ONR Physics Division Department of the Navy ONR Arlington, VA 22217		12. REPORT DATE
		13. NUMBER OF PAGES
14. MONITORING AGENCY NAME & ADDRESS(if different from Controlling Office) Arlington, VA 22217		15. SECURITY CLASS. (of this report)
		15a. DECLASSIFICATION/DOWNGRADING SCHEDULE

16. DISTRIBUTION STATEMENT (of this Report)

Approved for public release; distribution unlimited

17. DISTRIBUTION STATEMENT (of the abstract entered in Block 20, if different from Report)

18. SUPPLEMENTARY NOTES

Our group uses plasma theory and simulation as tools in order ot increase the understanding of instabilities, heating, transport, wall interactions, and large potentials. We perform plasma device computer experiments to compare with analytic models and laboratory experiments in order to accelerate device design.

19. KEY WORDS (Continue on reverse side if necessary and identify by block number)

Research in plasma theory and simulation, plasma-wall interactions, large potentials in plasma, bounded plasmas. Plasma device computer experiments.

20. ABSTRACT (Continue on reverse side if necessary and identify by block number)

This is a brief progress report, covering our research in general plasma theory and simulation, plasma-wall physics theory and simulation, and code development. Reports written in this period are included with this mailing. A publications list plus abstracts of major meetings are included.

DD FORM 1 JAN 73 1473 EDITION OF 1 NOV 65 IS OBSOLETE

S/N 0102-LF-014-6601

SECURITY CLASSIFICATION OF THIS PAGE (When Data Entered)

PLASMA THEORY AND SIMULATION GROUP

January 1 to December 31, 1991

Principal Investigator

Prof. C. K. Birdsall	191 M Cory Hall	643-6631	

Post-Doctoral Researchers

Dr. Xueqiao Xu	187 M Cory Hall	642-3477	
Dr. Alfonso Tarditi*	197 M Cory Hall	643-7577	
Dr. Greg DiPeso(Spr 91)	199 MD Cory Hall	642-1297	

* NATO-CNR Fellow (1991-92)

Research Assistants

Mr. Vahid Vahedi	199 MD Cory Hall	642-1297	
Mr. John Verboncoeur	199 MD Cory Hall	642-1297	
Mr. Payam Mirrashidi	199 MD Cory Hall	642-1297	
Mr. Frank Tsung	199 ME Cory Hall	642-1297	
Mr. Ed Chao	199 ME Cory Hall	642-1297	
Mr. Conway Gee	199 ME Cory Hall	642-1297	

Visiting Scientists

Dr. M. J. Gerver (from SatConTech, Massachusetts, for two weeks in August)
Dr. S. Ishiguro (JIFT Visitor from Tohoku University, Sendai, Japan, July-September)

Contributing Scientists

Dr. K. Theilhaber (from September on, completing work begun in Tokyo)
Dr. W. S. Lawson (from September on)

Administrative Staff

Mrs. Nancy Kern (until August)	191 M Cory Hall	643-6631	
Ms. Pora Park (from September on)	195 M Cory Hall	643-6633	

Our Advisers Are

Dr. Bruce Cohen	L630 LLNL	422–9823	
Dr. Alex Friedman	381-1337 LLNL	422–0827	
Dr. A. Bruce Langdon	L472 LLNL	422–5444	

Physicists, Lawrence Livermore Natl. Lab

Dr. Ilan Roth 304 SSL 642–1327
Physicist, Space Sciences Lab, UCB

Our research group uses both plasma theory and simulation as tools in order to increase the understanding of instabilities, heating, transport, plasma-wall interaction, and large potentials in plasma. We perform plasma device computer experiments to compare with analytic models and laboratory experiments in order to accelerate device design.

Our research for 1991 has been widely reported, as given by the listing following, of Journal Articles, ERL Reports, Talks, and Poster Papers.

Abstracts are attached for some of the talks.

Sent along with this Report are reprints of Journal Articles.

Our prior mode was to publish Quarterly Progress Reports; these then became Semi-Annual Reports, which ended in 1988. In 1989, we began publishing Annual Progress Reports. While QPR's were excellent exercises in reporting, they required an immense effort; in today's research climate, such effort is not available.

We trust that our reporting is still useful.

— C. K. Birdsall

RESEARCH SUPPORTED BY

DOE Contract DE–FG03–90ER54079
ONR Contract FD–N00014–90–J–1198
State MICRO 90–018
University of Arizona 15546
Varian Associates

Table of Contents

PLASMA THEORY AND SIMULATION GROUP
Professor C.K. Birdsall
EECS Department
University of California
Berkeley, CA 94720
U.S.A.

1. We have developed the following interactive, real-time, many particle plasma codes for desktop computing, complete with graphics:
   - SPAM: A single particle mover, in specified $\vec{E}$, $\vec{B}$ fields; runs on a PC.
   - ES1, XES1: An electrostatic 1 dimensional, periodic PIC code. Can be magnetized. Described in detail in Plasma Physics via Computer Simulation, by Birdsall and Langdon, McGraw-Hill 1985 and Adam Hilger 1991 (which has the ES1 disk with it). Input files for projects in Chapter 5. Runs on PC's, or on X-11 windows equipped computers.
   - EM1: An electromagnetic 1 dimensional code, periodic or bounded. Not yet fully debugged.
2. We have developed the following plasma device computer experiments; also for desktop computing, complete with graphics.
   - IBC: Interactive-beam-circuit code; a PIC traveling wave tube, with space charge.
   - PDP1, PDC1, PDS1 (planar, cylindrical and spherical bounding electrodes): 1d3v, bounded, magnetized or not, including electron and ion collisions with neutrals, external circuit, voltage or current sources.
   - PDP2: Planar in x, periodic in y, 2d3v. $R-\theta$ and $R-Z$ versions in early development.
3. PC versions of SPAM, ES1 IBC, PDP1, PDC1, PDS1 are available at cost of handling from:

   Software Distribution Office
   Industrial Liaison Program
   EECS Dept., Cory Hall
   University of California
   Berkeley, California 94720
   U.S.A.

4. Xgrafix(for $X-11$ windows) versions of SPAM, EM1, IBC, PDP1 and PDP2 will probably be available Spring 1992. Contact Prof. Birdsall on these; do not request from ILP.

September 9, 1991

PLASMA DEVICE COMPUTER EXPERIMENTS
or
PDCX

Plasma device computer experiments are evolving far beyond what we have called plasma simulation codes up until now.

Hence, let us spell out what characterizes **PDCX**, what is included in **PDCX**, and some of the **PDCX** methods and diagnostics. This is the purpose of this sheet.

PDCX are characterized by:

- whole devices: internal plasma and gas, external circuit;
- real-time displays in internal and external diagnostics(see partial list at bottom);
- interactive, in terms of ease of viewing and re-scaling, as well as ease of setting initial values of parameters, and in changing parameters any time during an experimental run.
- results in a form to be compared with laboratory experiments.

PDCX include the electromagnetics, atomic physics and chemical reactions among charged particles(electrons, ±ions, particulates) and neutral atoms and molecules, in three regions:

- surfaces, walls
- sheaths, edges
- bulk plasma

PDCX numerical methods involve a marriage among:

- **PIC**, particle in cell, for electron, ion, neutral motion, collective effects;
- **MIC**, molecule in cell, for electron ion, neutral collisions, short range velocity changes, Monte-Carlo;
- fluids, many kinds;
- hybrids (fluids plus particles)

PDCX integrations in $\vec{x}, \vec{v}$, t may be explicit (to include high frequencies, short wavelengths) or implicit (to keep only low frequencies, high wavelengths), or be multi-scaled in $\vec{x}$, $\vec{v}$ or t..

PDCX diagnostics are non-invasive, available in $\vec{x}$ or $\vec{k}$ or t or ω, and are done by species (e.g., phase spaces, $n_s(\vec{x},t), f_s(\mathrm{E},\theta),(\vec{J}\cdot\vec{E})_s$ in $\vec{x},t$), plus the usual EM quantities and collision statistics, plus whatever the problem at hand demands.

Comments are most welcome.

C.K. Birdsall, EECS Dept., University of California, Berkeley, CA 94720

September 1991

I. PUBLICATIONS FOR 1991

Journal Articles

Crystal, T.L., P.C. Gray, W.S. Lawson, C.K. Birdsall, and S. Kuhn, "Trapped Electron Effects on Time-Independent Negative-Bias States of a Collisionless Single-Emitter Plasma Device: Theory and Simulation," *Physics of Fluids B* 3(1), January 1991, pp. 244.

Vahedi, V., M.A. Lieberman, M.V. Alves, J.P. Verboncoeur, and C.K. Birdsall, "A One Dimensional Collisional Model for Plasma Immersion Ion Implantation," *J. Appl. Physics* 69(4), 15 February 1991, pp. 2008-2014.

Alves, M.V., M.A. Lieberman, V. Vahedi, and C.K. Birdsall, "Sheath Voltage Ratio for Asymmetric RF Discharges," *J. Appl. Physics* 69(7) 1 April 1991, pp. 3823-3829.

Birdsall, C.K., "Particle-in-Cell Charged-Particle Simulations, Plus Monte Carlo Collisions with Neutral Atoms, PIC-MCC," *IEEE Trans. Plasma Science* 19(2), April 1991, pp. 65-85 (Invited paper).

Procassini, R.J., and C.K. Birdsall, 'Particle Simulation model of Transport in a Bounded, Coulomb Collisional Plasma," *Phys. Fluids B* 3(8), August 1991, pp. 1876-1891.

Friedman, A., S.E. Parker, S.L. Ray, and C.K. Birdsall, "Multi-Scale Particle-In-Cell Plasma Simulation," *J. Comp. Physics* 96, September 1991, pp. 54-70.

Parker, S.E., and C.K. Birdsall, "Numerical Error in Electron Orbits with Large $\omega_{ce}\,\delta t$," *J. Comp. Physics* 97(1), pp. 91-102, November 1991.

Parker, S.E., X.Q. Xu, A.J. Lichtenberg, and C.K. Birdsall, "Evidence of Stochastic Diffusion across a Cross-Field Sheath," accepted for publication, *Phys. Rev. A.*

Parker, S.E., A. Friedman, S.L. Ray, and C.K. Birdsall, "Bounded Multi-Scale Plasma Simulation: Application to Sheath Problems," accepted by *J. Comp. Physics.*

Otani, N.F., J.-S. Kim, C.K. Birdsall, B.I. Cohen, W. Nevins, and N. Maron, "Elimination of Velocity Space Rings-and-Spokes Instabilities in Magnetized Electrostatic Particle Simulations of Plasmas," accepted by *J. Comp. Physics* (approx. June 1992).

Parker, S.E., R.J. Procassini, C.K. Birdsall, and B.I. Cohen, "A Suitable Boundary Condition for Bounded Plasma Simulation without Sheath Resolution," accepted by *J. Comp. Physics.*

Verboncoeur, J.P., M.V. Alves, and V. Vahedi, "Simultaneous Potential and Circuit Solution for Bounded Plasma Particle Simulation Codes," accepted by *J. Comp. Physics.*

Berk, H.L., D.D. Ryutov, Y. A. Tsidulko, R.H. Cohen, and X.Q. Xu, "Electron Temperature-Gradient and Endloss Driven Transport in SOL of Tokamak Plasmas," submitted to *Comments on Plasma Physics and Controlled Nuclear Fusion.*

Hua, D., X. Xu, and T.K. Fowler, "Ion-Temperature-Gradient Modes in Non-Circular Tokamak Geometry," to be submitted by end of year.

Xu, X.Q., G. DiPeso, V. Vahedi, and C.K. Birdsall, "Theory and Simulation of Plasma Sheath Waves," to be submitted by end of year.

Book, Chapter

Birdsall, C.K., and A.B. Langdon, *Plasma Physics via Computer Simulation*, Adam-Hilger edition (with ES1 disk) 1991.

Birdsall, C.K., and A.B. Langdon, "Particle Simulation Techniques," in *Computer Applications in Plasma Science and Engineering*, ed. A. T. Drobot (Springer-Verlag: New York), pp. 7-41, 1991.

ERL Reports

Parker, S.E., X.Q. Xu, A.J. Lichtenberg, and C.K. Birdsall, "Evidence of Stochastic Diffusion across a Cross-Field Sheath due to Kelvin-Helmholtz Vortices," Memo. No. UCB/ERL M91/79, September 30, 1991.

X.Q. Xu, G. DiPeso, V. Vahedi, and C.K. Birdsall, "Theory and Simulation of Plasma Sheath Waves," Memo. No. UCB/ERL M91/80, September 30, 1991.

Conference Proceedings, Poster Papers

Workshop on Edge Plasma Physics for BPX and ITER, Princeton, NJ, January 15-17, 1991:

Birdsall, C.K., R.J. Procassini, A. Tarditi, and V. Vahedi, "1D-3V Particle Simulation of Tokamak Scrape-Off Layer and Divertor Plasmas"

International Sherwood Fusion Conference, Seattle, WA, April 22-24, 1991:

Birdsall, C.K., X.Q. Xu, S.E. Parker, and A.J. Lichtenberg, "Evidence of Stochastic Diffusion across a Cross-Field Sheath"

Hua, D., Fowler, T.K., and Xu, X.Q., "Gyrokinetic Particle Simulation of ITG Modes in General Toroidal Geometry"

Tarditi, A., "2D-Hybrid Particle Model with Non-Linear Electron Distribution"

Xu, X.Q. G. DiPeso, V. Vahedi, and C.K. Birdsall, "Theory and Simulation Study of Surface Waves in Bounded Plasma"

IEEE International Conference on Plasma Science, Williamsburg, VA, June 3-5 1991:

Tsung, F., J. Trulsen, V. Vahedi, and C.K. Birdsall, "Simulation of Potentials Created by Particulates in RF Discharges: Residence at the Sheath Edges"

Vahedi, V., M.A. Lieberman, G. DiPeso, C.K. Birdsall, T.D. Rognlien, J.R. Hiskes, and R.H. Cohen, "An Atomic Physics Model in a Particle-in-Cell Code for Simulation Plasma Processing"

Sixth International Conference on Emerging Nuclear Energy Systems, Monterey, CA, June 16-21, 1991:

Avanzini, P.G., and A. Tarditi, "Progress Towards a Neutralized beam Experiment for a Colliding-beam Advanced-Fuel Fusion Process"

Tarditi, A., "Multi-Turn Electron-Ion Injection Study for Neutralized High-Density Beam Sustaining in a Closed Configuration"

International Conference on Phenomena in Ionized Gases, Pisa, Italy, July 8-12, 1991:

Tarditi, A., "Particle Simulation of Neutralized Ion Bernstein Waves"

14th Conference on Numerical Simulation of Plasmas, Annapolis, MD, September 4-6, 1991:

Vahedi, V., M. Surendra, G. DiPeso, and J. Verboncoeur, "Numerical Methods for Simulating Processing Plasmas"

Vahedi, V., J.P. Verboncoeur, and C.K. Birdsall, "Xgrafix: An X-Windows Environment for Real-Time Interactive Simulations"

44th Annual Gaseous Electronics Conference, Albuquerque, NM, October 22-25, 1991:

Vahedi, V., P. Mirrashidi, B.P. Wood, M.A. Lieberman, and C.K. Birdsall, "A Comparison of PIC Simulation and Experimental Results in a Capacitive RF Discharge"

Lieberman, M.A., V. Vahedi, and R.A. Stewart, "An Analytic Model for the Ion Angular Distribution Function in a Highly Collisional Sheath"

Vahedi, V., M.A. Lieberman, G. DiPeso, and C.K. Birdsall, "A Bounded Particle in cell Code with an Atomic Physics Model for Simulating Processing Plasmas"

Lieberman, M.A., V. Vahedi, and R.A. Stewart, "An Analytic Model of the Ion Angular Distribution Function in a Highly Collisional Sheath"

Mirrashidi, P., B.P. Wood, V. Vahedi, M.A. Lieberman, and C.K. Birdsall, "A Comparison of PIC Simulation and Experimental Results in a Capacitive RF Discharge"

Vahedi, V., M.A. Lieberman, G. DiPeso, C.K. Birdsall, T.D. Rognlien, J.R. Hiskes, and R.H. Cohen, "An Atomic Physics Model in a Particle-in-Cell Code for Simulation Plasma Processing"

33rd Annual Meeting of the American Physical Society, Division of Plasma Physics, Tampa, FL, November 4-8, 1991:

Xu, X.Q., G. DiPeso, V. Vahedi, and C.K. Birdsall, "Theory and Simulation of Sheath Waves in Bounded Plasmas"

Vahedi, V., M.A. Lieberman, G. DiPeso, C.K. Birdsall, T.D. Rognlien, J.R. Hiskes, and R.H. Cohen, "A Particle in Cell Code with an Atomic Physics Model for Simulating Processing Plasmas"

Cohen, R.H., and X.Q. Xu, "Scrapeoff-Layer Instabilities Driven by Temperature Gradients and End Loss"

Tarditi, A., "Hybrid Particle-Fluid Simulation fo Magnetized Ion Plasma-Sheath Waves"

Tarditi, A., "Merging-code approach for Realistic Simulation of Plasma Experiments"

Theilhaber, J., "Quantum-Molecular-Dynamics Simulations of Liquid Metals and Highly-Degenerate Plasmas" (Invited paper)

1st Brazilian Congress on Plasma Physics, Santos SP, Brazil, December 10-13, 1991:

Birdsall, C.K., "Particle-in-Cell Simulations Plus Monte-Carlo Collisions, PIC-MCC, for Partially Ionized Gases, in Bounded Systems" (Invited paper)

Short Course

"Plasma Simulation" was taught to third world professionals at the International Center for Theoretical Physics, Trieste, Italy, June 3-13, 1991, by C.K. Birdsall and V. Vahedi.

Invited Talks

C.K. Birdsall presented several talks and live demonstrations on bounded plasma computer experiments: Vienna (Technical University, June 18, 1991); Garching bei München (Max Planck Institute for Plasma Physics, July 2, 1991); Bochum (University, July 23, 1991); Saǫ Paolo (Conference, December 1991)

Awards

1. C.K. Birdsall was a Lecturer/Researcher at University of Innsbruck, Austria, February 15 to July 28, 1991. He presented a term-long course on plasma simulation and gave several lectures in the local plasma seminar
2. At the College of Engineering graduation in May, Prof. Birdsall was given the Berkeley Citation, in recognition of activity in plasma simulation and for helping found the Energy and Resources Group (ERG) in 1972-1974.
3. At the 14th International Conference on Numerical Simulation of Plasmas banquet on September 5, 1991, in Annapolis, MD, former students and post-doctoral researchers of PTSG (who now number almost 50) presented Prof. Birdsall a plaque (surprise!) inscribed:

> To Professor Charles K. (Ned) Birdsall
> In warm appreciation of your many important achievements in the sciences of electronics, plasma physics, and computer simulation; of your effective promotion of international cooperation in science; and of your contributions to the lives and careers of the many of us — students, post- doctoral researchers, and collaborators — who have benefited by interacting with you, our colleague and friend.

CKB comments*: *This is wonderful, especially as it comes from our simulation "family," which has been most productive and very warm friends over the past several decades. You all have made my 33 years at UC a very good life. Thank you!*

* Yes, I am now retired from UC; however, while this means no regular teaching schedule, I plan to continue in plasma research, with PTSG, for some time to come. —CKB

II. LIST OF REPRINTS AND REPORTS SENT WITH THIS REPORT

Crystal, T.L., P.C. Gray, W.S. Lawson, C.K. Birdsall, and S. Kuhn, "Trapped Electron Effects on Time-Independent Negative-Bias States of a Collisionless Single-Emitter Plasma Device: Theory and Simulation," *Physics of Fluids B* 3(1), January 1991, pp. 244

Vahedi, V., M.A. Lieberman, M.V. Alves, J.P. Verboncoeur, and C.K. Birdsall, "A One Dimensional Collisional Model for Plasma Immersion Ion Implantation," *J. Appl. Physics* **69**(4), 15 February 1991, pp. 2008-2014

Friedman, A., S.E. Parker, S.L. Ray, and C.K. Birdsall, "Multi-Scale Particle-In-Cell Plasma Simulation," *J. Comp. Physics* **96**, September 1991, pp. 54-70

Alves, M.V., M.A. Lieberman, V. Vahedi, and C.K. Birdsall, "Sheath Voltage Ratio for Asymmetric RF Discharges," *J. Appl. Physics* **69**(7) 1 April 1991, pp. 3823-3829

Birdsall, C.K., "Particle-in-Cell Charged-Particle Simulations, Plus Monte Carlo Collisions with Neutral Atoms, PIC-MCC," *IEEE Trans. Plasma Science* **19**(2), April 1991, pp. 65-85 (Invited paper)

Procassini, R.J., and C.K. Birdsall, 'Particle Simulation model of Transport in a Bounded, Coulomb Collisional Plasma," *Phys. Fluids B* 3(8), August 1991, pp. 1876-1891

Parker, S.E., X.Q. Xu, A.J. Lichtenberg, and C.K. Birdsall, "Evidence of Stochastic Diffusion across a Cross-Field Sheath due to Kelvin-Helmholtz Vortices," Memo. No. UCB/ERL M91/79, September 30, 1991

III. ABSTRACTS OF 1991 TALKS AND POSTERS, UNPUBLISHED

Workshop on Edge Plasma Physics for BPX and ITER, Princeton, NJ, January 15-17, 1991 (1 abstract)

International Sherwood Fusion Conference, Seattle, WA, April 22-24, 1991 (4 abstracts)

IEEE International Conference on Plasma Science, Williamsburg, VA, June 3-5 1991 (2 abstracts)

Sixth International Conference on Emerging Nuclear Energy Systems, Monterey, CA, June 16-21, 1991 (2 abstracts)

International Conference on Phenomena in Ionized Gases, Pisa, Italy, July 8-12, 1991 (1 abstract)

14th Conference on Numerical Simulation of Plasmas, Annapolis, MD, September 4-6, 1991 (2 abstracts)

44th Annual Gaseous Electronics Conference, Albuquerque, NM, October 22-25, 1991 (3 abstracts)

33rd Annual Meeting of the American Physical Society, Division of Plasma Physics, Tampa, FL, November 4-8, 1991 (6 abstracts)

WORKSHOP ON EDGE PLASMA PHYSICS FOR BPX AND ITER
15-17 JANUARY 1991 - PLASMA PHYSICS LABORATORY, PRINCETON, NJ

1D-3V PARTICLE SIMULATION OF TOKAMAK SCRAPE-OFF LAYER AND DIVERTOR PLASMAS

C.K. Birdsall, R.J. Procassini*, A. Tarditi, V. Vahedi

EECS, University of California at Berkeley, Berkeley, CA 94720
*LLNL, Livermore, CA 94550

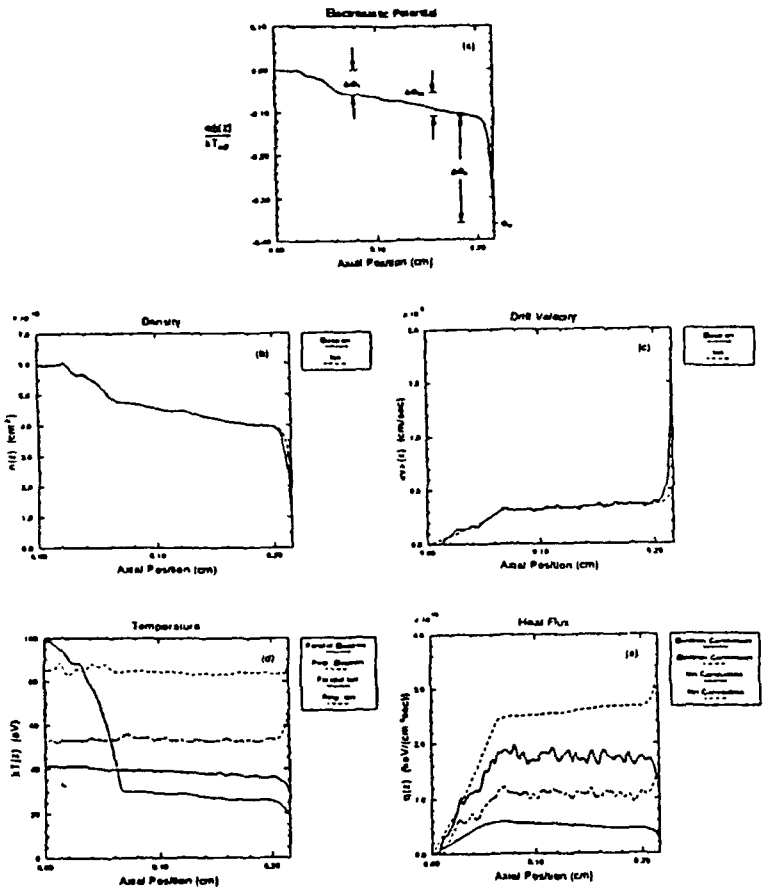

Spatial profiles of (a) the electrostatic potential, (b) plasma density, (c) drift velocity, (d) temperature and (e) heat flux.

3. SIMULATION OF TRANSPORT IN A HIGH-RECYCLING DIVERTOR SCRAPE-OFF LAYER

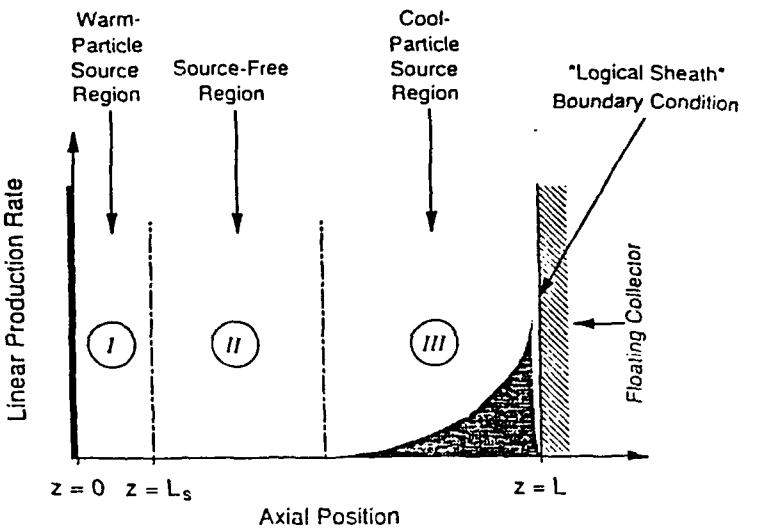

The one-dimensional particle-in-cell model of the high-recycling divertor scrape-off layer in a tokamak.

Simulations Parameters Used to Model Transport in a High-Recycling Divertor Scrape-Off Layer.

System Length:	$L = 2000\lambda_{De0} = 2.10$ cm
Source Region Width:	$L_S = L/3 = 0.70$ cm
Warm-Particle Injection Rate:	$R_{inj} = 2.25$ particles pairs per Δt
Electron Source Temperature:	$kT_{\|\|,e0} = kT_{\perp,e0} = 100$ eV
Ion Source Temperature:	$kT_{\|\|,i0} = kT_{\perp,i0} = 100$ eV
Equilibrium Density:	$n_{eq} = 5.0 \times 10^{13}$ cm^{-3}
Mass Ratio:	$m_i/m_e = 200$
Coulomb Collisionality:	$\nu^* \equiv \nu_{e0}/\nu_{be0} = 1$
Collisional Acceleration Factor:	$\alpha_{coll} = 26.5$
Peak Charge Exchange Cross Section:	$\hat{\sigma}_{ion} = 2.038 \times 10^{-15}$ cm^2
Peak Ionization Cross Section:	$\hat{\sigma}_{cx} = 1.978 \times 10^{-15}$ cm^2
Neutral Density e-Folding Length:	$L_n = 0.12$ cm
Neutral Particle Temperature:	$kT_n = 5$ eV

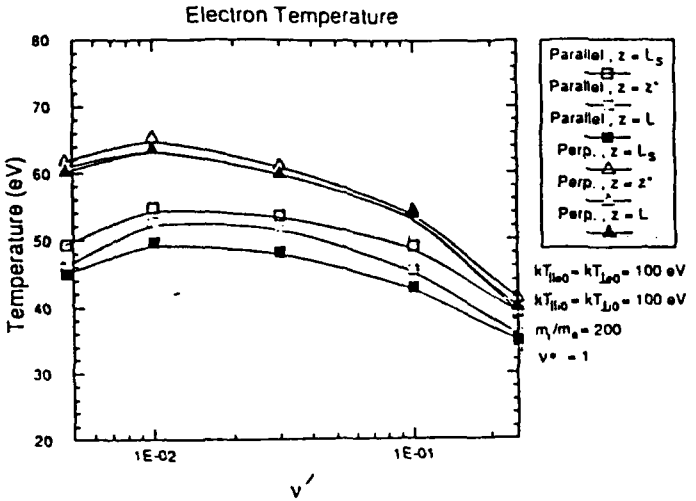

(a) Electron temperature.

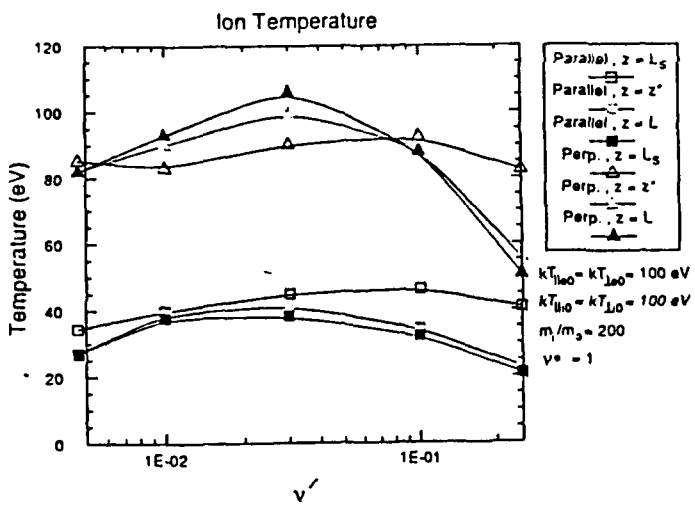

(b) Ion temperature.

The variation of the components of (a) the electron and (b) the ion temperature with neutral recycling intensity over the range $0 \leq \nu' \leq 0.25$.

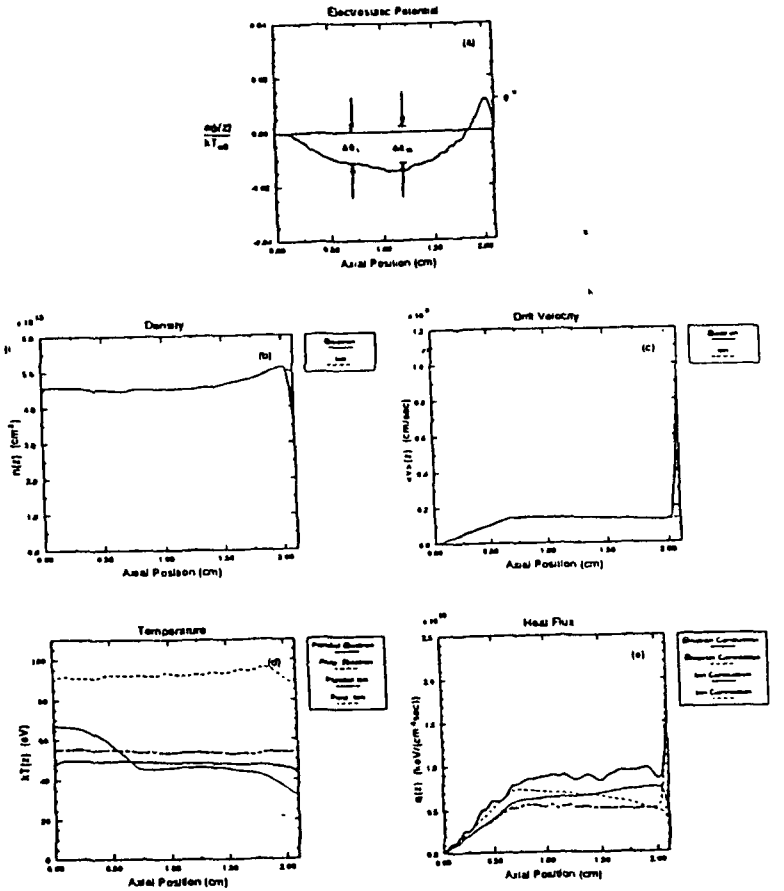

Spatial profiles of (a) the electrostatic potential, (b) plasma density, (c) drift velocity, (d) temperature and (e) heat flux from the simulation with $\nu' = 0.1$.

4. DIVERTOR PLASMA-SHEATH REGION REAL-TIME SIMULATION

An explicit 1D ES code has been used for the plasma sheath simulation in a high density divertor plasma (PDP1 code [3], [4]).

The code runs in a real-time, interactive graphics display environment (XGRAPHIC [4]) on workstations and fast PC's.
Monte Carlo binary collision and atomic physics models are implemented.

The simulation considers an emission plate to model the warm-plasma source region and a floating collector plate for the divertor. A region about 100 Debye lengths far from the plate was simulated.

Equal fluxes of thermal electron and ions are injected in a pre-loaded uniform, quiet, thermal plasma. This allows to avoid strong space-charge oscillations which hidden the plasma sheath potential.

ITER scenarios-like divertor plasma parameter have been used ($n=10^{20}$, $Te=Ti=100\,eV$, $10\,MW/m^2$ particle energy flux).

A careful choice of the model parameters allowed to eliminate the "source sheath", whose potential drop produces an unphysical acceleration effect.

The plasma-sheath formation, from its early stages to the regime condition, can be followed during the real time simulation.

[3] I.J. Morey, V. Vahedi, L. Verboncoeur, Bull. APS, 34,2028 (1989)
[4] Code available from Industrial Liaison Program, EECS Dept. UC Berkeley, CA 94720

SHEATH POTENTIAL FORMATION BEFORE THE REGIME CONDITIONS (PDP1 SIMULATION)

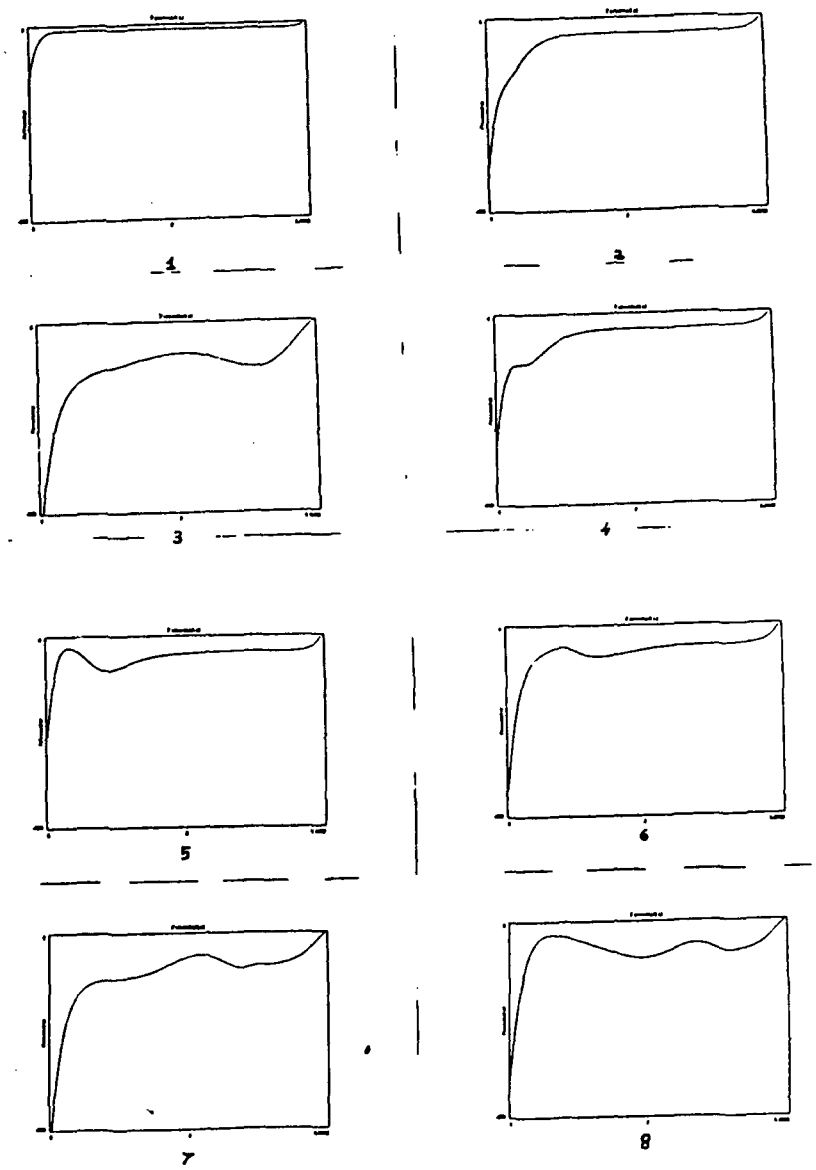

SHEATH POTENTIAL AND ELECTRON AND ION DENSITIES IN THE REGIME CONDITIONS (PDP1 SIMULATION)

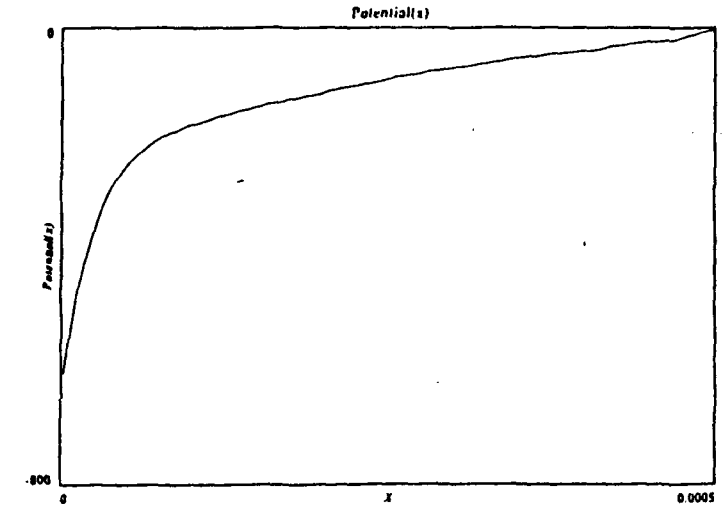

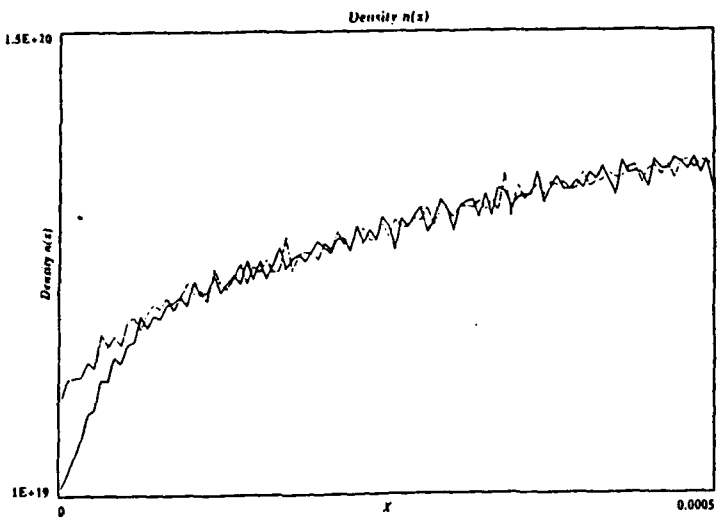

5. FUTURE DEVELOPMENTS

- Implementation of the implicit code DIPSI in a real-time graphics displaying environment.

- 2D, (implicit), magnetized bounded plasma particle code (including atomic physics 2D models).

- Improvement of atomic physics modeling including excitation collisional processes (for the impurity transport simulation) and radiative loss models (for the simulation of the effect of impurities on the SOL temperature).

Theory and Simulation Study of Surface Waves in Bounded Plasma

X. Q. Xu, G. DiPeso, V. Vahedi, C. K. Birdsall
Electronics Research Laboratory
U. C. Berkeley, CA 94720

Surface waves have been investigated analytically and with particle simulation for an unmagnetized 2d plasma slab with periodic boundary conditions in y and bounded in x with either vacuums (isolated plasma) or conducting walls. In the vacuum boundary case, the particle simulation results are found to agree reasonably with theory for high frequency surface waves.[1] For a plasma inside two absorted conducting walls, simulation indicate that surface waves propagate along the static sheath-plasma boundary. Analytically treating the sheath as a vacuum layer, the surface waves bear a resemblance to plasma-vacuum surface waves with the vacuum dielectric constant ϵ_0 replaced by $\epsilon_0 \arctan(k_y \Delta)$, where Δ is width of the static sheath. Nonlinear interaction of bulk and surface waves in the system will be discussed.

References

1. A. G. Sitenko, **Fluctuations and Non-linear Wave Interactions in Plasmas**, (Pergamon Press, Oxford, 1982)

Sherwood

Evidence of Stochastic Diffusion across a Cross-Field Sheath due to Kelvin-Helmholtz Vortices

C.K. Birdsall, X.Q. Xu, S. E. Parker[†], and A.J. Lichtenberg

Electronics Research Laboratory

University of California, Berkeley, California 94720

September 13, 1991

Abstract

Our objective is to identify the mechanisms for particle transport across a cross-field sheath. We present a study of $\mathbf{E} \times \mathbf{B}$ motion in a vortex in which the ions are perturbed by the finite gyroradii and electrons are perturbed by one or more traveling waves. Large scale vortices which are the result of a shear in the $\mathbf{E} \times \mathbf{B}$ drift velocity have been observed in plasma simulations of the cross-field sheath[1-3]. Small scale turbulence is also present. The vortices are the result of the nonlinear saturation of the Kelvin-Helmholtz instability. A vortex alone does not allow for the observed electron transport because the electron drift orbits simply circulate. On the other hand, the ion motion can be stochastic from resonant interaction between the drift motion and the gyromotion, independent of the background turbulence. The fluctuations in the ion density would then give rise to small amplitude wave spectrum. The combined action of the vortex fields and traveling wave fields on the electron motion can again lead to stochasticity. We study these effects, showing that the values of vortex fields, observed in the simulation, are sufficient to lead to both ion and electron stochastic diffusion. Furthermore, the rate of the the resulting diffusion is sufficient to account for the diffusion observed in the simulation.

[†] Present address: Plasma Physics Laboratory, Princeton University, Princeton, New Jersey 08543.

Sherwood

2D-HYBRID PARTICLE MODEL WITH NON-LINEAR ELECTRON DISTRIBUTION

A. Tarditi

Electrical Engineering and Computer Science, Electronic Research Lab.
University of California at Berkeley - Berkeley, CA 94720 (USA)

ABSTRACT

A 2D, hybrid (particle-ion, fluid-electron) simulation code characterized by the solution of the non-linear modified Poisson equation, which results assuming the Boltzmann distribution for the electrons, is presented.
Following [1], the field solution is achieved through an iterative procedure. Anyhow a new scheme is considered. The potential is not obtained by directly solving the finite difference equation but via the Green's function method.
The procedure begins with the first guess for the potential. This is found through the solution of the linearized modified Poisson equation. The Green's function for this equation, in the 2D case which is considered, can be found analytically in term of the Neumann functions [2], [3].
Once the potential corresponding to the linearized modified Poisson equation is known, the first approximation of the electron (Boltzmann) distribution can be calculated. This distribution, plus the one given by the (particle) ions, is considered as the source term for the Poisson equation (which now is not "modified" since the fluid electron component is taken into account in the source term itself).
The solution of this Poisson equation gives the second approximation of the electric potential and is still obtained via the Green's function method (as it comes from the Coulomb law, modified for the 2D case, [2]).
Each time step this procedure can be iterated according to the desired accuracy. The last iteration cycle is different: in fact the direct solution for the electric field can be obtained, without numerical differencing from the potential. It is sufficient in this case to consider the electric field Green's functions (x- and y-component) for the Poisson equation (in place of the electric potential Green's function).
The first results obtained with this new code are here presented and compared with previous simulation runs based on a linearized Boltzmann distribution model, as in [2], [3].

REFERENCES

[1] H. Okuda, J.M. Dawson, A.T. Lin , C.C. Lin, Phys. Fluids, 21, 476 (1978)
[2] A. Tarditi, Ph.D. Thesis, University of Genova (Italy), 1990
[3] A. Tarditi, submitted to the XX Int. Conf. on Phenomena in Ionized Gases, 1991

Sherwood

Gyrokinetic Particle Simulation of ITG Modes in General Toroidal Geometry

Daniel Hua, T.K. Fowler
Department of Nuclear Engineering
University of California
Berkeley, CA 94720

Xueqiao Xu
Electronics Research Laboratory
University of California
Berkeley, CA 94720

Abstract

We have generalized the 1-1/2 d linearized gyrokinetic particle simulation code of Xu et. al. [1] to tokamaks with non-circular corss section (i.e. elongation and triangularity) to study ion temperature gradient modes (ITG) in the presence of ion-ion collisions. We hope to determine the role of local magnetic shear, poloidal beta and various geometric factors in linear growth rate and transport coefficients. For comparison to DIII-D, we apply the code with input parameters calculated by the MacEquilibrium Code of Haney [2] using experimental measurements of DIII-D.

[1] Xueqiao Xu, to be published in Physics of Fluids B.

[2] Scott Haney, Ph.D. Thesis, MIT.

Sherwood

AN ATOMIC PHYSICS MODEL IN A PARTICLE-IN-CELL CODE FOR SIMULATING PLASMA PROCESSING[1]

Vahid Vahedi, M. A. Lieberman
G. DiPeso and C. K. Birdsall
University of California, Berkeley
Berkeley, CA 94720

T. D. Rognlien, J. R. Hiskes, and R. H. Cohen
Lawrence Livermore National Laboratory
Livermore, CA 94550

We are combining a particle-in-cell (PIC) model for particle with a Monte Carlo collision (MCC) scheme to model the collisions between the charged and neutral particles. The MCC model can also be extended to model Coulomb collisions between charged particles which tends to be significant at very low temperature RF discharges and in ECR discharges. We are comparing the merits of treating the neutrals as fluids and/or as particles. These models are incorporated into PDP1[2], a bounded one dimensional plasma simulation code. As a specific example, we consider oxygen RF discharges, at various neutral pressures and RF voltages. The atomic physics model for oxygen currently only includes the energy dependent processes of ionization, dissociation, recombination, detachment, and charge transfer. Electrons, O_2^+, O^-, and O are evolved as particles. We are studying the modification of the dynamics of the discharge owing to the presence of a substantial concentration of negative ions. The atomic physics model can also be used for many other types of processing discharges, such as ECR discharges.

---

1. Work performed for USDOE by LLNL under contract W-7405-ENG-48; a portion of the UCB work performed for NSF under grant ECS-8910827.

2. I. J. Morey, V. Vahedi and J. Verboncoeur, *Particle Simulation Code for Modeling Processing Plasmas*, Bull. APS, 34:2028, (1989) (Abstract); Codes available from Industrial Liaison Program, EECS Dept., UC Berkeley.

IEEE COPS

SIMULATION OF POTENTIALS CREATED BY PARTICULATES IN RF DISCHARGES: RESIDENCE AT THE SHEATH EDGES[1]

F. Tsung, J. Trulsen,
V. Vahedi, C. K. Birdsall

University of California, Berkeley
Berkeley, CA 94720

Heavy particles may play a role in determining the average potentials experienced by ions in RF discharges, hence ion acceleration into targets. Particulates or dust particles also may play a role in many other plasmas. Hence, it is desirable to find where these heavy particles reside (with respect to the edge of the plasma, or sheath) and their effect of the time average potential which accelerates ions through the sheath.

Using our many-particle PIC-MCC 1d3v simulation code PDP1[2], we have been able to show that the particulates tend to become charged negatively, using cross sections for electron and ion attachment worked out here by Trulsen, inspired by work of R. Carlile at Univ. Of Arizona[3]. We have placed one heavy particle at various locations in the sheath and found that special location where the time average field at the particle is zero; this is then the residence of the particle, which turns out to be very near the time average sheath edge. We are now putting in a large number of particulates and allowing them to move and affect the potential across the whole RF discharge; this is feasible only by lowering the particulate mass from about 10^8 argon ion mass to some smaller values, still running a long time (many RF cycles). We will report on the results at the meeting.

---

1. Work supported in part by Univ. Of Arizona Sematech Ctr. for Excellence, J. Prince, Dtr.

2. I. J. Morey, V. Vahedi and J. Verboncoeur, *Particle Simulation Code for Modeling Processing Plasmas*, Bull. APS, 34:2028, (1989) (Abstract); Codes available from Industrial Liaison Program, EECS Dept., UC Berkeley, CA 94720.

3. R. N. Nowlin and R. N. Carlile, "Electrostatic Nature of Contaminative Particles in a Semiconductor Processing Plasma", ECE Dept., Univ. Of Arizona (Submitted for publication)

IEEE COPS

PROGRESS TOWARDS A NEUTRALIZED BEAM EXPERIMENT FOR A COLLIDING-BEAM, ADVANCED-FUEL FUSION PROCESS

P.G. Avanzini and A. Tarditi

ANSALDO RICERCHE - Corso Perrone 25 -16161 Genova (ITALY)

Electrical Engineering and Computer Sciences - Electronic Research Laboratory
University of California at Berkeley - Berkeley, CA 94720 (USA)

ABSTRACT

The problem of sustaining a colliding ion beam process for advanced-fuel fusion power generation is considered. In order to overcome the space charge limit on the beam density, a concept based on a neutralized ion-electron beam is introduced.
A device with fairly novel features is described and preliminary design considerations for a basic neutralized beam experiment are outlined.

INTRODUCTION

An approach to a fusion process based on colliding beams has been studied for several years [1-4].
The optimal reactivity conditions for a given fusion reaction are obtained when two monoenergetic counterstreaming ion beams collide with relative velocity chosen reaching the maximum of the fusion cross section.
The generation of ion beams with energies of hundreds of keV, that is the typical range for the reactivity maxima of very energetic and "clean" reactions such as H-^{11}B or D-^{3}He [5] is rather easy (while these energies are prohibitive for confined plasma heating and ignition). A closed confinement geometry for the colliding beams has to be necessarily considered ("open beam" configurations are hopeless for energy production purpouses).
For a reactor with reasonable fusion power density a reacting fuel density of at least 10^{19} m^{-3} is required. Then, ion beams of such a density with energy in the 100 keV range have to be produced and confined while they collide.
At these densities, due to the space charge force the beams must be neutralized: for this purpose also a fast electron beam is considered. For electrodynamical stability reasons the two ion beams run in the same direction at a given relative velocity (there will be a fast and a slow beam) while the electrons will be counterstreaming.
A "neutralized" (and not "neutral") beam will then result because, being charge balanced, it shows global electrical neutrality but, due to the high electron-ion relative velocity, also low recombination (and elastic collision) rate.

THE OPTIMAL FUSION PROCESS

THE OPTIMAL REACTIVITY CONDITIONS

In order to estimate the fusion power production, the rate R_{ab} (number of fusions between the species "a" and "b" per time and volume unit) can be defined as

$$R_{ab} = n_a n_b \sigma_f u_{ab} \quad (\text{fusions}/(m^3 s))$$

where $n_{a,b}$ are the densities of the reacting species, u_{ab} their relative velocity and σ_f the fusion cross section. Here u_{ab} is the same for all the particles (case of two colliding monoenergetic beams).
The fusion power density will then be expressed as $p_f = R_{ab} \cdot E_f$ where E_f is the energy released per fusion.
The maximum rate is obtained when the quantity $\sigma_f u_{ab}$ ("reactivity") is maximum. The same definition holds when a non-monoenergetic velocity distribution is given: in this case the reactivity is defined as $\langle \sigma_f v \rangle$ by averaging over the velocity distribution [4].
The curves of σ_f versus particle relative energy are well referred in the literature [5]. Then the reactivity vs. particle energy trend can be readily found.
The reactivity maxima for colliding beams and thermal plasmas are summarized in table 1. Here the D-T reaction has been compared with the most important neutron free fusion reactions (characterized by high σ_f and E_f at the same time [4]).
These estimates show that the maximum ideal efficiency of the colliding beam approach is greater than that of the hot plasma roughly by a factor of two.
In a real device the Bremsstrahlung losses must be also taken into account: they set a limit to the temperature that can be reached in a plasma at ignition.

ICENES

For a neutralized beam (electron-ion) beam with axial velocity much greater than the thermal velocity (i.e. with small transversal temperature), the effect of Bremsstrahlung radiation losses is less important.

COLLIDING BEAMS VS. PLASMAS

The previous discussion about the expected maximum fusion efficiency must be integrated by taking into account the power losses. The optimal conditions will be reached when the gain $G=p_f/p_{loss}$ of the process is maximum, where p_{loss} is a power density that takes into account the energy absorbed during the process operation. Then the real "optimal" fusion cycle shall not necessarily correspond to the maximum fusion cross section since the greater p_f could be counterbalanced by an increase in p_{loss}.

	$\langle\sigma_f v\rangle\|_{max}$	$\sigma_f u\|_{max}$	E_f (MeV)	$E_f\sigma_f u\|_{max}$ (Jm^3/s)
H-^{11}B	$3.5\cdot10^{-22}$ (1 MeV)	$7.3\cdot10^{-22}$ (700 keV)	8.64	10^{-33}
D-^{3}He	$2.2\cdot10^{-22}$ (300 keV)	$5.8\cdot10^{-22}$ (420 keV)	18.35	$1.7\cdot10^{-33}$
D-T	$8\cdot10^{-22}$ (50 keV)	$2\cdot10^{-21}$ (100 keV)	17.59	$5.6\cdot10^{-33}$

Table 1.1 - Reactivity comparison for colliding beams and thermal plasmas in D-T, H-^{11}B and D-^{3}He reactions.

In a thermal plasma the Bremsstrhalung radiation loss increases with electron temperature imposing then a severe limit on the energy gain of the process and making prohibitive those high temperature regimes required by optimal reactivities in advanced fuel reactions [7]. In practice plasma breakeven will be possible only at a lower temperature than that maximizes the fusion cross section.
Then a hot plasma-based fusion cycle will be at most a sub-optimal process from the reaction ideal efficiency point of view (besides the problems concerning the heating, the ignition and the confinement of plasmas at tens of keV or more).
By trying to conceive a fusion process closer to the ideal fusion cycle conditions, a colliding beam approach seems to be a "natural" answer.
As pointed out previously, the attainment of ion beam energies of hundreds of keV does not represent a problem.
The first difficulty arises from power density considerations. For example, also by choosing the D-T reaction, in order to get just $p_f=10^3$ W/m^3 (a very small power density for a reactor) the beam density required for each species is $n=(10^3/5.64\cdot10^{-33})^{1/2}\simeq4\cdot10^{17}$ particles/m^3. However the stable confinement of such a beam density is unfeasible due to the space charge limits and the concept of neutralized beam has to be introduced.

ENERGY BALANCE CONSIDERATIONS

Output fusion power is produced as long as the ion beams keep on running with sufficient relative speed.
The particles "burned" in the fusion reactions represent an unavoidable loss and they shall be replaced in order to keep the density constant. Moreover there will be a flux of scattered particles (ions and electrons) which, for the high transversal velocity acquired, will tend to escape from the beam. Some of these particles will be lost and they have to be replaced, too.
Due to these losses input beams supplied by the injectors are also needed to preserve the achieved regime conditions for a longer time.
The system, in regime conditions, is then continuously fed by two ion accelerators and by an electron accelerator for replacing the particles scattered out of the beam or "burned".
The intrinsic gain (i.e. in the ideal, lossless case) of the process can be readily expressed by considering the power density required to supply the fuel particles "burned" in the fusion reactions. If W_a and W_b are the kinetic energies of the reacting ions, the power density the accelerators shall yield is $p_{prn}=R_{ab}\cdot(W_a+W_b)$, where R_{ab} is the fusion rate. Then the intrinsic gain will be simply

$$G_i = \frac{p_f}{p_{brn}} = \frac{E_f}{W_a+W_b}$$

By choosing $W_a+W_b=W_{ab}|_{opt}$ (the optimum relative beam energy quoted for $\sigma ru|_{max}$ in table 1) an intrinsic gain of about 12 for the H-^{11}B reaction, 44 for D-^{3}He and 176 for D-T is found.
This is really the maximum gain one could expect since the assumption $W_a+W_b=W_{ab}|_{opt}$ corresponds to the case of counterstreaming ion beams with zero center-of-mass velocity [3].
The long-range collisions produce a gradual thermalization and deteriorate the confinement but they do not throw the particles out of the beam, so particle losses are due directly only to short-range collisions.
However, not all the short-range scattered particles will be lost. This is mainly due to the fact that the center of mass in all these collisions is moving (w.r.t. the laboratory frame) because the ion beams are moving in

the same direction: the scattering cross-section is defined for a square-angle momentum deviation in the center of mass frame. By means of simple mechanical considerations [9], it is easy to show that when the ions are moving fast, the scattering angle in the laboratory frame is considerably reduced.

BASIC OPERATION OF A NEUTRALIZED BEAM DEVICE

The neutralized beam process is based on two fundamental items: *i*) an injection process that in the start-up phase creates a high-density neutralized beam by accumulating particles from low-density electron and ion injectors and in the final operating regime compensates the particles lost or "burned" in the fusion reaction; *ii*) a confinement system which provides a sufficient beam stability from the first injection (low-density) phase to the final high-density pinched condition.
The first item has been extensively studied and the last results are presented in [6].
Direct supply of very high-density, 100's keV ion and electron beams does not seem feasible due technical and economic issues; it was envisaged that a high-density neutralized beam can be produced in a ring configuration using low density, electrostatic, ion and electron accelerators. The basic principle is to keep a sufficient beam stability for the beam to allow a very fast accumulation of particles.

THE NEUTRALIZED BEAM

THE ION AND ELECTRON COMPONENTS

The basic idea is to "assemble" a high density "neutralized beam" by confining the ion and electrons together.
The electrons produce unavoidable collisions and radiation losses leading towards the thermalization of the whole system. However the faster the electrons run with respect to the ions, the lower is the electron-ion Coulomb collision cross section. Then a very fast electron neutralization component can reduce the collisional rate at an acceptable level.
Furthermore the high velocity electron beam will have a small energy spread, i.e. trasversal temperature, allowing a very small Bremsstrhalung loss.
Here the ion energy is typically greater than in a discharge-produced plasma since it is provided independently to ion and electron beams. The presence of these high momentum ions could have a favourable influence on stability against "kink" or "sausage" pinch instabilities.

THE LOW-DENSITY COLLISIONLESS BEHAVIOUR

The beam is "a priori" subjected to both the space charge fields produced by the other particles and to the external confinement fields.
A simple estimate, however, shows that during the injection phase the self-consistent fields are negligible with respect to the external confinement ones because the low beam densities. This means that a single-particle treatment can be applied to study the neutralized beam formation and confinement in the early phase of operation.
Then, at the injection phase, the particle trajectories are determinated only by external fields and the electron and ion beams constitute a non-collisional system which the single-particle treatment can be applied to.

THE INCREASE OF THE BEAM DENSITY

At the startup, low-density electron and ion beams are injected into the device. Each beam will be constrained in a circular path by an external confinement and focusing system [4, 6].
In the hypothesis of perfect confinement, if L is the length of the beam orbit, no is the beam density at the accelerator output and vo its (longitudinal) velocity, the density will increase linearly with time as

$$n(t) = n_0 v_0 t/L = n_0 t/\tau$$

being $\tau = L/vo$ the typical time constant.
For example, if $vo = 10^6$ m/s and L=1 m, a density increase by three orders of magnitude will take 10^{-3} s.

THE HIGH-DENSITY REGIME CONDITIONS

The regime conditions for a neutralized beam will be characterized by a strong poloidal magnetic field with the related pinch effect.
If the beam minor radius is much greater than the Debye lenght (defined through the transversal temperature) the neutralized beam is like a neutral, "soft" conductor carrying a strong current. In this condition the toroidal curvature radius could be imposed by an external dipolar field directed as the beam major axis.
The beam centrifugal force per volume unit is

$$f_c = \frac{m_e v_e^2 n_e + m_i v_i^2 n_i}{R_c}$$

where Rc is the curvature radius of the beam.
The force due to an external magnetic field Bo perpendicular to the beam plane is

$$F_m = i \cdot l \cdot B_0,$$

where

$$i = S \cdot (n_e v_e q_e + n_i v_i q_i)$$

is the total current ($S=\pi R_b^2$ is the beam section) and l is the beam circonference The global centrifugal force on the beam will be $F_c=f_c \cdot S \cdot l$. Writing down the force balance equation for a one-species neutralized beam one gets:

$$R_c = \frac{1}{B} \cdot \frac{m_e v_e^2 n_e + m_i v_i^2 n_i}{n_e v_e q_e + n_i v_i q_i}$$

By taking into account also the "hoop" expandig force the expression for R_c cannot be obtained anymore in a closed form since

$$B = \frac{1}{R_c} \cdot \left[\frac{m_e v_e^2 n_e + m_i v_i^2 n_i}{n_e v_e q_e + n_i v_i q_i} + \frac{\mu_0 i}{4\pi} \mathcal{L} \right]$$

$$\mathcal{L} = \left(\ln \frac{8R_c}{R_b} + \frac{l_i}{2} - 1 \right)$$

being "R_b" the beam minor radius and l_i the normalized inductance per unit lenght and $l_i = \langle H\phi^2 \rangle / H\phi^2(R_b)$ [8] ($H\phi$ is the poloidal field).

COULOMB COLLISIONS

Coulomb collisional effects can be studied by referring to the long-range and the short-range collisions.
Let it be considered "test" charges q (mass m, velocity v, density n) colliding with "field" charges q^* (mass m^*, velocity v^*, density n^*). The relative velocity is $u=v-v^*$; the present model holds until all the velocities are almost parallel, then the scalar notation will be used for velocities and momenta. The cross-section for long-range large-angle collision is [8]:

$$\sigma_{lr} = \frac{(qq^*)^2 \ln \Lambda}{4\pi\varepsilon_0^2 \mu^2 u^4}$$

where

$$\ln \Lambda = b_{max}/b_{min} = \lambda_D 4\pi\varepsilon_0 \mu^2 u^2 / (qq^*)^2$$

is the Coulomb logarithm and μ the reduced mass. By simple mechanical considerations it can be shown that [8]

$$\frac{d}{dt}(mv) = \frac{dp}{dt} \approx \frac{(qq^*)^2 \ln \Lambda}{4\pi\varepsilon_0^2 \mu u^2}$$

and then it can be derived that:

$$u(t) = (u_0^3 - 3Bt)^{1/3}$$

where

$$B = A\left[\frac{1}{m} + \frac{1}{m^*} \right] \quad A = \frac{(qq^*)^2 \ln\Lambda \, n^*}{4\pi\varepsilon_0^2 \mu}$$

The solution "u(t)" yields an estimate of the effect of the long-range collisions on the colliding beams velocity that is valid until the energy spread is low (since the approximation of almost parallel velocities). A stability time constants can be defined as the times at which u(t), v(t) or $v^*(t)$ reach, for example, the 90% of their initial value.
The short-range collision cross-section is simply σ_{lr} divided by a factor $4\ln\Lambda$.
A collisional rate for short-range scattering can be readily defined and taken into account as a loss term (the particles scattered out by short-range collisions could be considered lost).

THE "EXTRAP" HIGH-DENSITY CONFINEMENT

When the high-density regime is reached the neutralized beam looks like a current carrying plasma in a toroidal z-pinch configuration and the confinement cannot be ensured anymore only by the weak-focusing effect.
Lehnert's multipolar plus z-pinch "EXTRAP" configuration [10], seems to be naturally suitable for the confinement of a neutralized, high-density, pinched beam. Here the EXTRAP plasma-induced current could be replaced by the beam current.
It has been experimentally demonstrated [10] that EXTRAP shows an excellent degree of stability with respect to the MHD pinch disrupting modes.

EXAMPLE

Some of the most important parameters for the proposed process are calculated in an example case.
The D-^{3}He reaction was chosen and the basic features are listed below

Relative ion energy	420 keV
Relative ion beam velocity	$8.2 \cdot 10^6$ m/s
Energy released per fusion	18.3 MeV
Fusion cross section	$7 \cdot 10^{-29}$ m^{-2}
Slow beam energy	10 keV ($8 \cdot 10^5$ m/s)
Fast beam energy	843 keV ($9 \cdot 10^6$ m/s)
Electron beam energy	300 keV ($2.3 \cdot 10^8$ m/s)
Relativistic electron mass	$1.58 \cdot m_{e0}$

Assuming a regime ion density of 10^{19} m^{-3}, a current for the slow ion accelerator of 100μA, a 5 mm minor radius beam and a 2-m long ring, the following input parameters can be found:

Particle species	D	^{3}He	e^-
regime density (m^{-3})	10^{19}	10^{19}	$3 \cdot 10^{19}$
inject. density (m^{-3})	$9 \cdot 10^{11}$	10^3	$1.4 \cdot 10^{11}$
injection current (μA)	100	200	300

The time required to reach the regime density is here 2.5 s and a $3.8 \cdot 10^{-2}$ T external magnetic field is needed.
The fusion power density is $1.68 \cdot 10^{5}$ W/m^{3} and $0.78 \cdot 10^{4}$ W/m^{-3} are needed to replace the fuel burned. So an intrinsic gain of 21.4 is obtained. The power density required to replace all the short-range scattered particles is $7 \cdot 10^{5}$ W/m^{-3}, then in order to get the breakeven at least 76% of these particles must be confined within the beam. The radiated power density is about 10^{4} W/m^{3} (over-estimated).

CONCLUSIONS

A colliding beam fusion concept was introduced and some fundamental aspect of a possible experimental device configuration were discussed.
The proposed approach is suitable for the useof neutron-free fusion reactions. Besides further theoretical and simulation investigation, also an experimental activity for a basic, low-cost feasibility test on the neutralized beam concept seems worthwhile to be considered.

REFERENCES

[1] P.G. Avanzini, "A Colliding Beam, Advanced Fuel, Fusion Process", Proc. IV Int. Conf. on Emerging Nucl. Energy Systems, ICENES 86, Madrid (Spain), July 1986

[2] P.G. Avanzini, F. Rosatelli, A. Tarditi, "Neutralized Beams in Fusion as Alternative to Plasmas" Proc. 14th Eur. Conf. on Contr. Fusion and Plasma Phys., Madrid (Spain), June 1987

[3] P.G. Avanzini, F. Rosatelli, and A. Tarditi, "Neutralized Beams in Fusion as Alternative to Plasmas", Proc. II Eur. Fus. Theory Meeting, Varenna (Italy), December 1987

[4] P.G. Avanzini and A. Tarditi, "Beam Collider for Neutron-Free Fusion Power Generation", Proc. II Int. Symp. on Feasibility of Aneutronic Power, Washington, DC (USA), April 1989

[5] T.J. Dolan, "Fusion Research", Pergamon Press, New York 1980

[6] P.G. Avanzini and A. Tarditi, "Progress towards a Neutralized Beam Experiment for a Colliding Beam, Advanced Fuel, Fusion Process", submitted to this conference

[7] W. Kernbichler, IAEA-CN-44-/I-I-6, p. 429

[8] K. Miyamoto, "Plasma Physics for Nuclear Fusion", MIT Press, Cambridge Mass., 1980.

[9] W.I. Linlor, U.S. Pat. 4,246,067 (1981)

[10] B. Lenhert, "The EXTRAP Device" Nucl. Instr. Meth. 207, p. 223 (1983)

MULTI-TURN ELECTRON-ION INJECTION STUDY FOR NEUTRALIZED HIGH-DENSITY BEAM SUSTAINING IN A CLOSED CONFIGURATION

A. Tarditi

Electrical Engineering and Computer Sciences - Electronic Research Laboratory
University of California at Berkeley - Berkeley, CA 94720 (USA)

ABSTRACT

The problem of creating a high-density, high-current neutralized beam in a closed configuration via a continuous particle injection and accumulation has been considered in relation to the research on a colliding beam fusion process.
The last results, oriented to the development of a basic neutralized beam experiment, are discussed.
The theory of resistive wall injection of a charged particle ring is reviewed and the application to the simultaneous injection of electron and ion rings is introduced.

INTRODUCTION

A colliding-beam based fusion process has been proposed and studied [1-4]; one of the major issues for demonstrating its feasibility is to provide a technique for an efficient beam injection in a space-charge neutralized environment: low-density, 100's keV-range, electron and ion beams have to be injected and trapped in a closed geometry.
In order to provide the same equilibrium orbit for both the electron and ions, a special weak-focusing confinement system has been conceived [3].
By maintaining space-charge neutrality and through a continuous injection, a very fast increase in the circulating beam density should be achieved, leading to the formation of a high-density neutralized beam.
The injection process has to be effective from the early stage of the beam formation (low-density) to the final, high-density regime equilibrium in order to provide the necessary compensation for the particles lost (and "burned" if a fusion process were implemented).
In order to accomplish these requirements a "multi-turn", non-Liouvillian injection technique based on the axial motion damping of electron and ion rings through image currents induced in a resistive cylindrical shell has been envisaged. This technique was proposed and experimentally tested in the past for ion and electron rings separately (e.g. [5-8]). The present proposal is intended to take advantage of this previous experience in a new experimental environment.

DESCRIPTION OF THE PROCESS

A focusing-confinement system for holding electron and ion beams on the same stable orbit has been conceived [3]. Then low-density (compared to a fusion plasma density), counterstreaming, electron and ion beams are injected in a ring configuration.
Each beam is provided with a small axial velocity in order to miss the injector at the first turn. The ring motion generates image currents in a surrounding resistive cylindrical shell which provides the required damping (only in the axial direction, [6]).
The final condition is the merging of the two rings on the same equilibrium orbit resulting in the formation of a neutralized beam.

THE INJECTION PROBLEM

THE BASIC THEORY FOR THE INJECTION

The fundamentals of theory of the resistive injection are discussed in [5] and [6] for the case of a relativistic electron ring. There the solution of the e.m. problem and the self-consistent solution of field and motion equation for the particle ring are presented. Those results are here briefly reported.
The following simplifying assumptions are made in order to solve the problem analitically: *i*) the resistance of the cylindrical wall can be approximated by the surface resistivity ρ, *ii*) the velocity along 'z' is considered non-relativistic so that the contribution of image charges to the retarding force is negligible, *iii*) the current ring is considered infinitely thin.
In order to design properly the injection system the equation of motion for the particles moving along "z" (the axial direction of the cylindrical shell) must be solved with respect to the beam (particle ring) parameters.
In [6] the image current density j(z,t) on

ICENES

the shell is determined in terms of the total ring current I_R by taking into account self-consistently the motion of the current ring along "z".
Due to simmetry reasons the only non-vanishing components of the electromagnetic field are B_r, $E\phi$, B_z.

THE RETARDING FORCE ON THE PARTICLE RING

The force on each electron due to the B_r component produced by the image current on the resistive shell is:

$$F_M = -e\, v_\phi\, B_r$$

In the case the cylinder resistance can be approximated by the surface resistance the force depends only by this last quantity, (i.e. the product of the conductivity σ and the thickness "d", or $\sigma \cdot d = d/\rho$).
It can be demonstrated that, within the hypothesis made, the image charge gives a negligible contribution to the total force on the injected ring so F_M is the only force component that will be considered [6].
According to [5], for the case of a thin cylinder with and ring motion close to the wall the following expression for F_M can be derived (written here in MKSA units):

$$F_M = -\frac{c^2 m_e\, r_0\, N_e}{2\pi R a} \frac{2c\rho/377 v_z \gamma_z}{1 + (2c\rho/377 v_z \gamma_z)^2}$$

where m_e is the electron mass, ro the classical electron radius, N_e the number of electrons in the ring, R the ring radius, "a" the distance of this last from the resistive shell and $377=(\mu/\varepsilon)^{1/2}$ is expressed in Ohm.

THE EQUATION OF MOTION FOR THE INJECTED RING

The equation of motion along "z" for one electron (belonging to the particle ring producing the image current on the shell) writes as:

$$\gamma\, m_e\, \dot{v}_z = F_M$$

where $\gamma \cong [1-(v\phi/c)^2]^{-1/2}$ in the hypothesis that $v_z \ll v\phi$.
Furthermore if electric acceleration in the z-direction is assumed, then the transverse momentum is a constant of motion and it follows:

$$v_\phi = v_\phi^0\, \gamma_z \,,\quad v_\phi^0 = v_\phi(t=0),\quad \gamma_z = (1-v_z^2/c^2)^{-1/2}$$

Assuming $\gamma_z = 1$ it comes

$$\gamma = [1-(v_\phi^0/c)^2]^{-1/2} \,.$$

By substituting the expression of F_M it comes:

$$\dot{v}_z = -\frac{N_e r_0 c^2}{\gamma\, 2\pi R a} \frac{377 v_z/2\rho c}{1 + (377 v_z/2c\rho)^2}$$

This equation integrated by variable separation yields:

$$\ln(v_z/v_{z0}) + \left(\frac{377}{2c\rho}\right)^2 \frac{(v_z^2 - v_{z0}^2)}{2} = -\frac{377 r_0 N_e c}{\gamma\, 4\pi\, \rho\, Ra}\, t$$

This last equation gives (implicitely) the trend vs. time of the z-velocity of the particle ring with respect the injection parameters.

THE STOPPING LENGHT

An important design quantity is the "stopping lenght" required to bring the axial ring velocity to zero (reaching then the equilibrium position).
By dividing the eq. of motion by $v_z = dz_R/dt$ it is obtained:

$$\frac{dv_z}{dz_R} = -\frac{377 r_0 N_e c}{\gamma 4\pi\, \rho\, R\, a} \frac{1}{1 + (377 v_z/2c\rho)^2}$$

Integrating by variable separation and imposing $v_z = 0$ the stopping lenght $L_{st} = z_R - z_{R0}$ is found as

$$v_{z0} + (377/2\rho c)^2 \frac{v_{z0}^3}{3} = \frac{377 r_0 N_e c}{\gamma 4\pi\, \rho\, R\, a} L_{st}$$

or

$$L_{st} = \frac{2\pi\, Ra\, \gamma}{r_0 N_e} \left(\frac{\rho}{188.5} \frac{v_{z0}}{c} + \frac{188.5}{\rho} \frac{v_{z0}^3}{3c^3} \right)$$

(see eq. (38) [5] or eq. (21) in [6]). Then:

$$r_0 N_e = \frac{e^2}{4\pi\varepsilon_0^2 m_e c^2} \frac{2\pi R I_R}{e\, v_\phi} = \frac{e R I_R}{2\, \varepsilon_0^2 m_e c^2 v_\phi}$$

In the more general case of $v\phi \cong c$ the expression of L_{st} has to be divided by $v\phi/c$.
Then, finally, by considering that the ring current is given by:

$$I_R = \frac{e N_e v_\phi}{2\pi R} \Longrightarrow N_e = \frac{2\pi R I_R}{e\, v_\phi}$$

while the classical electron radius is

$$r_0 = \frac{e^2}{4\pi\varepsilon_0^2 m_e c^2}$$

it is obtained

$$L_{st} = \frac{4\pi a \gamma \varepsilon_0^2 m_e c^2 v_\phi}{e\, I_R} \left(\frac{\rho}{188.5} \frac{v_{z0}}{c} + \frac{188.5}{\rho} \frac{v_{z0}^3}{3c^3} \right)$$

It is important to notice that the dynamic of the particle due to the retarding force does not depend on its mass, so the stopping lenght for both ions and electrons which are in the same current ring are the same. The quantity m_e in the equation of L_{st} comes,

throught expression of the magnetic field produced by the ring current, from having imposed that the electrons are confined with a given Larmor radius.

THE EXTERNAL CONFINEMENT FIELD

ELECTRONS AND IONS WITH THE SAME LARMOR RADIUS

A vertical magnetic field (with respect the orbit plane) keeps the ions onto a circular orbit. A weak-focusing field profile gives them the required stability.
When two ion species are considered, if they are of different masses (like in all the most efficient advanced-fuel fusion reactions as well as the D-T one) it is possible to choose the velocities of the two species in order to both maximize the fusion cross section and making equal their Larmor radii.
However the electrons will have in general a much smaller Larmor radius then the ions. The only way to keep them rotating on the same, "reasonable" size ion orbit (i.e. in the order of the meter) is to use relativistic electrons.
By imposing the equality of the ion and electron Larmor radii it comes

$$\frac{r_{Le}}{r_{Li}} = \frac{m_e v_e}{m_i v_i} Z=1$$

where

$$m = \gamma m_{e0} = \frac{m_{e0}}{(1-v_e^2/c^2)^{1/2}}$$

so it comes

$$v_e^2 = \frac{c^2 m_i^2 v_i^2}{(m_i^2 v_i^2 + c^2 m_{e0}^2 Z^2)} = \frac{c^2}{1 + \frac{m_{e0}^2 Z^2 c^2}{m_i^2 v_i^2}}$$

The corresponding electron kinetic energy will be then

$$W_e = (\gamma-1) m_{e0} c^2$$

For the fusion process which it is referred to [1-4] using relativistic electrons with a few MeV energy would be unacceptable from the overall power gain (since electrons have to be supplied as well as ions to compensate the particle losses).

THE "CORRECTED LARMOR RADIUS" CONFIGURATION

In order to maintain electrons and ions on the same orbit without being forced to use relativistic electrons a special focusing system was conceived [3].
A vertical magnetic field B produces a deflecting inwards radial force, as usual. The electron Larmor radius is however much smaller than the ion one (more than one order of magnitude with the parameters here considered) and the neutralized beam could not form since the injection phase.
A radial electric field is then introduced (fig. 1). The additional radial force contribution acts in opposite ways for ions and electrons. Therefore by choosing proper values for E and B, the same equilibrium orbit for both ions and electrons can be imposed.
In the most general case, considering two species of charged particles with given charge $q_{e,i}$, mass $m_{e,i}$ and velocity $v_{e,i}$, the force balance equations for equilibrium orbits with radius $R_{e,i}$ are:

$$m_e v_e^2/R_e = q_e v_e B + q_e E$$

$$m_i v_i^2/R_i = q_i v_i B + q_i E$$

then

$$R_e = m_e v_e^2 / q_e (E+v_e B)$$

$$R_i = m_i v_i^2 / q_i (E+v_i B)$$

By imposing $R=R_e=R_i$ and solving for E and B it is found

$$B = \frac{m_e v_e^2 q_i - m_i v_i^2 q_e}{(v_i - v_e) q_e q_i R}$$

$$E = v_i v_e \frac{m_i v_i q_e - m_e v_e q_i}{(v_i - v_e) q_i q_e R}$$

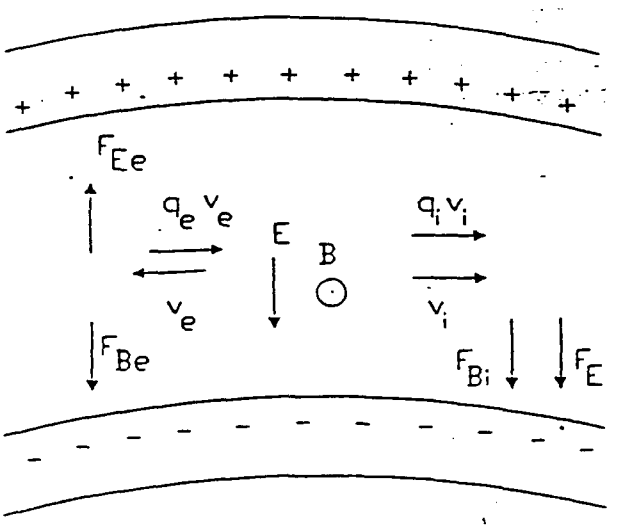

Fig. 1 - External confinement fields

For example, if one assumes (all MKSA units) $v_e = -10^8$, $v_i = 10^6$, R=0.05 for electrons and

protons respectively, it comes $E \cong 2 \cdot 10^5$ and the $B \cong 1.3 \cdot 10^{-2}$

It must be pointed out that the configuration of E and B here considered do not produce any $\underline{E} \times \underline{B}$ drift velocity on the particles because $\underline{E}$ remains always perpendicular to the particle trajectory. Another way to say this is observing that the particle guiding center will remain always fixed, at the centre of the ring.

WEAK FOCUSING WITH RADIAL ELECTRIC FIELD

The stability properties of the weak-focusing magnetic field profile remain unchanged with the added electric component. A charged particle (mass m, charge q) with velocity v perpendicular to a uniform magnetic field Bo will find an equilibrium orbit with radius Ro such that

$$qvB_0 + mv^2/R_0 = 0$$

The frame of reference in fig. 1 is considered: the equilibrium orbit is at r=Ro, centered at r=0, the magnetic field has the direction of the z-axis.

To achieve vertical focusing, for particle displacements in the "z" direction, the magnetic field must decrease with r, that is $\partial B/\partial r < 0$, like what is produced by two outwards diverging poles (fig. 2).

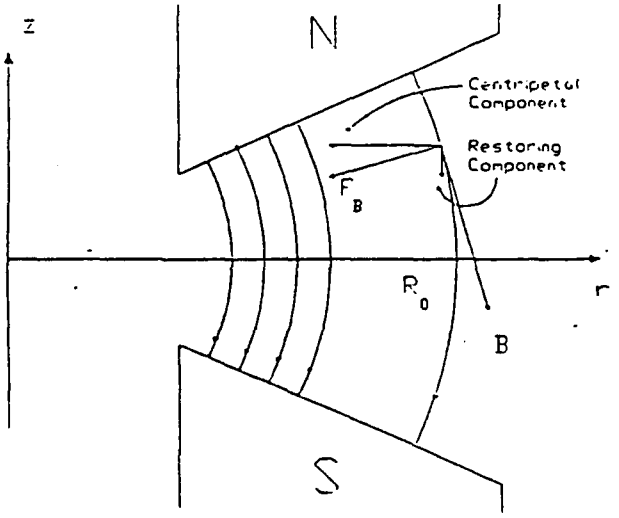

Fig. 2 - Magnetic weak focusing

To ensure at the same time the horizontal stability one must impose that the centrifugal force decreases with r faster than the magnetic one: then a restoring force component along r will be obtained. This condition is expressed as

$$\left.\frac{\partial F_m}{\partial r}\right|_{r=R_0} < \left.\frac{\partial F_c}{\partial r}\right|_{r=R_0}$$

where (F_m is directed inwards)

$$F_m = -qvB \ , \ F_c = mv^2/r \ .$$

It comes then immediately:

$$-qv \left.\frac{\partial B}{\partial r}\right|_{r=R_0} < -\frac{mv^2}{R_0^2}$$

or

$$-\frac{R_0}{B_0}\left.\frac{\partial B}{\partial r}\right|_{r=R_0} < -\frac{mv}{B_0 R_0 q} \cong 1$$

By defining the left-hand side of (5) as the field index "n" and recalling the previously stated condition $\partial B/\partial r < 0$ for the vertical focusing (which is equivalent to $n>0$) it comes that the stability of the particle trajectory will be ensured if $0<n<1$, that is the well-known weak-focusing condition.

The same considerations will be now applied in the case of the corrected Larmor radius configuration.

The equilibrium equation is

$$m\, v^2/R_0 = q\, v\, B_0 + q\, E_0$$

If $\partial E/\partial z = 0$ the vertical focusing will not be affected by the presence of the electric field (the electric field is only along the radial direction).

The condition for the horizontal stability will instead become

$$\left.\frac{\partial F_e}{\partial r}\right|_{r=R_0} + \left.\frac{\partial F_m}{\partial r}\right|_{r=R_0} < \left.\frac{\partial F_c}{\partial r}\right|_{r=R_0}$$

being $F_e = -qE$ the electric force (F_e must be directed outwards for the electrons and inwards for the ions).

Since it is considered a radial electric field produced by two coaxial cylindrical electrodes, then $E(r) \propto 1/r$ which can also be written as $E(r) = E_0 R_0 / r$, where $E_0 = E(R_0)$. So $\partial F_e/\partial r = qE_0R_0/r^2$ and the last equation becomes

$$\frac{qE_0}{R_0} - qv \left.\frac{\partial B}{\partial r}\right|_{r=R_0} < -\frac{mv^2}{R_0^2}$$

or

$$\frac{E_0}{B_0 v} - \frac{R_0}{B_0}\left.\frac{\partial B}{\partial r}\right|_{r=R_0} < -\frac{mv}{B_0 R_0 q}$$

Rewriting this equation in terms of the field index "n" the condition for the weak-focusing will be now

$$0 < n < -\frac{E_0}{B_0 v} - \frac{mv}{B_0 R_0 q}$$

BASIC DESIGN EXAMPLE

A calculation example is reported for giving an estimate of the injection parameters.
Electrons at 300 keV and protons at 100 keV are considered. Their velocities result respectively v_e=2.3e+08 and v_i=4.3·10^6 m/s.
For 100 keV protons electrons at 13 MeV are required for having the same Larmor radius. while for protons at 10 KeV electrons at 3 MeV are needed.
Using low energy protons could be a way for implementing a neutralized beam, low-cost, basic experiment to check the main issues of the proposed approach (injection, density increase, pinch effect).
For a electron beam injected at 2·10^8 m/s, density 5·10^{13} m^{-3}, minor radius 5 mm (then beam current 0.12 A) major radius 0.2 m, distance from the wall 0.01 m, wall surface resistance 20 Ω and axial ("z") velocity of 10^7 m/s, a stopping lenght of 6 cm is found.
With a ring radius of 0.5 m and distance from the wall 5 cm, a stopping lenght of 0.33 m is obtained.

CONCLUSIONS

A technique for continuous injection of electron and ion beams and their confinement on the same stable orbit in order to form a neutralized beam was proposed.
An experimental background experience which comes from previous experiments on electron and ion beams separately can be usefully applied.
The proposed approach seems suitable for a low-cost basic experiment.

REFERENCES

[1] P.G. Avanzini, "A Colliding Beam, Advanced Fuel, Fusion Process", Proc. IV Int. Conf. on Emerging Nucl. Energy Systems, ICENES 86, Madrid (Spain), July 1986

[2] P.G. Avanzini, F. Rosatelli, A. Tarditi, "Neutralized Beams in Fusion as Alternative to Plasmas" Proc. 14th Eur. Conf. on Contr. Fusion and Plasma Phys., Madrid (Spain), June 1987

[3] P.G. Avanzini and A. Tarditi, "Beam Collider for Neutron-Free Fusion Power Generation",Proc. II Int. Symp. on Feasibility of Aneutronic Power, Washington, DC (USA), April 1989

[4] P.G. Avanzini and A. Tarditi, "Progress towards a Neutralized Beam Experiment for a Colliding Beam, Advanced Fuel, Fusion Process", submitted to this conference

[5] P. Merkel, "Ohmic Losses of a Relativistic Electron Ring Moving along a Conducting Cylinder", Part. Accel., 7, 69 (1976)

[6] P. Merkel, "Stopping of a Relativistic Electron Ring by Image Currents in a Resistive Cylinder", Part. Accel., 8, 21 (1977)

[7] J.G. Kalnins, H.Kim, J.G. Linhart, "Stopping of an Electron Ring by Induced Image Currents in Resistive Wire Loops", IEEE-NS 20, 324 (1973)

[8] R.N. Sudan, P.M. Lyster, "Merging Ion Rings in Resistive Plasmas", Comm. Plasma Phys. Contr. Fus., 9, 23 (1984)

PARTICLE SIMULATION OF NEUTRALIZED ION BERNSTEIN WAVES

A. Tarditi

Electrical Engineering and Computer Sciences - Electronics Research Laboratory
Cory Hall - University of California at Berkeley - Berkeley, CA 94720 (USA)

ABSTRACT

The Neutralized Ion Bernstein Wave (NIBW) simulation via an electrostatic, two-dimensional hybrid particle-fluid model is approached.
Simulations are compared and confirmed by already published experimental results.

INTRODUCTION

Particle simulation of waves in plasmas, due to the intrinsic microscopic character of the model, is better concerned with the physics of the particle-wave interactions rather than with the representation of the whole wave pattern spatial evolution. This is particularly true when explicit particle models are used, since in the space discretization the grid cell size cannot be much larger than the electron Debye length.
The particle-fluid approach was developed in order to study plasma phenomena which are mainly affected by the ion dynamics [1]. The high-frequency plasma oscillations (due to the electrons) are dropped, the time step size is then determined from the ion motion time scale and no more from the electron one. Furthermore the spatial resolution is now linked to the ion Debye length in place of the electron one. This makes affordable problems which otherwise would require many thousands of time steps and grid cells per linear dimension.
Here ions are simulated as in a conventional particle model while no computer particles are used for electrons; they are considered like a "fluid" which maintains everywhere the plasma quasi-neutrality and their effect is considered only in the field solution procedure.

THE HYBRID PARTICLE-FLUID CODE ES2HYB

A 2D, ES quasi-neutral, hybrid (particle ions, fluid electrons) model is implemented in the code ES2HYB.
An uniformly magnetized plasma is simulated. The magnetic field is along the normal direction (z) with respect to the (x-y) simulation plane.
The Green's function technique is used (via FFT convolution) for a direct solution of the 2-D electrostatic field.
The field solver provides the electrostatic self-consistent field produced by the particles. The problem is usually afforded by solving the Poisson equation (directly, via inversion of the corresponding set of finite difference equations, or through a convolutional method by Fourier transform of the finite difference operators, see [2]) and then by numerical differencing the potential in order to obtain the electric field components.
Here a Green's function-based field solver has been developed for the quasi-neutral hybrid particle-fluid model and no direct reference to the Poisson equation is made in the numerical solution (the potential numerical gradient is also avoided).
The electric field due to a unitary 2D charge in the origin is considered as the Green's function (x and y components). Once the charge density distribution is collected from the particle positions the total field is found after the convolution between the Green's function and the charge density itself. The convolution is quickly performed by means of a 2D-FFT.
According to [1] the model assumes a Boltzmann equilibrium for the electrons with small density fluctuations (a few percent) in order to allow the linearization of the Boltzmann distribution.
The field solution proceeds as follows: first the modified Poisson equation, which takes into account the electron linearized Boltzmann distribution, is solved analytically in two dimensions for a unitary source in the origin. This gives the Green's function for the electrostatic, Debye-shielded potential due to the ions. Then the Green's functions for the electric field x-y components are found by analytical differencing.
The Boltzmann distribution for the electron density n_e expanded at the first order writes as:

$$n_e = n_o \exp(eV/k_B T_e) \cong n_o (1 + eV/k_B T_e)$$

where n_o is the equilibrium electron density.
By considering a small perturbation of the ion density as $n_i = n_o/Z_i + \delta n_i$ the Poisson equation becomes

$$\nabla^2 V + k_D^2 V = -e Z_i \delta n_i / \varepsilon_o$$

where $$k_D^2 = n_o e^2 / k_B T_e \varepsilon_o = 1/\lambda_D^2$$

being λ_D the electron Debye length.
Writing the corresponding homogeneous equation for the Green's function in cylindrical coordinates and supposing the circular symmetry it is found:

$$\frac{d^2}{dr^2} G_V + \frac{1}{r} \frac{d}{dr} G_V + k_D^2 G_V = 0$$

which is a zero-order Bessel equation. It can be shown [3] that the Green's function for this equation, in the case of an isolated source which is considered, is

$$G_V(r) = Y_o(k_D r)/2\pi$$

where Yo is the zero-th order Neumann function (or Bessel function of the second kind) in the argument "kDr".
In order to find the Green's functions for the electric field components it is observed that, since $\underline{E} = -\nabla V$, it comes

$$G_{Ex} = -\frac{\partial}{\partial x} G_V = -\frac{1}{2\pi} \frac{\partial}{\partial x} Y_o(k_D r)$$

Then it can be easily found that [3]:

$$G_{Ex} = \frac{1}{2\pi\lambda_D} Y_1(\xi) \frac{x}{r} \qquad G_{Ey} = \frac{1}{2\pi\lambda_D} Y_1(\xi) \, y/r$$

where Y_1 is the first order Neumann function.
The FFT convolution method used for the field calculation assumes the periodicity of the system which the density and field arrays are referring to. The code is then intrinsically periodic: the particles passing over the domain border from one side have to be made appearing on the other side with the same velocity.

THE SIMULATION RESULTS

It is essential to define a quantitative correspondence between the simulation model and the real plasma parameters. The computer particles can be chosen with the same charge-to-mass ratio as real particles, however, typically, the values of both charge and mass are many orders of magnitude above the

PISA

real ones.
The definition of the model parameters is a critical issue for the reliability of the simulation. A simple algorithmic procedure which finds the input data from the real plasma specifications has been used [3].

Since the external magnetic field is perpendicular to the x-y simulation plane ion plasma waves propagate as Ion Bernstein modes. Moreover due to the intrinsic quasi-neutrality of the model considered, only the Neutralized IBW occurs. In the case of NIBW in fact the electrons are able to perform a sort of neutralization reaching a Boltzmann equilibrium with the wave potential [4], [5].
The propagation of NIBW modes can be seen in a narrow angular region very close to 90° w.r.t. the magnetic axis. A 2D-3V (i.e. two-and-half dimensional) model would be appropriate for exploring the angular dependence of the mode propagation.
The first results on the NIBW simulation were shown in [3]. Here further calculation on the simulation of a real experiment are reported.
Experimental measurements on NIBW were recently obtained in the LMP (Linear Magnetized Plasma) device of CRPP-EPF in Lausanne [6]. The simulated (Argon) plasma, as in the experiment, has a density of 10^{17} m^{-3}. T_e=14 eV, T_i=0.1 eV, with an external magnetic field of 0.3 T.

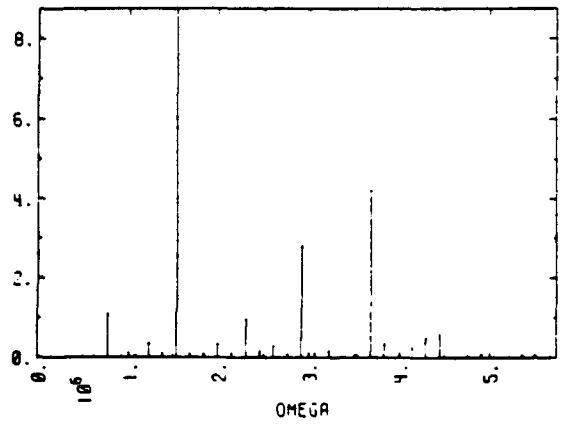

Fig. 1 - The electric field spectrum for the mode 3

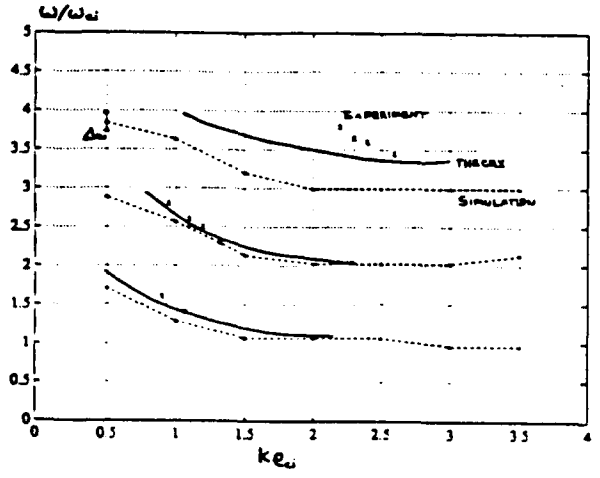

Fig. 2 - The NIBW dispersion relation: simulation is compared with theory and experiments.

These physical conditions give $\omega_{pi}/\omega_{ci} \cong 90$. Then, in order to obtain a sufficient frequency resolution the simulation has to be extended over many $1/\omega_{ci}$ but at the same time a time step $\Delta t < 1/\omega_{pi}$ ($\rightarrow \Delta t << 1/\omega_{ci}$) has to be used, as the usual requirement of explicit particle codes. Then a considerable number of time steps was needed (2048).

The former simulation results showed in [3] are here improved by increasing the number of particles and the spatial grid resolution.
The code was run on the CRAY-2 with 128×128 grid points and 65536 ($=256^2$) particles.
In fig. 1 an example for the electric field spectrum (for the 3rd mode) is shown. Up to eight modes were recorded with $k=m/2\rho_{ci}$, $m=1,2...8$.
The dispersion relation is obtained as in fig. 2. The experimental results and theoretical curves (both from [6]) are reported on the same plot for comparison. The frequency resolution was $\Delta\omega \cong \omega_{ci}/4.5$, 2048 time steps with $\Delta t = 2 \cdot 10^{-8}$ having been used. A very good agreement is found for the first two branches. The differences in the third one are attributed to the still not sufficiently large scale of the simulation considered so far.
A maxwellian plasma was initialized through a "quiet start" technique and a good stability of the thermal equilibrium was obtained as showed by the final distribution function in fig. 3 (after about 400 plasma periods).

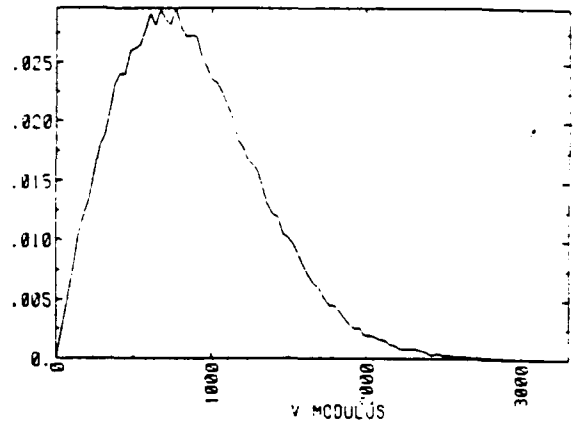

Fig. 3 - Ion distribution at the end of run

CONCLUSIONS

A 2D, ES quasi-neutral ,hybrid particle-fluid code, was applied to the simulation of NIBW.
The hybrid code exploits a new, rather sophisticated, field solver for a linearized, quasi-neutral, plasma model. The extension to the non-linear case could be made straightforwardly by successive field solving iterations within each time step. Work in this direction is in progress.
Techniques for defining correlations between the particle model and the real plasma were exploited.
The character of the simulation results is still that of an approach phase. Anyhow it is believed that a contribute to the improvement of the particle simulation method reliability and to the progress towards a closer link with plasma experiments has been given.

ACKNOWLEDGEMENTS

A particular acknowledgement is due to Dr. P.J. Paris of the CRPP of the Ecole Polytechnique Federale de Lausanne (CH) for a valuable discussion regarding the analysis of some of the first simulation results.

REFERENCES

[1] Ukuda H., Dawson J.M., Lin A.T. and Lin C.C., Phys. Fluids, 21, 476 (1978)
[2] Birdsall C.K., Langdon A.B., "Plasma Physics Via Computer Simulation", Mc Graw-Hill, New York (1985)
[3] Iarditi A. Ph.D. Thesis, University of Genoa (Italy), 1989-90
[4] Schmitt J.P.M., Phys. Rev. Lett., 31,982 (1973)
[5] Allen J.E., Phelps D.R., Rew. Mod. Phys. 40, 1968
[6] Anderegg F., LPP 375/89, Ecole Polytechnique Federale de Lausanne, 1988

NUMERICAL METHODS FOR SIMULATING PROCESSING PLASMAS

V. Vahedi, M. Surendra,
G. DiPeso, J. Verboncoeur
University of California, Berkeley
Berkeley, CA 94720

RF glow discharges and other processing plasmas are used extensively in the microelectronics industry. Self-consistent fluid equations have been used recently to study the structural features of RF and DC glows[1-3]. However, since these discharges are inherently complex and the particle distributions are non-Maxwellian, there has been a considerable effort in developing self-consistent kinetic models without making any assumptions on the distribution functions[4-8].

In order to use particle-in-cell simulation codes for modeling collisional plasmas and self-sustained discharges it is necessary to include interactions between charged and neutral particles. Monte Carlo methods have been used extensively in swarm simulations[9-14]. In many Monte Carlo schemes, the time (or distance) between collisions for each particle is calculated from a random number. This allows for efficient algorithms, especially when the null collision method is used[15]. This technique is however, not compatible with PIC simulations, since all particle trajectories are integrated simultaneously in time. Thus, the collision probability for the ith charged particle is calculated, based on the distance $\Delta s_i = v_i \Delta t$ traveled *in each time step* Δt, to be

$$P_i = 1 - \exp(-\Delta s_i \sigma_T(E_i) n)$$

where σ_T is the total collision cross section, E_i is the kinetic energy of the particles and n is the neutral density. A collision takes place if a uniformly distributed random number on the interval [0, 1] is less than P_i. The null collision method can be incorporated into the collision model by picking a constant collision frequency ν' such that,[11]

$$\nu' \geq n v \sigma_T$$

Thus, the computational cost of calculating P_i can be avoided. The fraction of the total number of particles (chosen at random) in the simulation that experience collisions is given by

$$P = 1 - \exp(-\nu' \Delta t)$$

The collision is assumed to take place at the current position of the particle. It should be noted that the choice of Δt will affect the accuracy of the collision model. For instance, Δs_i should not be much larger than simulation length scales of interest (e.g. grid spacing, λ_{De}) and $\Delta s_i \sigma_T(E_i) n$ should be about 0.1 or less[17]. Once a collision occurs, the type of collision, the energy of the ejected electron (for an ionizing collision) and the direction(s) are determined with new random

Num, Sim, Gen

numbers. These quantities are related back to the system coordinate axes. The procedure for electron-neutral collisions is describe in detail by Boeuf and Marode[10], and by Thompson *et al*[14] for ion-neutral collisions. Expressions for differential cross sections that are analytically integrable are useful as the computational cost of determining scattering angles and energy redistribution in ionizing collisions is minimized[4, 10, 16, 17].

A Monte Carlo collision handler as described above, including the null collision method, has been developed as an addition to the PIC scheme as shown in Fig. 1. The full three dimensional character of a collision is modeled with three velocity components. The neutrals are assumed to be uniformly distributed between the boundaries with a constant density and a Maxwellian profile. The model is still valid if the neutral density is a weak function of position and time (small variations across the mean free path and collision times). This scheme can also be extended to model Coulomb collisions between charged particles.

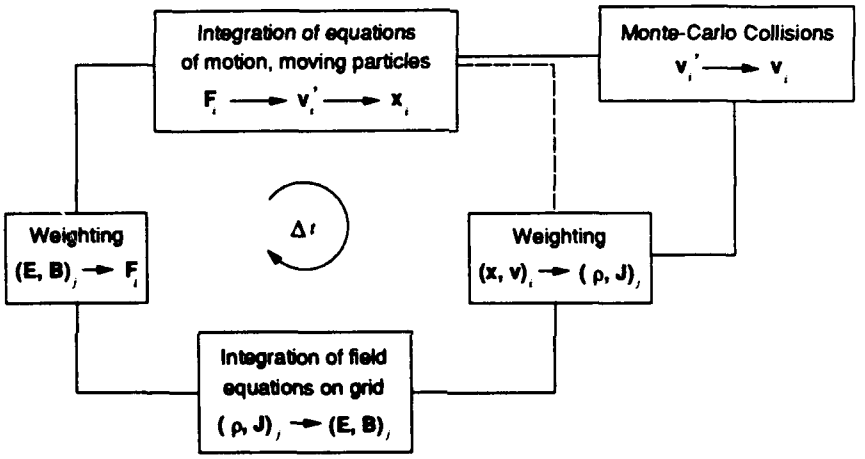

FIG. 1. The flow chart for an explicit PIC scheme with the addition of the collision handler, called PIC-MCC[4].

RF discharge modeling displays many physical time scales, e.g. $\omega_{RF} \ll \omega_{pe}$. With a PIC model including an electrostatic response, the highest frequency that must be resolved by the explicit numerical methods used to solve the particle and field equations is ω_{pe}. If $\omega_{pe}\Delta t > 1$, numerical instabilities can occur for explicit methods[18]. To observe the physics of interest, one needs to resolve th RF timescale only, and therefore much computing time is wasted resolving the plasma oscillation time scale.

Implicit particle simulation[19] has been developed to relax the numerical stability constraint. We will now briefly review implicit particle simulation techniques. Implicit particle movers advance the postion of the *i*th super particle by the equation

$$x_i^{n+1} = \alpha' E^{n+1}(x_i^{n+1}) + \bar{x}_i^{n+1}$$

where $\bar{x}$ is the portion of the position advanced, dependent on quantities known at present and previous time levels, $\alpha' = \beta \Delta t^2 q/m$, and β depends on the particular implicit scheme. The field at a particle location is interpolated from the field known at the grid in space. Note that the particle location at the future n+1 time step depends on the field at that time step, but the field at the future time step depends on the particle location at that time step through the Poisson equation.

One way to get around this problem is to linearize the locations x_i^{n+1} about the locations $\bar{x}_i^{n+1}$ in the superparticle-to-grid weighting equations. Then

$$\rho^{n+1} = \tilde{\rho}^{n+1} - \partial_x[\tilde{\rho}^{n+1}\delta x^{n+1}]$$

where $\tilde{\rho}^{n+1}$ is determined by weighting superparticles at $\bar{x}_i^{n+1}$ to the grid. The minus sign is from the functional dependence of the particle positions in the superparticle-to-grid weighting equations. Strictly speaking, $\delta x_i^{n+1} = x_i^{n+1} - \bar{x}_i^{n+1}$ is an individual quantity for each superparticle and is given by the advancing equation. Instead, $\delta x_i^{n+1} \approx \delta x^{n+1} \approx \alpha' E^{n+1}$, i.e., the perturbations are taken to be grid quantities while maintaining the form as given by the advancing equation. Inserting the above form of the perturbation into the equations for the density and combining with the Poisson equation gives the numerically implicit Poisson equation

$$\partial_x[1 + \alpha\tilde{\rho}^{n+1}]\partial_x\phi^{n+1} = -\tilde{\rho}^{n+1}/\varepsilon_0$$

where $\alpha = \alpha'/\varepsilon_0$.

The equation is solved on a spatial grid. Simple boundary conditions for the RF discharge are a zero potential at the left wall and an RF source voltage at the right wall. The electric field is found at the interior points by central differencing the potential. The electric field at the walls is given by a numerically implicit Gauss' law which is the integral form of the numerically implicit Poisson equation. The electric field, at the left wall for example, is then derived by taking a Gaussian pill box about the wall,

$$[(1 - \alpha\tilde{\rho})E]_{j=1/2} = \sigma_0/\varepsilon_0 + \tilde{\rho}_0 \Delta x/2\varepsilon_0$$

The enclosed charge (RHS) includes the wall surface charge density $\sigma_0 = \varepsilon_0 E_0$ where the 0 subscript indicates the left wall quantity and j=1/2 indicates an evaluation between the 0 and 1 grid points. It is then possible to solve for the electric field on the left wall. A similar proceedure is used for the right wall. The equations may be generalized to included more complicated boundary conditions including external circuit elements.

Many accuracy constraints still remain. One important constraint is that the fastest particle species should resolve spatial gradients in the field, i.e., $v_{max}\Delta t/s < 1$ where s is the gradient length. Another important constraint is that all particles should sample the field on the grid in a continuous manner over a single time step. This gives $v_{max}\Delta t/\Delta x < 1$. A problem with implicit methods is excessive numerical cooling which is due to poor sampling of fast particles in simulations with large time steps. Resolving fast particles is particularly important in RF discharges because it is

the fast electrons which maintain the discharge through ionization collisions with the neutrals. A possible way out of this problem is to do multi-scale[20] simulations. That is, the few fast electrons that maintain the discharge may be pushed with a small time step while the remaining slow particles, essentially residing in the bulk plasma, may be pushed with a large implicit time step.

ACKNOWLEDGEMENT

This work is supported in part by DOE Contract DE-FG03-90ER54079 and ONR Contract N00014-85-K-0809, and the San Diego Supercomputer Center.

REFERENCES

[1] D. B. Graves and K. F. Jensen, *IEEE Trans. Plasma Sci.* **PS-14**, 78 (1986).

[2] J. P. Boeuf, *Phys. Rev. A* **36**, 2782 (1987).

[3] E. Gogolides, J. P. Nicolai, and H. H. Sawin, *J. Vac. Sci. Technol. A* **7**, 1001 (1989).

[4] Birdsall C. K., *IEEE Trans. Plasma Sci.* **19**, 65 (1991).

[5] Surendra M., and D. B. Graves, *IEEE Trans. Plasma Sci.* **19**, 144 (1991a).

[6] V. Vahedi, M. A. Lieberman, M. V. Alves, J. P. Verboncoeur, and C. K. Birdsall, *J. Appl. Phys.* **69**, 2008 (1991).

[7] Vender D., and R. W. Boswell, *IEEE Trans. Plasma Sci.* **18**, 725 (1990).

[8] Sommerer T. J., W. N. G. Hitchen, R. E. P. Harvey, and J. E. Lawler, *Phys. Rev. A* **43**, 4452 (1991).

[9] S. R. Hunter, *Aust. J. Phys.* **30**, 83 (1977).

[10] J. P. Boeuf and E. Marode, *J. Phys. D* **15**, 2169 (1982).

[11] Y. Kaufman, *J. Phys. D* **21**, 442 (1988).

[12] M. J. Kushner, *J. Appl. Phys.* **58**, 4024 (1985).

[13] M. J. Kushner, *J. Appl. Phys.* **54**, 4958 (1983).

[14] B. E. Thompson, H. H. Sawin and D. A. Fisher, *J. Appl. Phys.* **63**, 2241 (1988).

[15] S. L. Lin and J. N. Bardsley, *J. Chem. Phys.* **66**, 435 (1977).

[16] M. Surendra, D. B. Graves, and I. J. Morey, *Appl. Phys. Lett.*, **56**, 1022 (1990).

[17] M. Surendra, D. B. Graves, and G. M. Jellum, *Phys. Rev. A* **41**, 1112 (1990).

[18] C. K. Birdsall and A. B. Langdon, *Plasma Physics via Computer Simulation* (McGraw-Hill, New York, 1985).

[19] A. B. Langdon, B. I. Cohen, A. Friedman, *J. Comp. Phys.* **51**, 107 (1983).

[20] "Multi-Scale Particle Simulation of Bounded Plasmas", S. E. Parker, A. Friedman, S. L. Ray, and C. K. Birdsall, *Proc. 13th Conf. on Numerical Simulation of Plasmas*, Santa Fe, New Mexico (1989).

XGRAFIX: AN X-WINDOWS ENVIRONMENT FOR REAL-TIME INTERACTIVE SIMULATIONS

V. Vahedi, J. P. Verboncoeur,
and C. K. Birdsall

University of California, Berkeley
Berkeley, CA 94720

We have developed a real-time user interface environment, XGRAFIX, for simulations running under X-Windows. XGRAFIX is written in C in an object oriented style, and since it uses only the lower level X-Windows function-calls, it can be compiled with any superset of X-Windows, e.g. Motif, and is compatible with many systems. XGRAFIX allows the user to display multiple diagnostics and view them as they evolve in time. Like most other X environments, XGRAFIX provides keyboard and mouse supports. The simulation codes are structured as shown in Fig. 1.

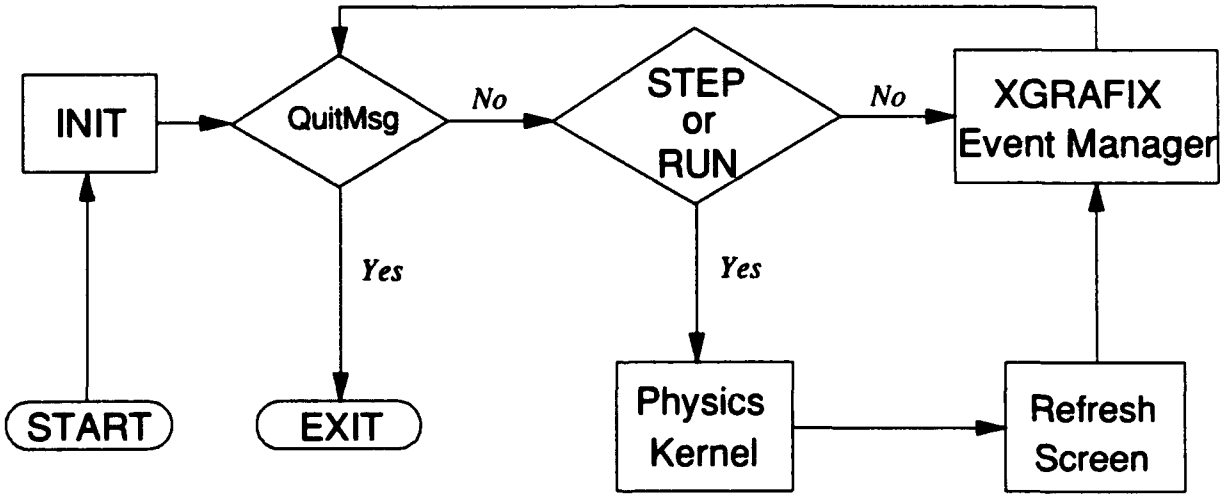

Figure 1. Schematic representation of the interaction between XGRAFIX and the physics kernel.

The physics kernel is portable to any machine supporting standard C. The INIT module scans the input file containing the physical parameters of the problem and initializes the diagnostic windows. INIT also sets up memory for array storage. The environment provides hooks for the physics kernel to run continuously (there is no time limit - the code can run indefinitely) or step through individual timesteps. The windows are refreshed each timestep, and all user requests are processed by the XGRAFIX Event Manager. When the simulation is in the running state, the

Num. Sim. Conf

Event Manager is invoked at each time step to process the events; if not running, the Event Manager is constantly invoked. The events include moving, resizing, and iconifying windows as well as mouse button clicks and keyboard inputs. XGRAFIX also supports PostScript output of the plots.

The environment currently offers three types of plots: linear, semi-log, and scattered. XGRAFIX provides the user with menus, dialogboxes, and smart windows. Each window has (currently) four standard buttons for rescaling the graph, viewing traces of plots, PostScript output, and a crosshair for measurements. The menus, dialogboxes, and the mouse make the environment especially user-friendly.

XGRAFIX is being currently rewritten in C++ which offers pre-defined classes and hierarchies used in the object-oriented style for such objects as buttons, menus, windows, etc. This modification should make it easier to handle future additions to XGRAFIX. We are also adding optimized three dimensional plotting routines to the environment which will make XGRAFIX even more useful for 2D and 3D simulations.

We are presently running three of our codes, ES1 (Electrostatic 1 Dimensional periodic plasma simulation)[1], PDP1 (Plasma Device, Planar 1 Dimensional)[2] and PDP2 (Plasma Device, Planar 2 Dimensional) in XGRAFIX.

This work will be presented at the *14th International Conference on the Numerical Simulation of Plasmas*.

---

1. C. K. Birdsall and A. B. Langdon, *Plasma Physics via Computer Simulation* (McGraw-Hill, New York, 1985; Adam Hilgar, 1991).

2. I. J. Morey, V. Vahedi and J. Verboncoeur, *Particle Simulation Code for Modeling Processing Plasmas*, Bull. APS, **34** 2028 (Abstract 1989)

A Comparison of PIC Simulation and Experimental Results in a Capacitive RF Discharge,[1] P. MIRRASHIDI, B. P. WOOD, V. VAHEDI, M. A. LIEBERMAN, and C. K. BIRDSALL, EECS Dept. University of California, Berkeley - Simulation results from PDP1, a *1d3v bounded particle-in-cell code*,[2] are compared to recently published experimental results[3] over a pressure range of 10-100 mTorr and 100-1000 V applied RF voltage in a symmetric, parallel plate, argon discharge. We show that where similar results are obtained, the simulation allows insight into plasma parameters which are not experimentally accessible, such as details of the electron power sources and losses.

---

1. Work supported in part by the ONR, DOE and NSF.
2. Available from C. K. Birdsall, Plasma Theory and Simulation Group, EECS Dept., UC Berkeley.
3. V. A. Godyak, and R. B. Piejak, and B. M. Alexandrovich, IEEE Trans. Plasma Sci., August 1991.

An Analytic Model of the Ion Angular Distribution Function in A Highly Collisional Sheath,[1] M. A. LIEBERMAN, V. VAHEDI, R. A. STEWART, University of California, Berkeley - An analytic model is developed that predicts the ion angular distribution function in a highly collisional sheath. In a previous study[2], the normal ion velocity distribution was obtained under the assumption that charge-exchange is the dominant ion-neutral collision mechanism. In the present model, we assume $\lambda_s > \lambda_{cx}$, where λ_s and λ_{cx} are the mean free paths for ion-neutral scattering and charge-exchange collisions, respectively. With this assumption, we consider the angular distribution to arise mainly from ions that strike the electrode after undergoing only one scattering collision following the last charge-exchange collision.

---

1. Work supported in part by a gift from Applied Materials, Inc. and a grant from the California Office of Competitive Technology.
2. V. Vahedi, M. A. Lieberman, M. A. Alves, J. P. Verboncoeur, and C. K. Birdsall, *J. Appl. Phys.*, 69 2008 (1991).

A Bounded Particle in Cell Code with an Atomic Physics Model for Simulating Processing Plasmas,[1] V. VAHEDI, M. A. LIEBERMAN, G. DIPESO, C. K. BIRDSALL, University of California, Berkeley, T. D. ROGNLIEN, J. R. HISKES, and R. H. COHEN, Lawrence Livermore National Laboratory- We are combining a particle-in-cell (PIC) model for particle and field dynamics with a Monte Carlo collision (MCC) scheme to model the collisions between the charged and neutral particles. The MCC model can also be extended to model Coulomb collisions between charged particles which tends to be significant at very low temperature discharges. These models are incorporated into PDP1, a bounded one dimensional plasma simulation code. As a specific example, we consider oxygen RF discharges at various neutral pressures and RF voltages. Electrons, O_2^+, O^-, and O are evolved as partilces. These models can be used to model other processing discharges.

---

1. Work performed for USDOE by LLNL under contract W-7405-ENG-48; a portion of the UCB work performed for NSF under grant ECS-8910827.

GEC

Theory and Simulation of Sheath Waves in Bounded Plasmas,* X. Q. XU, G. DIPESO, V. VAHEDI, AND C. K. BIRDSALL, *University of California, Berkeley*—Sheath waves have been investigated analytically and with particle simulation for an unmagnetized two dimensional plasma slab with periodic boundary conditions in y and conducting walls in x. Analytically treating the sheath as a vacuum layer, the sheath wave bears a resemblance to plasma vacuum surface waves. The simulations are in good agreement with the theory for both bulk Bohm Gross waves and edge sheath waves. We have also simulated a magnetized plasma in both the pure (PIBW) and neutralized (NIBW) ion Bernstein wave regimes to look for sheath waves in these cases. For PIBW and NIBW, the ions are fully magnetized while for PIBW, the electrons are treated as a background and for NIBW, they are treated in the drift kinetic approximation. Ultimately, we want to do magnetized simulations to gain understanding of the impurity and edge heating problem for ICRF experiments.

*This work was performed under U. S. Department of Energy Contract DE-FG03-90ER54079.

A Particle in Cell Code with an Atomic Physics Model for Simulating Processing Plasmas,* V. VAHEDI, M. A. LIEBERMAN, G. DIPESO, C. K. BIRDSALL, *University of California, Berkeley*, T. D. ROGNLIEN, J. R. HISKES, R. H. COHEN, *Lawrence Livermore National Laboratory*—We are combining a particle in cell (PIC) model for particle and field dynamics with a Monte Carlo (MCC) scheme to model the atomic physics of particle collisions with a background neutral gas. These models are incorporated into PDP1, a one dimensional bounded plasma simulation code. As a specific example, we consider oxygen RF discharges at verious neutral gas pressures and RF voltages. Electrons, O_2^+, O^-, and O are evolved as particles. These models can be used for other processing discharges. Due to the varying time scales of electric field and collisional dynamics, discharge equilibrium is difficult to reach in the simulations. We will discuss methods to acheive equilibrium more rapidly.

*Work perfomed for USDOE by LLNL under contract W-7405-ENG-48; a portion of the UCB work performed for NSF under grant ECS-8910827.

Scrapeoff-Layer Instabilities Driven by Temperature Gradients and End Loss* R. H. COHEN, *LLNL;* X. Q. XU, *U.C. Berkeley*—We have performed a kinetic analysis of an instability[1] driven by electron temperature gradients in the presence of end loss, and examined its applicability to tokamak scrapeoff layers. This instability is strong enough that it could set the width of the scrapeoff layer. In addition to kinetic effects, our analysis adds secondary electrons, recycling, energy endloss and (where appropriate) electron Landau damping, and additional finite-gyroradius terms. The dispersion relation is unchanged significantly by the transition from a collision-dominated fluid regime to a more collisionless kinetic regime, so long as the ordering [1] $v_{ti}/L_{||} << \omega << v_{te}/L_{||}$ and a lower bound on collisionality are satisfied, but the energy endloss introduces a threshold in $L_{||}/L_T$. The atomic-physics corrections reduce growth rates and raises the threshold. We re-analyze the mode with alternate orderings. For realistic parameters the ordering expansions are marginally justified; furthermore, axial gradients in equilibrium quantities are significant. For these reasons, and to begin to assess nonlinear effects, we have developed a 2D gyrokinetic simulation model. We report analytic and simulation results for DIII and ITER parameters.

APS-DPP

*Performed by LLNL and UCB for USDOE under Contracts W7405-ENG-48 and DE-FG03-90ER54079.

[1]H. L. Berk *et al.*, Phys. Fluids B **3**, 1346 (1991).

Hybrid particle-fluid simulation of magnetized ion plasma-sheath waves. *A. Tarditi, EECS University of California at Berkeley, Berkeley, CA (USA).* A 2D electrostatic particle-ion, fluid-electron code has been developed for studying ion waves in a magnetized ion-sheath region close to an absorbing conducting wall. A semi-infinite plasma slab model is considered, x-bounded and y-periodic. In a hybrid model the particles (ions) are advanced on the ion time-scale while a fluid-like electron component is simulated by providing an analytic expression for a non-uniform density which takes into account the overall effect of the guiding center electron diffusion. Then in the sheath region a non-Boltzmann electron density profile (function of the plasma potential), which is eventually merged with the Boltzmann distribution in the "bulk" plasma region, is considered. An iterative field solver for a non-linear Poisson equation has been implemented in the code, so virtually any expression of electron density profile vs. potential can be considered.

Work supported by NATO Advanced Fellowship Program, US DOE contract DE-FG03-90ER54079 and US ONR contract no. FD-N00014-90-J-1198

Merging-code approach for realistic simulation of plasma experiments. *A. Tarditi, EECS University of California at Berkeley, Berkeley, CA (USA).* A merging-code approach for complex, space-time multiscale simulation of plasma experimental devices is proposed. This study is particularly oriented to the Numerical Tokamak eXperiment (NTX) project. Different codes, operating on different space and/or time scales as well as dealing with different sets of physical parameters, run at the same time while sharing and exchanging interactively their I/O data fluxes. The information interchange is performed through physical quantities (i.e. density profiles, current distribution, etc.) rather than through numerical quantities (like computer particles) which are code-dependent.
Physics and Computer Science issues relevant to the development of a multi-task integrated simulation are discussed. The features of a versatile software environment (shell), based on a merged-code standard shell communication protocol and provided with a modular structure which allows the use of even previously written codes, are described. A simple simulation example is also referenced.

Work supported by NATO Advanced Fellowship Program, US DOE contract DE-FG03-90ER54079 and US ONR contract no. FD-N00014-90-J-1198

Ion-Temperature-Gradient Modes in Non-Circular Geometry.* D. Hua, X. Xu, and T.K. Fowler, UC Berkeley. — A $1\frac{1}{2}$-D linearized gyrokinetic code employing a δf particle algorithm for ion temperature gradient mode calculations is extended to non-circular cross-section to study scaling with the elongation κ. The growth rate, wave numbers and stability thresholds are calculated for κ ranging from 1 to 2, for a flat density profile characteristic of H-mode operation. Calibration with a hot-ion H-mode shot in DIII-D gives fair agreement between mixing length estimates of χ_i derived from the theory and experimentally-derived values. Agreement requires taking into account $T_e \ll T_i$ in the core, which reduces χ_i near the axis. However, the theory fails to account for the strong dependence on κ at fixed q implicit in empirical scaling laws for the energy confinement time.

*Supported by U.S. DOE Contracts DE-FG03-89ER5116 and DE-FG03-90ER54079..

APS-DPP

Abstract for an Invited Paper
for the Tampa, Florida, Meeting of the
American Physical Society
4-8 November 1991

Quantum-Molecular-Dynamics Simulations of Liquid Metals and Highly-Degenerate Plasmas.

J. THEILHABER, University of Tokyo. (25 min.)

A first-principles scheme for the simulation of systems of classical ions and highly degenerate electrons has been developed, with the aim of modeling metals and strongly-coupled, degenerate plasmas[1]. While the ions move according to Newton's laws of motion, the electrons are represented in a fully quantum-mechanical way by a set of three-dimensional wavefunctions[2]. The latter obey one-particle Schroedinger equations evolving in an effective potential, which accounts for both long-range electrostatic interaction, as well as local quantum-mechanical exchange and correlation between electrons. A pseudospectral scheme is used for the solution of the Schroedinger equations, coupled to a traditional molecular-dynamics scheme for the ions. For a model system of 54 sodium ions, results for thermal equilibration, radial distribution functions, ionic velocity auto-correlation, ionic self-diffusion and melting have been obtained for both the solid and liquid metal. Extensions of the method to other metallic elements and to the electron-proton plasma will be discussed, as well as the prospects for dealing with much larger systems through parallel computation.

*Collaborators S. Ichimaru, H. Iyetomi, S. Ogata. Supported by the Japan Society for the Promotion of Science and the National Science Foundation.

[1] J. Theilhaber, S. Ichimaru, Presented at the Meeting of the Japan Physical Society, Tokyo, March 24-27 1991.

[2] R. Car, M. Parrinello, Phys. Rev. Lett. 55, 2471 (1985).

APS-DAP

IV. WORK NOW IN PROGRESS

Vahedi, V., and G. DiPeso, "Direct Implicit Multi-Time Scale Particle Simulation for Modeling Discharges"

G. DiPeso, "Some Ideas on $\omega_{pe}\Delta t \gg 1$ Particle Simulation"

Mirrashidi, P., B.P. Wood, V. Vahedi, and G. DiPeso, "A Comparison of PIC Simulation and Experimental Results in a Capacitative RF Discharge"

DiPeso, G., and V. Vahedi, "Progress on PDP2, A Two Dimensional Bounded Particle Simulation Code"

Xu, X.Q., G. DiPeso, V. Vahedi, and C.K. Birdsall, "Theory and Simulation of Plasma Sheath Waves"

Ishiguro, S., "Progress on Conversion of ES2B to Xgrafix"

Gee, C., "Progress Report: RZ Project"

Chao, E.H., and C.K. Birdsall, "A New Approach to Traveling Wave Tube Simulation and Design"

Tsung, F.S., J. Trulsen, V. Vahedi, and C.K. Birdsall, "Simulation of Potentials Created by Particulates in RF Discharges: Residence at the Sheath Edges"

Direct Implicit Multi-Time Scale Particle Simulation for Modeling Discharges

Vahid Vahedi and Gregory DiPeso

September 30, 1991

Abstract

In recent years particle-in-cell techniques with Monte Carlo collisions have shown to be of great use in modeling discharges and processing plasmas [1] [2] [3] [4]. A better understanding of these plasmas, e.g. RF driven discharges, has enabled us to device a scheme to optimize the modeling code. It will be shown how direct implicit particle simulation [5] and multi-time scale scheme [6] are incorporated into the bounded one dimensional plasma simulation code PDP1 in order to relax the $\omega_{pe}\Delta t$ time constraint.

1 Introduction

In planar RF discharges, a plasma is bounded between two parallel plates and is driven by an external source as shown in Fig. 1. The electrons responding to the instantaneous applied field gain energy by colliding with the moving sheath, and the electron distribution develops a high energy tail. A typical electron energy distribution function is shown in Fig. 2. Although the population of the high energy tail is down by several order of magnitude from the bulk plasma population, it is the electrons on the tail of the distribution which overcome the ionization threshold to keep the discharge alive through ionization collisions with the neutral particles. In modeling discharges, one must pay s careful attention to resolve the orbit of the high energy electrons accurately.

With a particle simulation model based on an electrostatic plasma response, i.e. particle equations of motion coupled to the Poisson equation, the highest frequency that must be resolved by the explicit numerical methods used to solve the particle and field equations is ω_{pe}. That is, if $\omega_{pe}\Delta t > 1$, numerical instabilities can occur [7]. Direct implicit particle simulation [5] relaxes the $\omega_{pe}\Delta t$ time constraint. However, The temptation to use a larger Δt is foiled because the accuracy condition $v\Delta t/\Delta x < O(1)$ would be violated for the fast electrons. The poor sampling of the fast

electron orbits may lead to numerical cooling of the high energy tail of the distribution making it impossible for the electrons in the model to reach ionization threshold.

A multi-time scale scheme is deviced to allow the fast electrons to move with a small time step while the majority of the electrons in the bulk plasma are pushed with a larger implicit time step. We will now review the direct implicit particle simulation and describe the multi-time scale scheme in the code.

2 Direct Implicit Particle Simulation

Direct implicit particle simulation will now be presented for the case of a one dimensional unmagnetized electrostatic plasma. Following Langdon, Cohen, and Friedman [5], implicit particle movers advance the particle position by the equation

$$x^{n+1} = \beta \Delta t^2 a^{n+1} + \tilde{x}^{n+1}, \tag{1}$$

where $\tilde{x}$ is the portion of the position advance dependent on quantities known at time level n and β depends on the particular implicit scheme. Now let the electric field E be defined on a spatial grid. Then,

$$a^{n+1} = qE^{n+1}(x^{n+1})/m, \tag{2}$$

where weighting, e.g. linear, NGP, etc., would be used to determine E at particle location x^{n+1} from E on the grid. Combining Eq. (1) and (2)

$$x^{n+1} = \alpha' E^{n+1}(x^{n+1}) + \tilde{x}^{n+1}, \tag{3}$$

where $\alpha' = \beta \Delta t^2 q/m$.

Note that a logistical problem with the implicit method is that E^{n+1} depends on ρ^{n+1} which in turn depends on the particle locations x^{n+1}. Unfortunately, all of the particle locations depend on E^{n+1}. One way to get around this problem is to linearize the locations x^{n+1} about the locations $\tilde{x}^{n+1}$ as in Reference 1. Then ρ^{n+1} on the grid is written as

$$\rho^{n+1} = \tilde{\rho}^{n+1} + \delta\rho^{n+1}, \tag{4}$$

where $\tilde{\rho}^{n+1}$ depends on $\tilde{x}^{n+1}$ and

$$\delta\rho^{n+1} = -\partial_x[\tilde{\rho}^{n+1}\delta x^{n+1}]. \tag{5}$$

Equation (5) is derived from linearizing the particle to grid weighting equations about $\tilde{x}^{n+1}$. Strictly speaking, $\delta x^{n+1} = x^{n+1} - \tilde{x}^{n+1}$ is an individual quantity for each particle and is given by Eq. (3).

Instead, δx^{n+1} is approximated as a grid quantity while maintaining the form as given by Eq. (3). That is,

$$\delta x^{n+1} = \alpha' E^{n+1}. \tag{6}$$

Equations (5) and (6) may be combined and then substituted into the right hand side of the Poisson equation to get an implicit version

$$\partial_x[1 + \alpha\tilde{\rho}^{n+1}]\partial_x\phi^{n+1} = -\tilde{\rho}^{n+1}/\epsilon_0, \tag{7}$$

where $\alpha = \alpha'/\epsilon_0$. The $\tilde{\rho}$ terms are determined by weighing the $\tilde{x}$ terms to the grid.

3 Implicit Particle Advance, Field Solve, and Boundary Conditions for RF Discharge Modeling in PDP1

There are several possible implicit finite difference approximations to the particle equations of motion. Here, Friedman's adjustable damping scheme is chosen [8]. The scheme is

$$x^{n+1} = x^n + \Delta t v^{n+1/2}, \tag{8}$$

$$v^{n+1/2} = v^{n-1/2} + \Delta t[a^{n+1} + \theta a^n/2 + (1 - \theta/2)A^{n-2}]/2, \tag{9}$$

$$A^{n-2} = (1 - \theta/2)a^{n-1} + \theta A^{n-3}/2, \tag{10}$$

where $a^{n,n+1} = qE^{n,n+1}(x^{n,n+1})/m$ is the acceleration of the particle which is found by interpolating the field known on a spatial grid to the particle location. The A terms are the lag accelerations which damp high frequency oscillations. $\theta = 0$ gives no damping and $\theta = 1$ gives the D1 scheme. For this scheme, $\beta = 1/2$.

Equation (7), the time implicit Poisson equation, was written for a single species. For multiple species, Eq. (7) is generalized to

$$\partial_x[1 + \chi]\partial_x\phi = -\tilde{\rho}/\epsilon_0, \tag{11}$$

where the $n + 1$ superscript is suppressed and

$$\tilde{\rho}j = \Sigma_s q \Sigma_{i,j} W_j(\tilde{x}), \tag{12}$$

$$\chi_j = \Sigma_s(q^2\Delta t^2/2m\epsilon_0)\Sigma_{i,j} W_j(\tilde{x}). \tag{13}$$

As in the previous section, $\tilde{x}$ is the portion of the advance dependent on quantities known at time level n. The W terms indicate weighing particles to the grid. The finite difference version of Eq. (11) is

$$[1 + \chi_{j-1/2}]\phi_{j-1} - [2 + \chi_{j-1/2} + \chi_{j+1/2}]\phi_j + [1 + \chi_{j+1/2}]\phi_{j+1} = -\Delta x^2\tilde{\rho}_j/\epsilon_0, \tag{14}$$

where $\chi_{j\pm1/2} = (\chi_j + \chi_{j\pm1})/2$, $j = 1, 2, ..., nc-2, nc-1$, and nc is the number of grid cells. For the RF discharge, left plate is biased at the RF source voltage and the right plate is referenced to 0 potential. This gives $\phi_{j=0} = V_{RF}(t)$ and $\phi_{j=nc} = 0$.

The electric field at the interior grid points can be determined by the finite difference version of $E = -\partial_x \phi$, i.e.,

$$E_j = (\phi_{j-1} - \phi_{j+1})/(2\Delta x). \tag{15}$$

At $j = 0$ and $j = nc$, an implicit Gauss law must be used to determine the field. An implicit Poisson equation can be written in vector notation as

$$\nabla \cdot (1 + \chi)\mathbf{E} = \tilde{\rho}/\epsilon_0. \tag{16}$$

The integral representation of Eq. (16) gives the implicit Gauss law:

$$\int_S (1 + \chi)\mathbf{E} \cdot \mathbf{dS} = Q/\epsilon_0, \tag{17}$$

where Q, the approximation to the enclosed charge, is due to $\tilde{\rho}$ and the surface charge density. Drawing a Gaussian pillbox for Eq. (17) around the left wall and spanning the distance $j = -1/2$ to $j = 1/2$ gives

$$[(1 + \chi)E]_{j=1/2} = \sigma_0/\epsilon_0 + \tilde{\rho}_0 \Delta x/2\epsilon_0, \tag{18}$$

where σ_0 is the wall surface charge density. Inside the perfectly conducting wall, $E_{j<0} = 0$. At the wall, Gauss law gives $E_{j=0} = \sigma_0/\epsilon_0$. Substituting this expression into Eq. (18) and solving for $E_{j=0}$ gives

$$E_0 = [(1 + \chi_{1/2})(\phi_0 - \phi_1)/\Delta x] - \tilde{\rho}_0 \Delta x/2\epsilon_0, \tag{19}$$

and similarily, for the right wall,

$$E_{nc} = [(1 + \chi_{nc-1/2})(\phi_{nc-1} - \phi_{nc})/\Delta x] + \tilde{\rho}_{nc} \Delta x/2\epsilon_0. \tag{20}$$

Finally, it is assumed that if $\tilde{x}$ penetrates the wall, then the particle's final location will be in the wall.

4 Numerical Procedure for Direct Implicit

The numerical procedure for direct implicit simulation without multi-time scale scheme is as follows.

- Take the particle quantities x^n, v^n, a^{n-1}, A^{n-3} and the grid quantities E^n, ϕ^n, ρ^n as known.
- In the prepush for each species, calculate A^{n-2} using Eq. (10), then calculate a^n using linear weighting from the grid to the particles, and finally, calculate $\tilde{x}^{n+1}$ using the known quantities in Eqs. (8) and (9).

- Use linear weighting from the particles to the grid to determine $\tilde{\rho}^{n+1}$ and χ^{n+1} as in Eqs. (12) and (13). Solve Eq. (14) for ϕ^{n+1} with a tridiagonal matrix inverter. Calculate E^{n+1} using Eqs. (15), (19), and (20).
- In the postpush for each species, determine x^{n+1} and v^{n+1} using the a^{n+1} terms in Eqs. (8) and (9) for all particles with $\tilde{x}^{n+1}$ not in the walls. Here, $a^{n+1} \approx qE^{n+1}(\tilde{x}^{n+1})/m$ and this quantity is not saved.
- Repack the particle arrays to remove particles lost to the walls. Do Monte Carlo collisions.

5 Multi-Time Scale Criteria

We now describe the scheme for the electrons only, knowing that ions can also be pushed with the large implicit time step. The $v_x - x$ phase space is divided into two regions by placing a rectangle in phase space. Inside the rectangle, electrons are pushed with Δt and outside the rectangle, electrons are pushed with δt where $\Delta t > \delta t$. The rectangle boundaries in x are the sheath plasma boundaries averaged over an RF cycle. The rectangle boundaries in v are $\pm\varepsilon\Delta x/\Delta t$ where $0 < \varepsilon < 1$. The boundary in x is necessary because the electric field in the sheath has large spatial gradient.

6 Multi-Time Scale Method

Here, we construct a very simple multiscale method for electrons as a correction to our original implicit scheme. The correction is an attempt to accurately model the fast electrons. Suppose $\Delta t = 4\delta t$, where δt is chosen to accurately model the fast electrons. The fast electrons are advanced in the time steps

$$n = 0, 1, 2, 3, 4, 5, 6, 7, 8, ...$$

The slow electrons are advanced in the time steps

$$N = 0, 4, 8, ...$$

Both fast and slow particles are moved with the direct implicit simulation technique for consistency. If the fast and slow electrons were moved independently, the implicit corrections to the free stream densities are

$$\delta\rho_F^n = -\partial_x[(\beta q/m)\tilde{\rho}_F^n \delta t^2 E^n],$$

for the fast (F) electrons and

$$\delta\rho_S^N = -\partial_x[(\beta q/m)\tilde{\rho}_S^N \Delta t^2 E^N],$$

for the slow (S) electrons. β depends on the particular implicit scheme used to push the electrons.

The field must be calculated at every time step with the Poisson equation:

$$\partial_x^2 \phi^n = -(\tilde{\rho}_F^n + \delta\rho_F^n + \tilde{\rho}_S^n + \delta\rho_S^n)/\epsilon_0.$$

The key is to determine $\tilde{\rho}_S$ and $\delta\rho_S$ at the n time steps during which the slow electrons are NOT pushed, e.g. 4 to 5, 5 to 6, etc. Since we view fast electron motion as a correction to the implicit scheme, $\delta\rho_S$ retains the same form:

$$\delta\rho_S^n = -\partial_x[(\beta q/m)\tilde{\rho}_S^n \Delta t^2 E^n],$$

where we keep the same Δt as if we were actually pushing the slow particles from $t - \Delta t$ to t.

The approximation to $\tilde{\rho}_S$ for the time steps in which the slow electrons are not pushed is given by linear weighting:

$$\tilde{\rho}_S^5 = (3/4)\tilde{\rho}_S^4 + (1/4)\tilde{\rho}_S^8,$$

$$\tilde{\rho}_S^6 = (2/4)\tilde{\rho}_S^4 + (2/4)\tilde{\rho}_S^8,$$

$$\tilde{\rho}_S^7 = (1/4)\tilde{\rho}_S^4 + (3/4)\tilde{\rho}_S^8.$$

Note that $\tilde{\rho}_S^{4,8}$ *are due to* the actual free streaming of the slow electrons. The implicit Poisson equation becomes

$$\partial_x[1 + \chi]\partial_x\phi^n = -(\tilde{\rho}_S^n + \tilde{\rho}_F^n)/\epsilon_0,$$

where $\chi = (\beta q/m)(\Delta t^2 \tilde{\rho}_S^n + \delta t^2 \tilde{\rho}_F^n)$. Boundary conditions may be worked out from an implicit Gauss law based on the above equation.

7 Numerical Procedure for Multi-Time Scale

The numerical procedure for moving the simulation from time step 4 to 8 is outlined below. The procedure is the same for moving the simulation from 8 to 12, 12 to 16, etc.

- Determine which electrons are slow and which electrons are fast.
- Prepush slow electrons from 4 to 8.
- Calculate $\tilde{\rho}_S$ for 5,6,7.
- Prepush fast electrons from 4 to 5.
- Field solve at 5.

- Postpush fast electrons from 4 to 5.
- Repeat fast electron steps for 5 to 6, 6 to 7, 7 to 8.
- Postpush slow electron from 4 to 8.

8 Acknowledgement

Discussions with Dr. Alex Friedman and Dr. Tom Rognlein of Lawrence Livermore National Laboratories is gratefully acknowledged.

References

[1] Birdsall C. K., *IEEE Trans. Plasma Sci.* **19**, 65 (1991).

[2] Surendra M., and D. B. Graves, *IEEE Trans. Plasma Sci.* **19**, 144 (1991a).

[3] V. Vahedi, M. A. Leiberman, M. V. Alves, J. P. Verboncoeur, and C. K. Birdsall, *J. Appl. Phys.* **69**, 2008 (1991).

[4] Vender D., and R. W. Boswell, *IEEE Trans. Plasma Sci.* **18**, 725 (1990).

[5] A. B. Langdon, B. I. Cohen, and A. Friedman, *J. Comp. Phys.* **51**, 107 (1983).

[6] **Multi-Scale Particle Simulation of Bounded Plasmas**, S. E. Parker, A. Friedman, S. L. Ray, and C. K. Birdsall, *Proc. 13th Conf. on Numerical Simulation of Plasmas*, Santa Fe, New Mexico (1989).

[7] C. K. Birdsall and A. B. Langdon, *Plasma Physics via Computer Simulation* McGraw-Hill (1985), Adam Hilger (1991).

[8] A. Friedman, *UCRL Memo PT803002*, (1988).

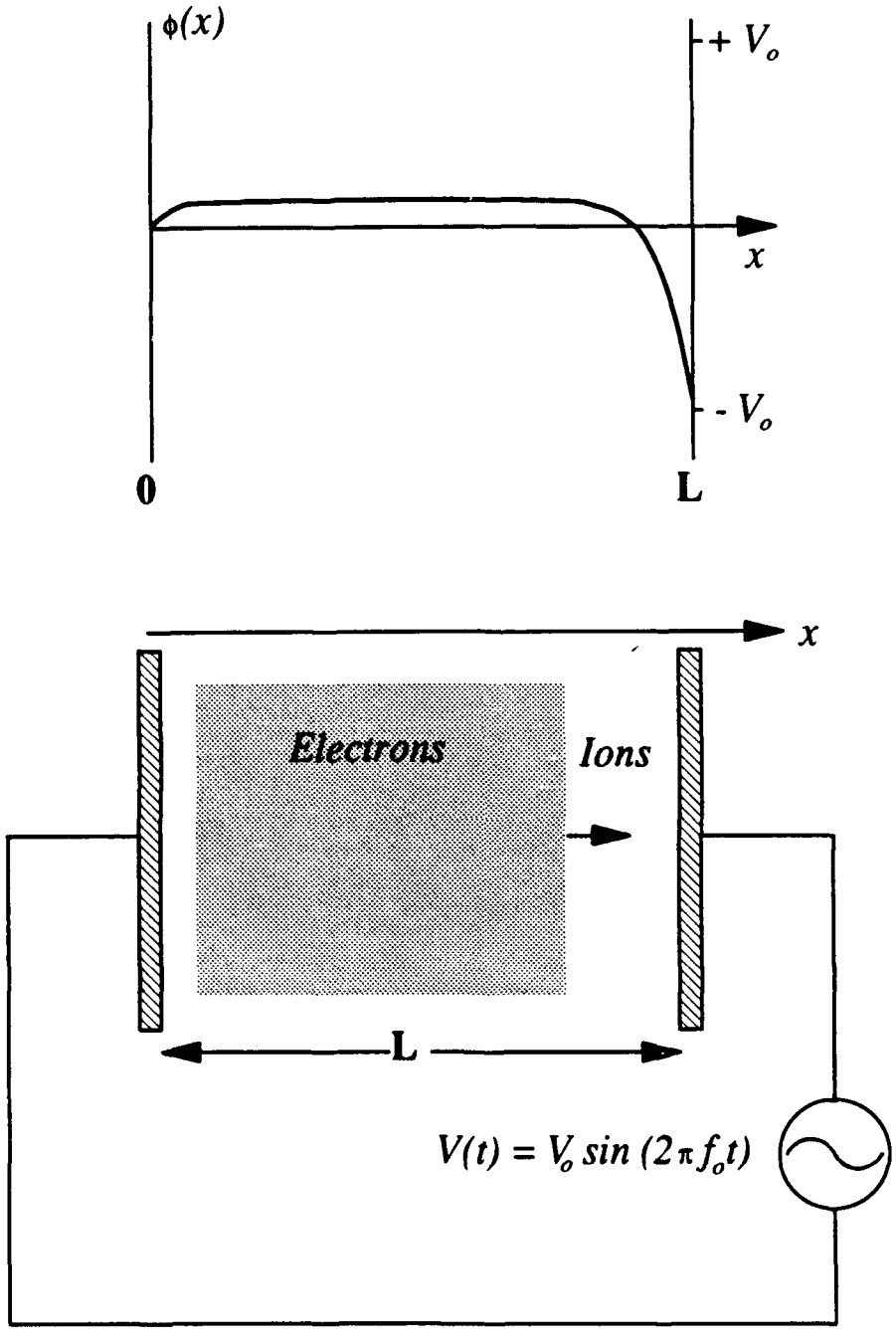

Fig. 1. A parallel plate RF discharge

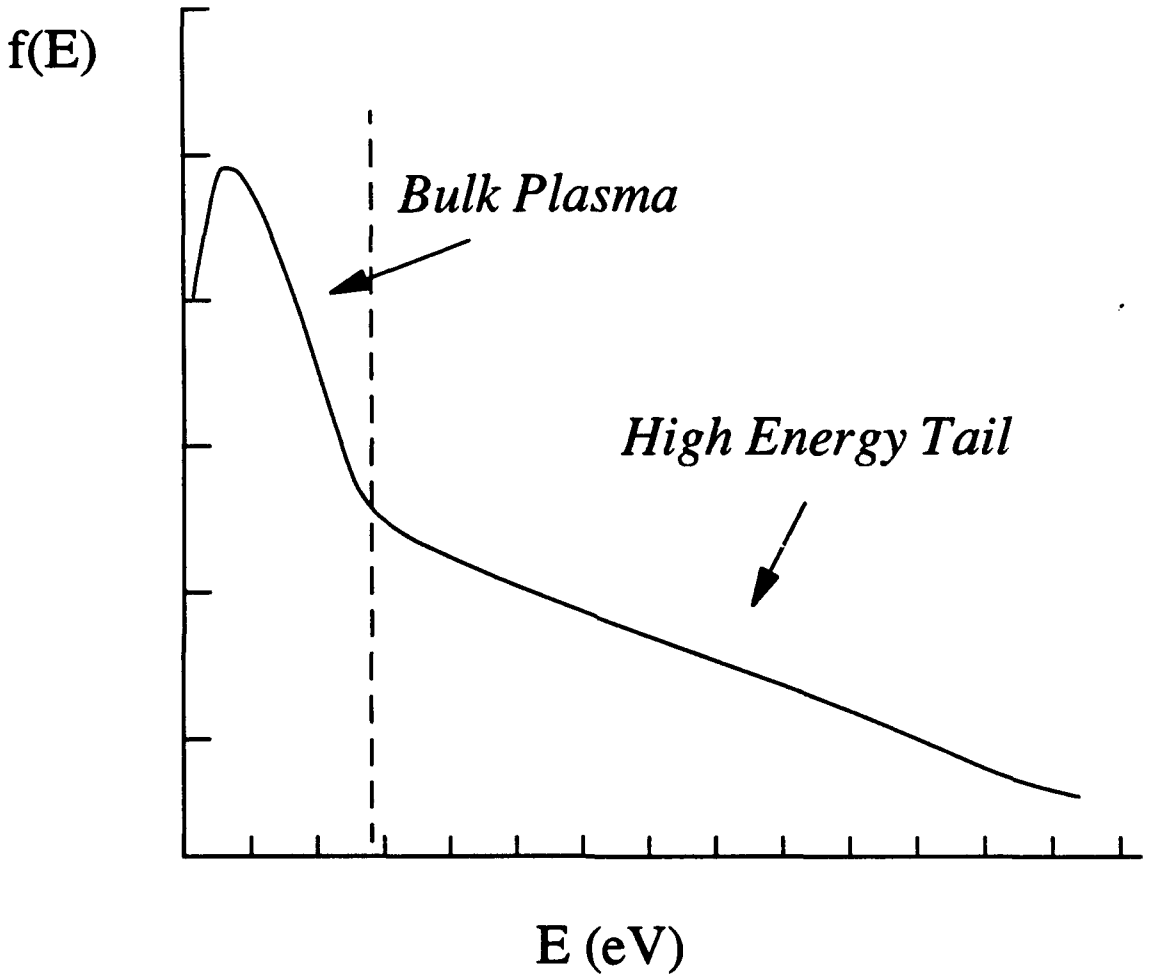

Fig. 2. A typical electron energy distribution function in an RF discharge

Some Ideas on $\omega_{pe}\Delta t >> 1$ Particle Simulation

Gregory DiPeso

September 24, 1991

Abstract

Two methods are presented for $\omega_{pe}\Delta t >> 1$ particle simulation. The first method pertains to cases where there is no $v_{te}\Delta t/L < 1$ restriction. For this case, an alternate form of the direct implicit particle simulation method is presented. The second method pertains to cases where there is a $v_{te}\Delta t/L < 1$ restriction, where L is a sheath length that must be resolved by the particles. The method uses quasineutrality in the plasma bulk with a logical sheath on the plasma boundary. Quasineutrality removes the $\omega_{pe}\Delta t < 1$ restriction and the logical sheath allows some resolution of the sheath physics.

1 Introduction

Very often, one wants to simulate a plasma phenomenon with a characteristic frequency $\omega << \omega_{pe}$. However, if the model equations include ω_{pe} physics as well as ω physics, such as the equations of electrostatic particle simulation, then the ω_{pe} time scale must be resolved or there will be a numerical instability. Furthermore, there are often spatial scales L such as sheath lengths or gradient lengths that also need to be resolved. For the case of particle simulation, this gives the restriction $v_{te}\Delta t/L < 1$. This restriction has nothing to do with numerical stability but everything to do with modeling the particular physical problem accurately.

To overcome the stability restriction $\omega_{pe}\Delta t << 1$, one can either alter the equations used to model the physical phenomenon or use implicit methods to solve the original equations. Both methods may fail if there are other restrictions. For example, one may introduce quasineutrality into the model to remove the ω_{pe} time scale, but this approximation breaks down in the sheath region where the plasma is very non-neutral. As another example, one may introduce implicit methods, but $v_{te}\Delta t/L < 1$ must be obeyed for sheath resolution and if $L \sim \lambda_{De}$, one still has the $\omega_{pe}\Delta t$ restriction.

Here, two methods are presented to allow large $\omega_{pe}\Delta t$. The first method is just an alternative form of direct implicit particle simulation [?], but this alternative form may be more accurate. This method would apply to the case of an RF driven sheath simulation. For this problem, the plasma sheath region is large due to the Child Langmuir law and $v_{te}\Delta t/L < 1$ is not too limiting. The second method attempts to remove both the ω_{pe} time scale and the L space scale restrictions by using a quasineutral Poisson equation [?] to model the plasma bulk and a logical sheath [?] to model the plasma boundary layers. This method would apply to the case of a plasma between two floating conductors. For this problem, the sheath is on the order of a few λ_{De}.

The plan of this report is as follows. In the second section, an alternative form of direct implicit particle simulation is presented. In the third section, a numerical proceedure for this method, in the remainder of this report called method a, is outlined. In the fourth section, the derivation of a quasineutral Poisson equation is given and the highest frequency that the quasineutral model can resolve is calculated. In the fifth section, the logical sheath is reviewed and it is shown how to merge the bulk's quasineutral model with the boundary's logical sheath. In the sixth section, a numerical proceedure for this method, in the remainder of this report called method b, is outlined. Finally, in the seventh section, some concluding remarks are made.

2 Method A: An Alternative Form of Direct Implicit Particle Simulation

A form of direct implicit particle simulation will be presented for the case of a one dimensional unmagnetized electrostatic plasma. Following Langdon, Cohen, and Friedman [?], implicit particle movers advance the particle position by the equation

$$x^{n+1} = \beta\Delta t^2 a^{n+1} + \tilde{x}^{n+1}, \tag{1}$$

where $\tilde{x}$ is the portion of the position advance dependent on quantities known at time level n and β depends on the particular implicit scheme. Now let the electric field E be defined on a spatial grid. Then,

$$a^{n+1} = qE^{n+1}(x^{n+1})/m, \tag{2}$$

where weighting, e.g. linear, NGP, etc., would be used to determine E at particle location x^{n+1} from E on the grid. Combining Eq. (1) and (2)

$$x^{n+1} = \alpha' E^{n+1}(x^{n+1}) + \tilde{x}^{n+1}, \tag{3}$$

where $\alpha' = \beta\Delta t^2 q/m$.

Note that a logistical problem with the implicit method is that E^{n+1} depends on ρ^{n+1} which in turn depends on the particle locations x^{n+1}. Unfortunately, all of the particle locations depend on E^{n+1}. One way to get around this problem is to linearize the locations x^{n+1} about the locations $\tilde{x}^{n+1}$ as in Reference 1. Then ρ^{n+1} on the grid is written as

$$\rho^{n+1} = \tilde{\rho}^{n+1} + \delta\rho^{n+1}, \tag{4}$$

where $\tilde{\rho}^{n+1}$ depends on $\tilde{x}^{n+1}$ and

$$\delta\rho^{n+1} = \partial_x[\tilde{\rho}^{n+1}\delta x^{n+1}]. \tag{5}$$

Equation (5) constitutes the linearization. Strictly speaking, $\delta x^{n+1} = x^{n+1} - \tilde{x}^{n+1}$ is an individual quantity for each particle and is given by Eq. (3). Instead, δx^{n+1} is approximated as a grid quantity while maintaining the form as given by Eq. (3). That is,

$$\delta x^{n+1} = \alpha' E^{n+1}. \tag{6}$$

Equations (5) and (6) may be combined and then substituted into the right hand side of the Poisson equation to get an implicit version

$$\partial_x[1 + \alpha\tilde{\rho}^{n+1}]\partial_x\phi^{n+1} = -\tilde{\rho}^{n+1}/\epsilon_0, \tag{7}$$

where $\alpha = \alpha'/\epsilon_0$.

Another approach will now be described which does not depend on linearization or the approximation used to arrive at Eq. (6). Suppose a one dimensional grid is defined with grid points 0 to N. Let h^{n+1} be the nearest left grid point for a particle located at x^{n+1}, i.e.,

$$h^{n+1} = int(x^{n+1}/\Delta x), \tag{8}$$

where Δx is the space between grid points. Given h^{n+1} and E^{n+1} on the grid, Eq. (3), with linear weighting, would be

$$x^{n+1} = \alpha[E^{n+1}_{h^{n+1}} + (E^{n+1}_{h^{n+1}+1} - E^{n+1}_{h^{n+1}})(x^{n+1} - x_{h^{n+1}})/\Delta x] + \tilde{x}^{n+1}. \tag{9}$$

Equation (9) can be solved for $W_{h^{n+1}+1}(x^{n+1}) = (x^{n+1} - x_{h^{n+1}})/\Delta x$, which is the linear weighting factor from a particle at x^{n+1} to the $h^{n+1} + 1$ grid point. Equation (9) becomes

$$W_{h^{n+1}+1}(x^{n+1}) = \frac{[\gamma E^{n+1}_{h^{n+1}} + W_{h^{n+1}}(\tilde{x}^{n+1})]}{[1 - \gamma(E^{n+1}_{h^{n+1}+1} - E^{n+1}_{h^{n+1}})]}, \tag{10}$$

where $\gamma = \alpha/\Delta x$. Also,

$$W_{h^{n+1}}(x^{n+1}) = 1 - W_{h^{n+1}+1}(x^{n+1}). \tag{11}$$

Now for any species, density on the grid, ρ^{n+1}, is formed as

$$\rho^{n+1}_j = Q\Sigma_{i,j} W_j(x^{n+1}_i), \tag{12}$$

where the sum is over particles that contribute density to the j grid point and $Q = q/\Delta x$ for one dimensional weighting. Particles in the grid cells immediantly to the left and right of the grid point j contribute the density. $W_{j=h^{n+1}+1}$ contributes from the left grid cell and $W_{j=h^{n+1}}$ contributes from the right grid cell. With this in mind, Eq. (12) can be written

$$\begin{aligned} \rho_j^{n+1} &= Q\Sigma_{i,h^{n+1}+1=j} W_{h^{n+1}+1}(x^{n+1}) \\ &+ Q\Sigma_{i,h^{n+1}=j} W_{h^{n+1}}(x^{n+1}), \end{aligned} \tag{13}$$

where the first summation is for contributions from the left grid cell and the second summation is for contributions from the right grid cell.

Substituting Eqs. (10) and (11) into Eq. (13) gives

$$\begin{aligned} \rho_j^{n+1} &= Q\Sigma_{i,h^{n+1}+1=j} \frac{[\gamma E_{h^{n+1}}^{n+1} + W_{h^{n+1}}(\tilde{x}^{n+1})]}{[1-\gamma(E_{h^{n+1}+1}^{n+1} - E_{h^{n+1}}^{n+1})]} \\ &+ Q\Sigma_{i,h^{n+1}=j} \left(1 - \frac{[\gamma E_{h^{n+1}}^{n+1} + W_{h^{n+1}}(\tilde{x}^{n+1})]}{[1-\gamma(E_{h^{n+1}+1}^{n+1} - E_{h^{n+1}}^{n+1})]}\right). \end{aligned} \tag{14}$$

For the first summation, $j-1$ is substituted for h^{n+1} inside the summation. For the second summation, j is substituted for h^{n+1} inside the summation. The subscript j and $j \pm 1$ field terms are constant over the summations. Therefore,

$$\begin{aligned} \rho_j^{n+1} &= Q\left(\frac{[N_{h^{n+1}+1=j}\gamma E_{j-1}^{n+1} + \Sigma_{i,h^{n+1}+1=j} W_j(\tilde{x}^{n+1})]}{[1-\gamma(E_j^{n+1} - E_{j-1}^{n+1})]}\right) \\ &+ Q\left(\frac{[N_{h^{n+1}=j}(1-\gamma E_{j+1}^{n+1}) - \Sigma_{i,h^{n+1}=j} W_{j+1}(\tilde{x}^{n+1})]}{[1-\gamma(E_{j+1}^{n+1} - E_j^{n+1})]}\right), \end{aligned} \tag{15}$$

where $N_{h^{n+1}+1=j}$ is the number of particles weighing in from the left and $N_{h^{n+1}+1=j}$ is the number of particles weighing in from the right.

To use Eq. (15) to form the density, one must know h^{n+1} before knowing x^{n+1}. A possible solution to this problem is to guess $h^{n+1} = int(\tilde{x}^{n+1}/\Delta x)$. This is a good guess since particle Courant conditions require $v_t \Delta t/\Delta x < 1$, and so one may expect $\mid x^{n+1} - \tilde{x}^{n+1} \mid << \Delta x$. For particles very close to a grid point, there may be a jump from one grid cell to the next making the above guess for h^{n+1} incorrect. However, particles very close to a grid point are moved mostly by a field located at that grid point and these particles contribute charge mostly to that grid point. Therefore, any errors due to the wrong h^{n+1} being used only appear in side terms, i.e. a small push from and a small contribution to $j \mp 1$ instead of $j \pm 1$. Linear weighting, on which this method is based, minimizes these kinds of errors.

Eq. (15) is substituted into the right hand side of the Poisson equation. The resulting set of equations would have the form

$$\partial_x^2 \phi^{n+1} = \Sigma_s \rho^{n+1}(E_j^{n+1}, E_{j\pm1}^{n+1}), \tag{16}$$

$$E^{n+1} = -\partial_x \phi^{n+1}. \tag{17}$$

From Eq. (15), it can be seen that the particle quantities need only be summed over once. Then Eqs. (16) and (17) must be solved simultaneously over the grid. This cannot be done by simple matrix inversion techniques because of the nonlinear form of Eq. (15). Instead, some matrix iteration technique may be used. There are continuing advances in matrix iteration techniques which may be applied to this case.

Method A has been presented for a one dimensional system with linear weighting from the particle to the grid and visa versa. It is not difficult to see how the method may be generalized to higher dimensions, however, the equations would be quite messy even for two dimensions. Using higher order weighting would make even the one dimesional equations cumbersome also. Also, it is difficult to see how to incorporate NGP weighting due to the form of the equations presented.'

Finally, one can compare this method to Appendix C in Langdon, Cohen, and Friedman [?]. In that appendix, the authors present a correction to the perturbed particle position which has a form similar to Eq. (10). However, that perturbed particle position is still substituted into the linearized theory as outlined in Eqs. (5)-(7). Here, an attempt is made to use $n+1$ particle positions, written in terms of $n+1$ fields on a spatial grid, without appealing to a linearization form as represented by Eq. (5). Whether this is just nitpicking or if this method is worth the trouble remains to be seen.

3 Method A: Numerical Proceedure

A numerical proceedure by which the above method may be implemented will now be presented. For a one dimensional unmagnetized electron and ion plasma, the following equations describe the evolution of the particle orbits and the electrostatic field:

$$\dot{x} = v, \tag{18}$$

$$\dot{v} = qE(x)/m, \tag{19}$$

$$\partial_x^2 \phi(x) = -\Sigma_s \rho(x)/\epsilon_0, \tag{20}$$

$$E(x) - \partial_x \phi(x). \tag{21}$$

The time implicit discretized form of these equations may be written

$$x^{n+1} = x^n + \Delta t(v^{n+1} + v^n)/2, \tag{22}$$

$$v^{n+1} = v^n + q\Delta t[E_j^{n+1}(x^{n+1}) + E_j^n(x^n)]/2m, \tag{23}$$

$$\partial_x^2 \phi_j^{n+1} = -\Sigma_s \rho_j^{n+1}/\epsilon_0, \tag{24}$$

$$E_j^{n+1} = -\partial_x \phi_j^{n+1}, \tag{25}$$

where Eqs. (22) and (23) are advanced for all particles in both species and Eq. (15) is substituted into the right hand side of Eq. (24). The trapezoidal scheme for the particle advance is chosen for illustrative purposes only. There are other schemes that contain adjustable damping [?].

The first step of the particle advance is to calculate the part of the advance dependent on known time level n quantities:

$$\tilde{v}^{n+1} = v^n + q\Delta t E_j^n(x^n)/2m, \tag{26}$$

$$\tilde{x}^{n+1} = x^n + \Delta t(\tilde{v}^{n+1} + v^n)/2, \tag{27}$$

$$h^{n+1} \approx int(\tilde{x}^{n+1}/\Delta x). \tag{28}$$

Next, the weighting factors in Eq. (15) are calculated. Note that this means two grid quantities must be found. Particles weighing in from a left grid cell to a grid point, i.e. the summation over $h^{n+1} + 1 = j$, is calculated as a grid quantity. Particles weighing in from a right grid cell to a grid point, i.e. the summation over $h^{n+1} = j$, is also calculated as a grid quantity. Then Eq. (24), with Eq. (15) used on the right hand side, and Eq. (25) are iterated on the grid to find the potential and the electric field.

Finally, the particles must complete their advance:

$$v^{n+1} \approx \tilde{v}^{n+1} + q\Delta t E_j^{n+1}(\tilde{x}^{n+1})/2m, \tag{29}$$

$$x^{n+1} \approx \tilde{x}^{n+1} + \Delta t(v^{n+1} - \tilde{v}^{n+1})/2. \tag{30}$$

The scheme presented can be considered a first step in an interation over particle and grid quantities if one wants to make the computational effort. The boundary conditions can be treated in the same manner as in explicit methods.

4 Method B: The Quasineutral Model for the Plasma Bulk

Now consider a problem of a quasineutral plasma bulk. One can expect important physics in long wavelength low frequency modes. Therefore, the plasma approximation, $n_e = n_i$ but electrostatic $E \neq 0$, can be used explicitly in constructing a physical model. Hewett derived the quasineutral equations for a particle ion, fluid electron, electromagnetic Darwin model [?]. A quasineutral model, complete with a quasineutral Poisson equation, will now be derived for the simpler unmagnetized, electrostatic case where both species are treated as particles.

The fluid equations, in vector form, for an unmagnetized, electrostatic, non resistive plasma with electrons and singly charged ions are

$$-e\partial_t n_e + \nabla \cdot \mathbf{J}_e = 0, \tag{31}$$

$$e\partial_t n_i + \nabla \cdot \mathbf{J}_i = 0, \tag{32}$$

$$\partial_t \mathbf{J}_e - e\nabla \cdot n_e < vv >_e = e^2 n_e \mathbf{E}/m_e, \tag{33}$$

$$\partial_t \mathbf{J}_i + e\nabla \cdot n_i < vv >_i = e^2 n_i \mathbf{E}/m_i, \tag{34}$$

where $\mathbf{J} = \pm enu$ and u and $< vv >$ are first and second moments of the distribution which, like n, can be found by particle weighting.

The basic idea behind the quasineutral Poisson equation is to use the plasma approximation $n_e = n_i$ directly and ignore the regular Poisson equation which, with this approximation, would give $\nabla^2\phi = 0$. With the plasma approximation, the sum of the continuity equations, Eqs. (31) and (32), gives

$$\nabla \cdot (\mathbf{J}_e + \mathbf{J}_i) = 0. \tag{35}$$

With the plasma approximation, the sum of the current equations, Eqs. (33) and (34), gives

$$\partial_t(\mathbf{J}_e + \mathbf{J}_i) + e\nabla \cdot n_i(< vv >_i - < vv >_e) = e^2(1/m_e + 1/m_i)n_i\mathbf{E}. \tag{36}$$

With the definitions $\mathbf{P} = \nabla \cdot n_i(< vv >_i - < vv >_e)$ and $\mu = m_e m_i/(m_e + m_i)$, Eq. (36) becomes

$$\partial_t(\mathbf{J}_e + \mathbf{J}_i) + e\mathbf{P} = e^2 n_i \mathbf{E}/\mu. \tag{37}$$

Operating on Eq. (37) with $\nabla\cdot$ and cancelling the resulting $\mathbf{J}$ terms using Eq. (35) gives, after some manipulation, the quasineutral Poisson equation:

$$\nabla^2\phi = \mathbf{E} \cdot \nabla n_i/n_i - \mu\nabla \cdot \mathbf{P}/en_i, \tag{38}$$

where

$$\mathbf{E} = -\nabla\phi. \tag{39}$$

A numerical solution of Eqs. (38) and (39) will not require iteration on the grid because the right hand side of Eq. (38) is linear in $\mathbf{E}$.

It should be noted that because the ions and electrons are treated as particles, one could calculate both n_e and n_i on the grid. The above theory only requires n_i because it is assumed that $n_e = n_i$. In a particle simulation, $n_e \approx n_i$ even in a quasineutral model because of particle noise. However, in the spirit of a low frequency long wavelength quasineutral simulation, n_i as determined by the ions weighed to the grid will be used in Eq. (38) and the definition of $\mathbf{P}$. n_e could be calculated and then compared to n_i for diagnostic purposes.

To calculate the natural frequency present in the model equations, one starts with Eqs. (31) to (34), takes $n_e = n_i$, and then perturbs the equations such that $n = n_0 + \delta n$ and $u = \delta u$. Ignoring the $\delta\delta$, letting $\delta \propto \exp[i(\mathbf{k}\cdot\mathbf{x} - \omega t)]$, and taking $\nabla \cdot n < vv >= v_t^2 \nabla n$, one gets a linear dispersion relation of the form

$$\omega^2 = k^2(T_e + T_i/m_e + m_i), \tag{40}$$

which predicts ion acoustic waves. These waves have the highest frequency that needs to be resolved by the numerical analogues of the particle advance and quasineutral Poisson equations.

5 Method B: The Logical Sheath Model for the Plasma Boundary Layer

The quasineutrality of the plasma ends near a bounding wall since the more mobile electrons charge up the wall while leaving the plasma near the wall ion rich. This region is called the sheath and is usually a few λ_{De} wide for an undriven wall. The sheath is analagous to boundary layers in fluid flow. In this region quasneutrality breaks down. Furthermore, even in steady state, the sheath represents a sharp gradient and the accuracy condition $v_t \Delta t/L < 1$ forces small Δt despite the large Δt that can be used in the bulk.

Fortunately, the logical sheath boundary condition can be used so that the basic features of the sheath can be modeled without creating an accuracy condition on Δt [?]. The logical sheath derivation is based on the fact that a potential drop near a floating wall always adjusts itself so that the electron and ion fluxes into the plate are equal at steady state. The model collapses the sheath potential drop into a step function with the sheath width approaching zero. To the plasma particles just touching the wall, the electric field and the wall charge still appear to be zero. This allows the boundary conditions for Eqs. (38) and (39) to be

$$\mathbf{E}_0 = 0, \tag{41}$$

$$\phi_0 = \phi_1, \tag{42}$$

where subscript 0 indicates the zeroeth grid point at the left wall. There are similar conditions at the right wall.

The electric field tangential to the wall is always zero while the logical sheath allows the electric field normal to the wall to be zero thus giving Eq. (41). Equation (42) proceeds from a Gaussian pill box drawn about the wall. The charge enclosed in that pill box is zero because the logical sheath suggests that there is no surface charge density on the wall and quasineutrality suggests that there

is no charge density near wall or any other place in the plasma. The bulk is allowed to press up against the wall.

In reality, there is an electric field near the wall, but only the particles that can cross the potential barrier and can go into the wall feel the field. This effect is modeled as follows. The number of electrons N_e and the number of ions N_i crossing into the wall are counted. If $N_e > N_i$, the N_e electrons are ordered in velocity from fastest to slowest. All N_i ions and the fastest N_i electrons are absorbed into the wall to give equal fluxes while the slower $N_e - N_i$ electrons are reflected as if they were in a potential well. For the rare case $N_e < N_i$ all particles are absorbed and a positive wall surface charge density σ_w is calculate which leads to a modification in Eq. (42):

$$\phi_0 = \phi_1 + \sigma_w \Delta x/\epsilon_0. \tag{43}$$

No modification in Eq. (41) is needed since the activity of the electric field at 0 is modeled by the particles themselves.

6 Method B: Numerical Proceedure

A numerical proceedure for method b will now be presented. It will contain less detail than the proceedure presented for method a because method b is rooted in physics whereas method a is rooted in numerics. Furthermore, the numerical proceedure to be presented is explicit. However, the logical sheath boundary condition has been used with implicit codes that solve the regular Poisson equation in the bulk [?] and there is no reason why the particle advance and quasineutral Poisson equations cannot be solved by implicit numerical methods.

Equations of motion for electrons and ions take the usual form

$$\dot{\mathbf{x}} = \mathbf{v}, \tag{44}$$

$$\dot{\mathbf{v}} = q\mathbf{E}(x)/m, \tag{45}$$

where $\mathbf{E}$ is known on a grid and the field is interpolated to the particle. After the advance, the logical sheath boundary conditions are calculated. Then, the $< vv >$ and n terms are accumulated on the grid and $\mathbf{P}$ is calculated. Eqs. (38) and (39) can be solved by matrix inversions or iterative methods so that the field at the next time step is determined.

7 Conclusion

Two methods have been presented to simulate plasmas with the $\omega_{pe}\Delta$ constraint relaxed. Method a pertains to the case where there are no gradient constraints whereas method b pertains to the case

of a thin sheath layer. Both methods would require $v_t \Delta t / \Delta x < 0.5$ for accuracy. It now remains for both methods to be tried for some simple bounded plasma test cases.

References

[1] A. B. Langdon, B. I. Cohen, and A. Friedman, *J. Comp. Phys.* **51**, 107 (1983).

[2] A. Friedman, *UCRL Memo PT803002*, (1988).

[3] D. W. Hewett and C. W. Nielson, *J. Comp. Phys.* **29**, 219 (1978).

[4] S. E. Parker, *PhD Dissertation, UC Berkeley*, (1990).

A Comparison of PIC Simulation and Experimental Results in a Capacitative RF Discharge[1]

P. Mirrashidi, B.P. Wood, V. Vahedi, G. DiPeso

September 24, 1991

Simulation results from PDP1, a 1d3v bounded particle-in-cell code[2], are compared to recently published experimental results[3] over a pressure range of 10-100mTorr and 100-1000V applied RF voltage in a symmetric, parallel plate, Argon discharge. We show that where similar results are obtained, the simulation allows insight into plasma parameters which are not experimentally accessible, such as details of the electron power sources and losses.

We have been exploring the numerical effects of various algorithms of moving particles. , In particular, how employing certain algorithms lead to either numerical cooling or heating. Implicit codes, for example, are not able to model the collision of the fast tail of electrons in a RF discharge with the plasma sheath accurately. Over long periods of time, the lack of stochastic heating in the simulated plasma will result in a completely inaccurate system. The large time steps associated with implicit codes curtails their use in the simulation of RF discharges.

Below are two examples of phase-space snapshots of PDP1, showing both an explicit result(physically correct) and an implicit result(which is numerically cooled) for RF discharges; note that the latter does not have any fast electrons.

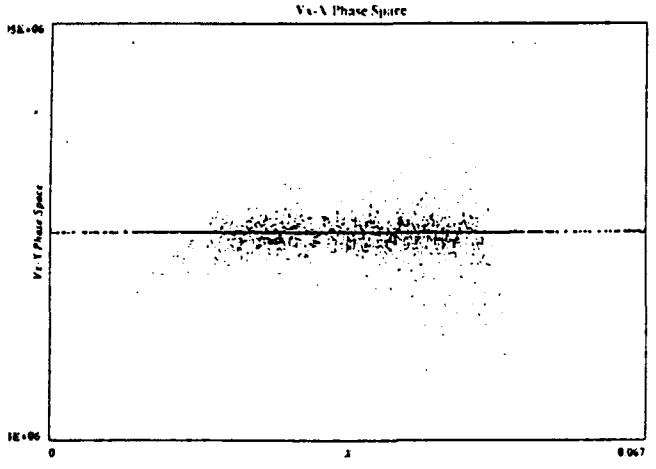

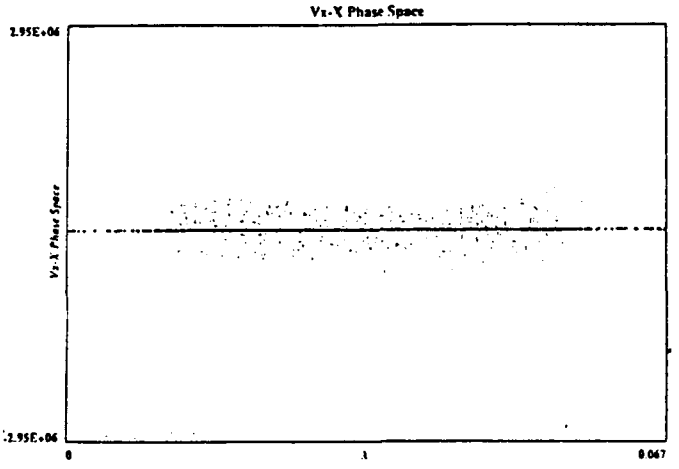

References

[1] Work supported in part by the ONR, DOE and NSF.

[2] Available from the Industrial Liasqn Program Software Office, EECS Dept., UC Berkeley, CA 94720.

[3] V.A. Godyak, R.B. Piejak and B.M. Alexandrovich, IEEE Trans. Plasma Sci., August 1991.

Progress on PDP2, A Two Dimensional Bounded Particle Simulation Code

Gregory DiPeso and Vahid Vahedi

September 30, 1991

Abstract

PDP2, a two dimensional bounded electrostatic particle simulation code for plasmas, is a fairly straightforward extension of the one dimensional bounded particle simulation code PDP1. In this report, we will describe in detail the extension of the field and circuit solve to a second dimension in space with periodic boundary conditions. We will also discuss particle loading, pushing, and weighting in two dimensions. Like the current workstation version of PDP1, PDP2 is run in the Xwindows environment and so we will describe the available diagnostics. Finally, we will conclude with the additional physics and diagnostics that should be added before PDP2 can acheive its full potential.

1 Introduction

Two dimensional particle simulation of plasmas is not new. Previous examples of two dimensional particle models in the electrostatic limit include the work of Decyk and Dawson [1] and the work of Thielhaber and Birdsall [2]. Decyk and Dawson developed a Poisson solver for generalized boundary conditions based on two dimensional Fourier transforms. They successfully simulated surface waves at a vacuum plasma interface. Thielhaber and Birdsall developed a Poisson solver for a plasma bounded by perfectly conducting walls in x and periodic in y [3] in their code ES2 to study Kelvin Helmholtz modes.

The model used in PDP2 is basically the same as that used in ES2. The differences between PDP2 and ES2 are inherited from PDP1. The physics differences are that PDP2 will use the charged particle neutral collision model of PDP1 [4] and uses the external circuit solver of PDP1 [5] where as ES2 uses collisions only as a source of electrons and ions to counter particle losses to the walls and uses the external circuit solver of Lawson [6]. The PDP1 collisional model is an improvement in

that it treats collisions in a more sophisticated manner. The PDP1 circuit solver is an improvement in that it allows a greater range of input parameters. The diagnostic differences are that PDP2 runs in an Xwindow environment like PDP1 [8]. This allows the viewing of physics as it happens and interactive measurements of any diagnostic via crosshair and rescaling mechanisms. ES2 runs on the CRAY in which graphics files can only be viewed at the end of execution.

The development of PDP2 is incomplete. The actual addition of the collisional package and the corresponding changes to input parameter reads are required. The options of particle injection from the walls and distributed sources could be added. PDP1's dumping and restarting capability should be added. Furthermore, all of the PDP1 diagnostics must be included in PDP2. Nonetheless, PDP2 has already been used to sucessfully simulate sheath waves in an unmagnetized plasma [9]. Perhaps a more obvious test would be to temporarily use the ES2 collision package and try to recover the results of Thielhaber and Birdsall.

2 Field and Circuit Solve

Consider a plasma bounded in x by perfectly conducting walls and assume the plasma is periodic in y as in Fig. 1. The conducting walls are attached to an RLC external circuit with a voltage source. The wall to wall distance is L_x. Let grid numbers run from $i = 0, M$ in x and $j = 0, N$ in y. The walls are at grid point $i = 0$ and $i = M$. Zero net Charge over the entire system gives the relation

$$\sum_{j=0}^{N-1}(\Delta y L_z \sigma_{0j}^t + \Delta y L_z \sigma_{Mj}^t) + \sum_{j=0}^{N-1}\sum_{i=0}^{M} \Delta x \Delta y L_z \rho_{ij}^t = 0, \tag{1}$$

where the superscript denotes the time level. The surface charge density σ varies in y because of its relation to the internal charge density ρ. Since the z dimension does not figure into the model, L_z may be chosen to be the unit length, e.g. $1m$ in MKS. Next, Kirchhoff's Laws are employed at the left $i = 0$ wall and the right $i = M$ wall which gives

$$Q_{p0}^t + Q_{c0}^t - Q_{c0}^{t-\Delta t} = \sum_{j=0}^{N-1} \Delta y L_z \sigma_{0j}^t - \sum_{j=0}^{N-1} \Delta y L_z \sigma_{0j}^{t-\Delta t}, \tag{2}$$

and

$$Q_{pM}^t + Q_{cM}^t - Q_{cM}^{t-\Delta t} = \sum_{j=0}^{N-1} \Delta y L_z \sigma_{Mj}^t - \sum_{j=0}^{N-1} \Delta y L_z \sigma_{Mj}^{t-\Delta t}, \tag{3}$$

where Q_p is the net charge extracted or deposited on the wall due to absorption of plasma charged particles or emission of charge particles to the plasma and Q_c is the charge on the external capacitor. Note that Q_{cM} is available from Q_{c0} by adding Eqs. (2) and (3) and substituting Eq. (1).

The external circuit equation is

$$L\ddot{Q}_{c0} + R\dot{Q}_{c0} + Q_{c0}/C = V(t) + \phi_M + \phi_0, \tag{4}$$

where ϕ indicates an equipotential at the wall (no j subscript) and V is a voltage source. The solution to this equation can be written as [5]

$$Q_{c0}^t = (V(t) - K^t + \phi_M^t - \phi_0^t)/\alpha_0, \tag{5}$$

where α_0 and K^t are numerical factors defined in [5].

To develop boundary conditions in x for the Poisson equation, we draw a Gaussian pillbox about some grid point j. This is shown on Fig. 2 for the left $i = 0$ wall. Noting that the electric field directed along the wall (along y) and inside the wall is zero and that E_x at $i = 1/2$ is given by $(\phi_{0,j} - \phi_{1,j})/\Delta x$, the finite differenced version of Gauss' Law is

$$(\phi_0^t - \phi_{1,j})/\Delta x = \Delta x(\rho_{0,j}/2 + \sigma_{0j}^t/\Delta x)/\epsilon_0, \tag{6}$$

where the superscript indicating the time level is dropped for internal ϕ and ρ . For the right hand wall, a similar equation may be written as

$$(\phi_M^t - \phi_{M-1,j})/\Delta x = \Delta x(\rho_{M,j}/2 + \sigma_{Mj}^t/\Delta x)/\epsilon_0. \tag{7}$$

The boundary conditions for y are periodic. Finally, the Poisson equation is written numerically as

$$(\phi_{i-1,j} - 2\phi_{i,j} + \phi_{i+1,j})/\Delta x^2 + (\phi_{i,j-1} - 2\phi_{i,j} + \phi_{i,j+1})/\Delta y^2 = -\rho_{i,j}/\epsilon_0 \tag{8}$$

for the internal ϕ. This completes the fundamental set of equations for the field and circuit solve routine. For more discussion see Chap. 16 in Birdsall and Langdon [3] and Lawson [7].

We solve the set of above coupled equations by Fourier transform methods as discussed in Chap. 14 of Birdsall and Langdon [3]. The y periodic boundary conditions are taken into account naturally and wave spectrum (in k_y) diagnostics are a by_product of the transformations. The Fourier transform of Eq. (8) in the y direction is

$$\phi_{i-1,k} + D_k\phi_{i,k} + \phi_{i+1,k} = -\Delta x^2\rho_{i,k}/\epsilon_0, \tag{9}$$

where the subscript k is the same as k_y and $D_k = -2[1 + 2(\Delta x \sin(\pi m/N))^2]$ is a term that accounts for the finite difference terms in Eq. (8) [3], $\phi_{i,k}$ is the Fourier transform of $\phi_{i,j}$, $k \geq 0$, and $i = 1, M-1$. Since ϕ is constant in space along the conducting walls, e.g., $\phi_{0,j} = \phi_0^t$ for all j, then $\phi_{0,k} = 0$ for $k > 0$ and $\phi_{0,k=0} = \phi_0^t$. Similarily, $\phi_{M,k} = 0$ for $k > 0$ and $\phi_{0,k=0} = \phi_M^t$. $\phi_{i,k}$ is generally a complex quantity where as $\phi_{i,j}$ is real. The $k = 0$ mode Fourier transformed *phi* has a zero imaginary part and the real part is just the average over the periodic length L_y. The Fourier transform of Eq. (6) for $k = 0$ is

$$(\phi_0^t - \phi_{1,k=0}) = \Delta x^2(\rho_{0,k=0}/2 + \sigma_{0,k=0}^t/\Delta x)/\epsilon_0, \tag{10}$$

where

$$\sigma^t_{0,k=0} = \sum_{j=0}^{N-1} \sigma^t_{0j}/N. \tag{11}$$

We do not need the equations for the higher modes of σ.

Substituting Eqs. (5) and (11) into Eq. (2) gives

$$\phi^t_0 + \alpha_0 \Delta y L_z N \sigma^t_{0,k=0} = \beta^t, \tag{12}$$

where $\beta^t = V(t) - K^t + \alpha_0(Q^t_{p0} - Q^{t-\Delta t}_{c0} + \Delta y \Delta z N \sigma^{t-\Delta t}_{0,k=0})$. This equation relates the average left wall surface charge density $\sigma^t_{0,k=0}$ to the left wall potential ϕ^t_0. Rearranging Eq. (10) gives

$$\phi^t_0 - \phi_{1,k=0} - \Delta x \sigma^t_{0,k=0}/\epsilon_0 = \Delta x^2 \rho_{0,k=0}/(2\epsilon_0). \tag{13}$$

Finally, writing Eq. (9) for $k = 0$ gives

$$\phi_{i-1,k=0} + D_{k=0}\phi_{i,k=0} + \phi_{i+1,k=0} = -\Delta x^2 \rho_{i,k=0}/\epsilon_0, \tag{14}$$

where $i = 1, M-1$. Recall that the $k = 0$ mode Fourier transforms are real quantities. For $i = 1$, $\phi_{0,k=0} = \phi^t_0$ as usual and for $i = M-1$, $\phi_{M,k=0} = \phi^t_M = 0$ as a reference potential. There are $M+1$ unknowns which are $\sigma^t_{0,k=0}$, ϕ^t_0, and $\phi_{i,k=0}, i = 1, M-1$. Equations (12)-(14) constitute $M+1$ equations for all of the unknowns. The resulting matrix for this system is tridiagonal which is easily inverted. The above set of equations couples the zero mode portion of the Poisson equation to the circuit equation. For the $k > 0$ modes, no coupling to the circuit is present since $\phi_{0,k} = \phi_{M,k} = 0$ for $k > 0$. For this case, Eq. (9) gives $M-1$ equations for the $M-1$ unknowns $\phi_{i,k}, k = 1, M-1$. Good algorithms for fast Fourier transforms of real quantities and tridiagonal matrix inversion can be found in **Numerical Recipes in C** by Press et al [10]. These algorithms are used in PDP2.

Finally, the $\phi_{i,k}$ can be inverse Fourier transformed into $\phi_{i,j}$. Eqs. (6) and (7) can be then used to get $\sigma_{0,j}$ and $\sigma_{M,j}$,

$$\sigma^t_{0,j} = \epsilon_0(\phi^t_0 - \phi_{1,j})/\Delta x - \Delta x(\rho_{0,j}/2), \tag{15}$$

$$\sigma^t_{M,j} = \epsilon_0(\phi^t_M - \phi_{M-1,j})/\Delta x - \Delta x(\rho_{M,j}/2). \tag{16}$$

Once $\sigma_{0,j}$ and $\sigma_{M,j}$ are calculated, E_x on the wall is given by,

$$E_{x,0,j} = \sigma_{0,j}/\epsilon_0, E_{x,0,j} = \sigma_{0,j}/\epsilon_0. \tag{17}$$

$E_{y,0,j} = E_{y,M,j} = 0$ on the wall, and for the internal points, the electric field is obtained from the finite difference version of $\mathbf{E} = -\nabla\phi$,

$$(E_x)_{i,j} = (\phi_{i-1} - \phi_{i+1})_j/(2\Delta x), \tag{18}$$

$$(E_y)_{i,j} = (\phi_{j-1} - \phi_{j+1})_i/(2\Delta y). \tag{19}$$

At $y = 0 = L_y$, periodicity is used to complete the finite difference. For a short circuit, $\phi_0^t = V(t)$ and $\phi_M^t = 0$ as a reference potential. Then, Eq. (14) can be solved independently of Eqs. (12) and (13). For an open circuit, the Q_{c0} terms in Eq. (2) vanish, leaving

$$\sigma_{0,k=0}^t = Q_{p0}^t/(\Delta y L_z N), \tag{20}$$

so that Eqs. (13) and (14) can be solved with Eq. (17) instead of Eq. (12).

3 Particle Manipulation

A particle in a simulation is often called a superparticle since it represents many actual plasma particles. For instance, if a plasma chamber volume is $1m^3$ with a density of $10^{18}m^{-3}$ for each of two species, then there are 2×10^{18} plasma particles in the chamber. For even the fastest computers with the largest storage space, it is impossible to represent the actual number of particles. If we use 200,000 simulation particles to represent the system, then each of these superparticles is worth 10^{13} plasma particles. Despite the seemingly poor representation, many theoretical and experimental results have been observed via simulation. In this section, the word particle will refer to the simulation superparticles.

Manipulation of the particles consists of loading, solving of the orbit equations, and calculating density on the grid from the particle positions. Particle injection and particle collisions, not yet implemented in PDP2, are discussed elsewhere [3, 4].

Loading of particles consists of choosing the initial conditions for the problem of interest and then setting the initial locations and velocities of all of the particles so as to represent the initial state. In PDP2, we assume an initial drifting Maxwellian distribution in velocity and a uniform distribution in space. The Maxwellian takes the usual isotropic form

$$f(v) = C \exp(-v^2/2v_T^2), \tag{21}$$

where v_t is the thermal spread in velocity and $v^2 = (v_x - v_{x0})^2 + (v_x - v_{x0})^2 + (v_x - v_{x0})^2$. The zero subscripted values are the user specified drift velocities. Once Eq. (18) is inverted to yield v [3], the velocities in each direction are chosen via regular random numbers and the drifts are then added. The uniform loading in configuration space is done by using bit reversed random numbers in y and random numbers in x. At this time, there is no option to add a perturbation to the particle orbits. Any waves that are to be excited must come from the thermal noise in velocity.

Once the particles are loaded, their equations of motion must be solved to advance the velocities and positions in time by one Δt. Then charge density on the grid is accumulated (using linear

weighting) so that the Poisson equation may be solved and the electric field can be calculated for the next time advance. The equations of motion are simply

$$\dot{\mathbf{x}} = \mathbf{v}, \tag{22}$$

$$\dot{\mathbf{v}} = (q/m)[\mathbf{E}(\mathbf{x}) + \mathbf{v} \times \mathbf{B}_0], \tag{23}$$

where $\mathbf{B}_0$ is a user specified magnetic field. The user may specify the magnitude and direction of the magnetic field. Equations (19) and (20) are advanced by the well known Boris mover [3]. Particles that go beyond $y = 0$ or $y = L_y$, are simply reintroduced into the other end in y to satisfy the periodic boundary conditions. Particles that hit the wall on the left side contribute to Q_{p0}. Since Q_{pM} is not used, the particles that hit the wall on the right side do not contribute to the physics except indirectly through the circuit equations. Any particle that hits a wall is deleted from the particle list. To reduce the number of multiplications and divisions, the following internal normalizations are used:

$$q \leftarrow qN_C/(L_z \Delta x \Delta y),$$

$$x \leftarrow x/\Delta x,$$

$$y \leftarrow y/\Delta y,$$

$$v_x \leftarrow v_x \Delta t/\Delta x,$$

$$v_y \leftarrow v_y \Delta t/\Delta y,$$

$$v_z \leftarrow v_z,$$

where N_C is the ratio of plasma particles to superparticles.

Finally, one needs to calculate the charge density on the grid. To do this, simple linear weighting is used. It should be mentioned that linear weighting is used to determine $\mathbf{E}$ at the particle for the Boris mover. From Fig. 3, the fraction of the particle charge contributed to grid point l (or the fraction of electric field contributed from grid point l as needed by the Boris mover) is given by the ratio of the area of square l to the total cell area $\Delta x \Delta y$ where $l = 1, 2, 3, 4$.

We have also added the option of a drift kinetic species. In this approximation, the gyromotion of the superparticles is neglected. The equations of motion take the form

$$\dot{\mathbf{x}} = \mathbf{E}_\perp/B + v_\parallel \mathbf{B}/B, \tag{24}$$

$$\dot{v_\parallel} = qE_\parallel/m, \tag{25}$$

where $\mathbf{E}_\perp = \mathbf{E} \times \mathbf{B}/B$, $E_\parallel = \mathbf{E} \cdot \mathbf{B}/B$, and B is the magnitude of $\mathbf{B}$. Note that the electron superparticles follow motions parallel to $\mathbf{B}$ and the $\mathbf{E} \times \mathbf{B}$ drift. Since there are no gradients or curves in the magnetic field, ∇B and curvature drifts are absent from the equations. $\mathbf{E}$ varies in

space which gives a correction to the $\mathbf{E} \times \mathbf{B}$ drift on the order of r_{ce}^2. For small r_{ce}, this correction can be ignored. $\mathbf{E}$ also varies in time which sets up a polarization drift which is not accounted for in the Eqs. (24) and (25).

The numerical method used to advance Eqs. (24) and (25) cannot be a simple leapfrog because the advance of $\mathbf{x}$ depends on the field quantities directly. Here, we propose the following multistep centered leapfrog scheme

$$\tilde{\mathbf{x}}^{n+1} = \mathbf{x}^{n-1} + \Delta t[\mathbf{B}v_{\parallel}^{n-1/2} + 2\mathbf{E}_{\perp}^{n}(\mathbf{x}^n)]/B, \tag{26}$$

$$v_{\parallel}^{n+1/2} = v_{\parallel}^{n-1/2} + q\Delta t E_{\parallel}^{n}(\mathbf{x}^n)/m, \tag{27}$$

$$\mathbf{x}^{n-1} = \tilde{\mathbf{x}}^{n+1} + \Delta t[\mathbf{B}v_{\parallel}^{n+1/2}]/B, \tag{28}$$

where $\mathbf{E}_{\perp}$ and $E_{\parallel}$ are defined on the grid. Note that fields calculated at $\mathbf{x}^n$ are used to move both $v_{\parallel}$ from $n-1/2$ to $n+1/2$ and $\mathbf{x}$ from $n-1$ to $n+1$. In the next pass through this algorithm, $\mathbf{x}^n$ is moved to $\mathbf{x}^{n+2}$, $v_{\parallel}^{n+1/2}$ is moved to $v_{\parallel}^{n+3/2}$, and the fields used in these moves are calculated at $\mathbf{x}^{n+1}$. The algorithm has been programmed but has yet to be tested for accuracy and stability.

4 Concluding Remarks: A Wish List

The basic changes to PDP2 are in order of importance:

- Add the charge particle neutral collision package and all of the input deck and reading paraphanalia that is needed.
- Add all of the diagnostics already present in PDP1. This includes number versus time for any species which is a very basic and important diagnostic.
- Incorporate the new version of Xgraphics including three dimensional visualization.
- Add the file dumping and restarting options already present in PDP1.
- Include particle injection from either wall.

Other changes to PDP2 are conceivable. For example, one may want to consider the case of walls in the y as well as the x direction. Then one could use either the field solve of Decyk and Dawson or opt for the many elliptic solvers currently available. If PDP2 is to be run on a parallel computing machine, obviously one would want to choose a Poisson solver that takes the most advantage of parallel architecture. Depending on the application, one may want to model walls that are not perfect conductors or walls which change material properties along their length. A wall with a time and space varying potential could be added. Cylindrical and spherical shapes are possible.

PDP2 could be made into a direct implicit or even a multiscale code. The collisonal model could be made even more sophisticated by taking into to account charged particle collisions. The possibilities are of course endless, but with its present sophistication, PDP2 could be a good base from which other particle simulation codes can be developed.

References

[1] V. K. Decyk and J. M. Dawson, *J. Comp. Phys.* **30**, 407 (1979).

[2] K. Thielhaber and C. K. Birdsall, *Phys. Fluids B* **1**, 2244, 2260 (1989).

[3] C. K. Birdsall and A. B. Langdon, **Plasma Physics via Computational Simulation**, McGraw-Hill (1985), Adam Hilger (1991).

[4] V. Vahedi, M. Surendra, G. Dipeso, and J. Verboncouer, **Numerical Methods for Simulating Processing Plasmas**, presented at the 14th International Conference on the Numerical Simulation of Plasmas (abstract 1991).

[5] J. Verboncoeur, V. Vahedi, and M. V. Alves, submitted to *J. Comp. Phys.* (1990).

[6] W. S. Lawson, UCB/ERL Memo M87/14 (1987).

[7] W. S. Lawson, *J. Comp. Phys.* **80**, 253 (1989).

[8] V. Vahedi and J. Verboncoeur, **XGrafix: An X-Windows Environment for Real-Time Interactive Simulations**, presented at the 14th International Conference on the Numerical Simulation of Plasmas (abstract 1991).

[9] X. Q. Xu, G. DiPeso, V. Vahedi, C. K. Birdsall, to be submitted to *Phys. Fluids* (1991).

[10] Press, Flannery, Teukolsky, and Vettering, **Numerical Recipes in C**, Cambridge Press, 1988.

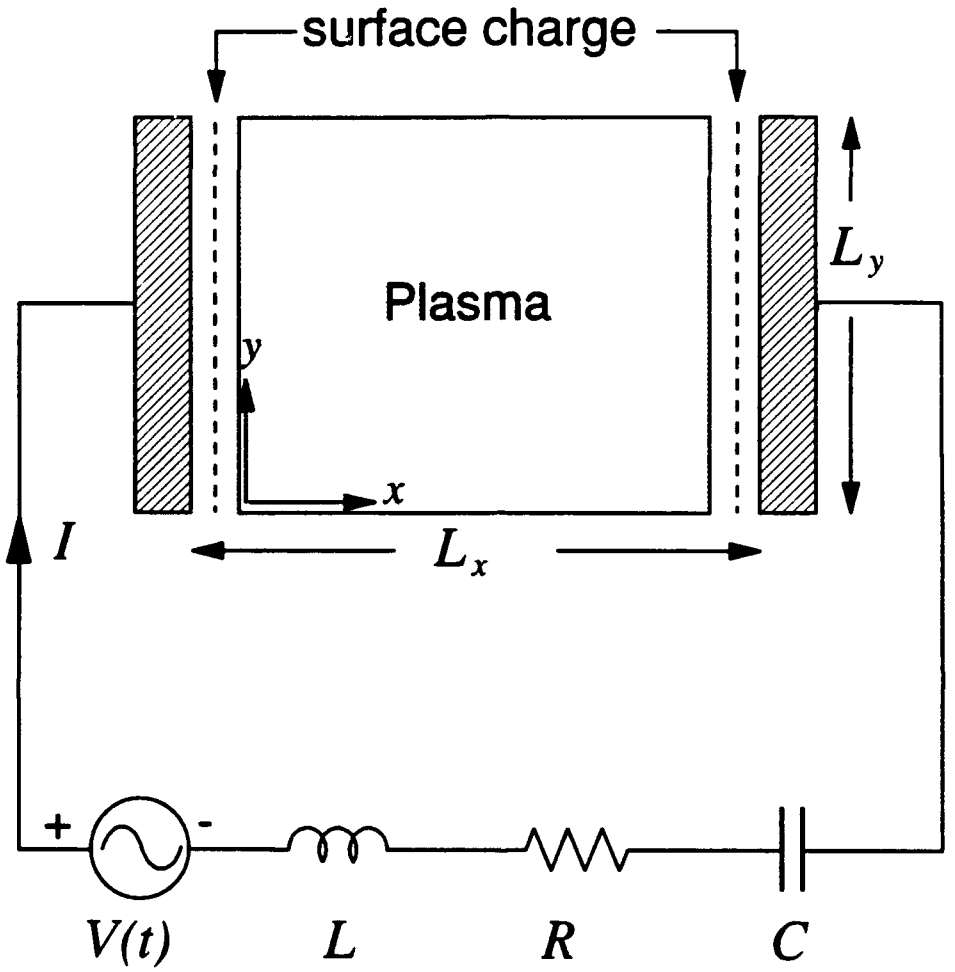

Fig. 1. Physical model

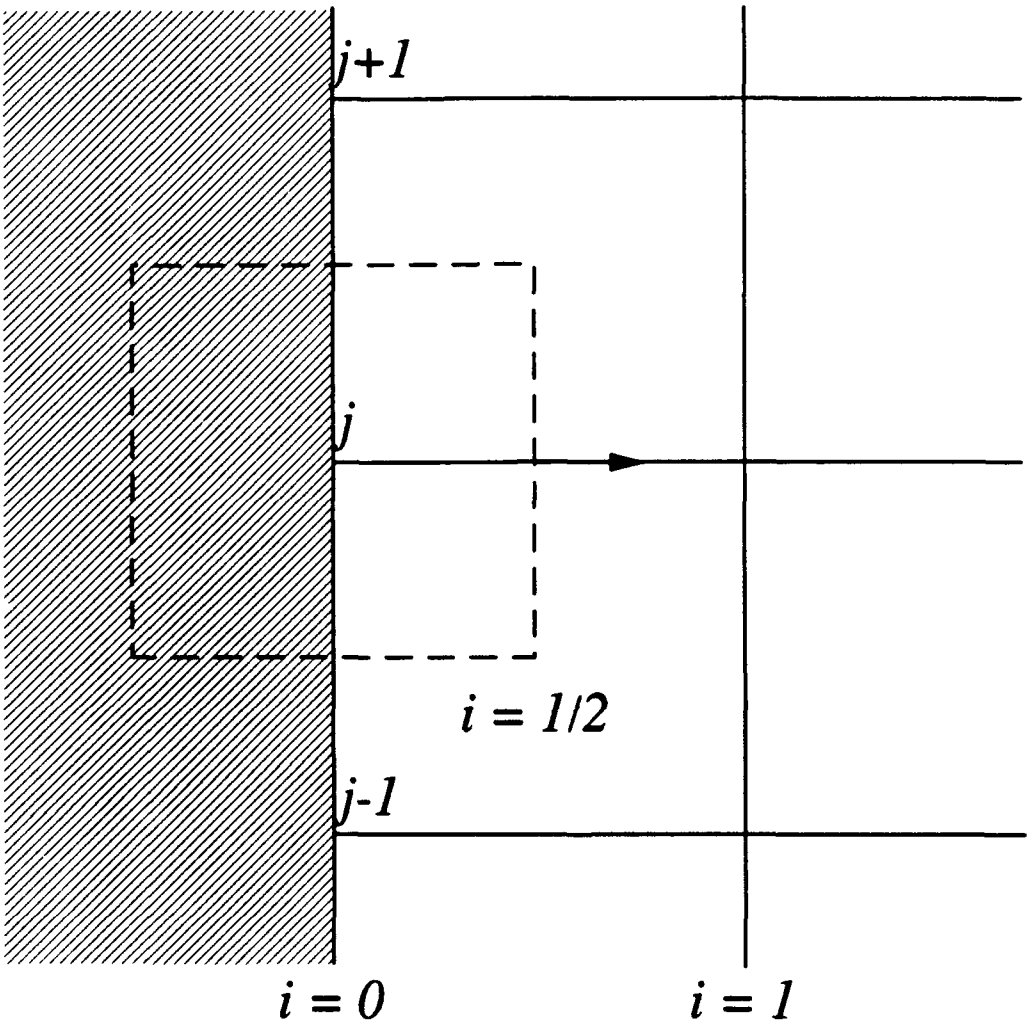

Fig. 2. Gaussian pillbox Non-zero electric field indicated by the arrow.

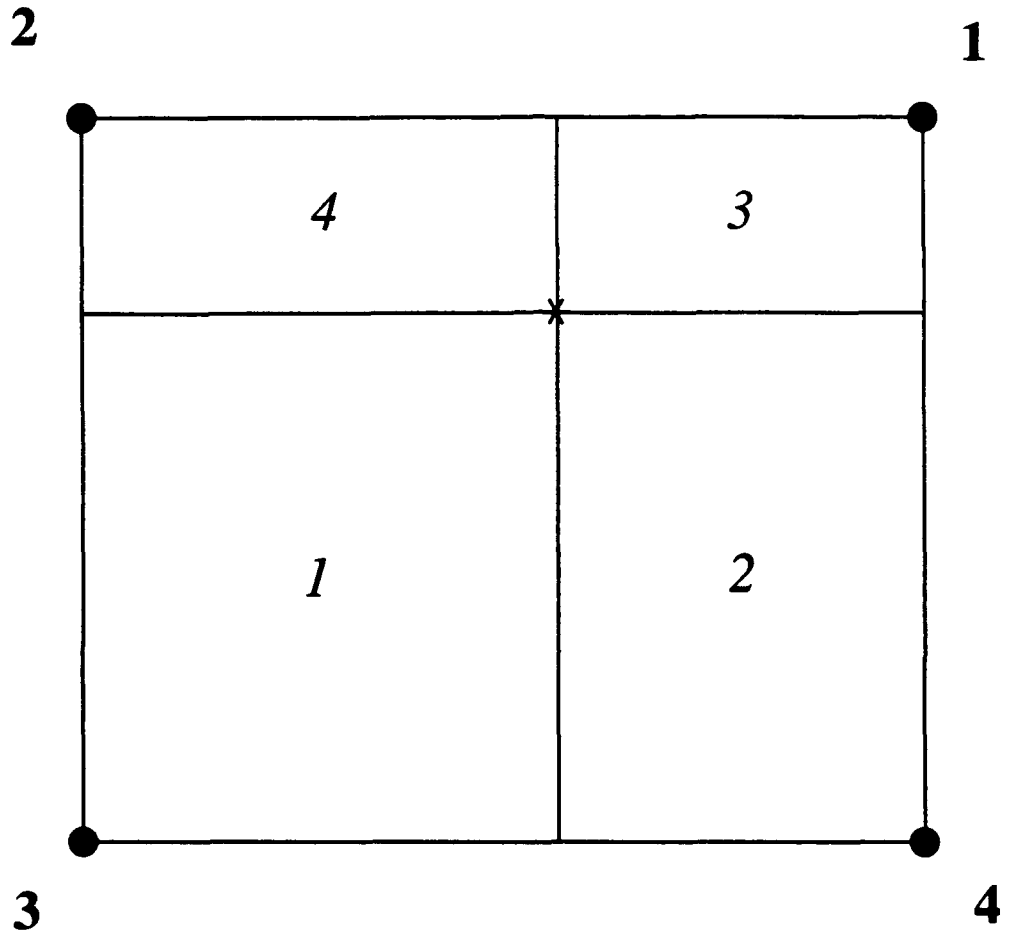

Fig. 3. Area Weighting. Star indicates particle center, dots indicate grid points

Theory and Simulation of Plasma Sheath Waves

X. Q. Xu, G. DiPeso, V. Vahedi, C. K. Birdsall

September 17, 1991

Abstract

Sheath waves have been investigated analytically and with particle simulation for an unmagnetized two dimensional plasma slab with periodic boundary conditions in y and conducting walls in x. Analytically treating the sheath as a vacuum layer, the sheath wave bears a resemblance to plasma vacuum surface waves. The simulations are in good agreement with the theory for both bulk Bohm Gross waves and edge sheath waves.

1 Introduction

It is well known that there is a great variety of waves in a plasma that is well neutralized ($n_i \simeq n_e$) and does not have sharp gradients in field or density quantities. Waves also exist at the plasma edge or sheath where there is large charge imbalance ($n_i \neq n_e$) and where the gradient scale lengths are on the order of the electron Debye length in the unmagnetized case or on the order of the ion gyroradius in the magnetized case. These waves have received less attention in the literature. This paper is a report on electrostatic waves propagating along the unmagnetized plasma edge or sheath. Both analytic theory and computer simulation are used to study the sheath waves. The computer simulation may be viewed as an experiment if the simulation model is constructed from first principal physics with a minimum of approximations or assumptions.

Before we start on the two dimensional theory and simulations, let us review the results of one dimensional simulations [1]. The one dimensional simulations are bounded by perfectly conducting walls which are connected by an external RLC circuit with optional voltage and current sources. The simplest boundary conditions for which sheath formation is observed is the short circuit where the reference potential or voltage on both walls is set to zero. The device is initially filled with warm electrons at a density n_{e0}. The electrons have a full Maxwellian velocity distribution at a temperature T_e. The ions are treated as an immobile background with a density $n_{i0} = n_{e0}$ so that the system is initially neutral. The device length is about $50\lambda_{De}$.

PROGRESS ON CONVERSION OF ES2B TO XGRAFIX

Dr. S. Ishiguro
Tohoku University
JIFT Visitor July-September
and
C. Gee

We connected the 2d3v electrostatic magnetized bounded particle simulation code ES2B, which has been developed at Tohoku University in Japan, to Xgrafix. ES2B is an x-y two dimensional code. A uniform magnetic field is pointing in the positive x-direction. The electrons and ions are continuously emitted from the boundary at $x = x_1$, where x_1 is the system length in x-direction. The potential at $x = x_1$, $y = 0$, and $y = y_1$ are zero, where y_1 is the system length in a y-direction. We can arbitrarily specify the potential at the boundary at $x = 0$. Poisson's equation is solved by the method of superposition. We modified the code so that we can apply a time varying potential at the boundary at $x = 0$. The Berkeley group will now use this code for fully bounded plasmas and as a key to an RZ model.

PROGRESS REPORT: RZ Project

SUBJECT: Two Dimensional, Cylindrical (in r and z directions) Multigrid Poisson Solver

BY: Conway Gee

Motivation

The ultimate goal will be to write a computer code that will simulate plasma in two dimensional cylindrical coordinates. Many physical systems are in cylindrical coordinates.

An interesting mathematical problem has arisen from the project. And the problem is coming up with a 'fast' method to solve the two dimensional, cylindrical Poisson's equation in the r and z directions.

$$\frac{1}{r}\frac{\partial}{\partial r}\left(r\frac{\partial \Phi(r,z)}{\partial r}\right) + \partial^2\Phi(r,z)/\partial z^2 = -\rho(r,z),$$

where ρ is the known charge, and Φ the potential to be solved,

and zero value boundary conditions.

The system looks like this.

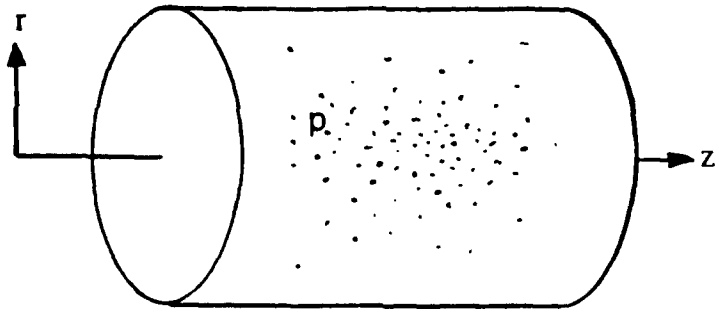

At first we looked at a Fast Sine (Fourier) Transform to find the solution along the z direction and perhaps a 'fast' Bessel series in the r direction. The FST requires O(N logN) arithmetic operations, which is nearly optimal in terms of efficiency (i.e. it is very fast). The algorithm for the FST is already well known. However, the suggested 'fast' Bessel series will require some study for it is not so well known.

The disadvantage of using the FST is that it is rather specialized. The FST can be applied primarily to systems which arise from separable self-adjoint boundary value problems.

References

Strang, Gilbert, Introduction to Applied Mathematics, ©1986

Briggs, William L., A Multigrid Tutorial, © 1987

McCormick, Stephen F., editor, Multigrid Methods, © 1987

The Multgrid Method

Introduction

The mulrigrid method is a culmination of results from trial and error ever since iterative, or relaxation, methods were first used to achieve a solution. Ideas about making the iterative methods converge faster were known for many years, but only until recently has these ideas been formalized as the multigrid method.

Review of the Classical Methods

If the original operator matrix A in the system $Ax = b$ is too difficult to work with (via Gaussian elimination, etc.), then another, simpler matrix can be used in place of A. Calling the new matrix M, we have

$$M x = (M - A)x + b \qquad (1)$$

In the classical iterative methods, (1) is solved iteratively by successive substitutions. Beginning with an initial guess x_0, it may be the vector of zeros, the current guess x_k leads to the next approximation.

$$M x_{k+1} = (M - A)x_k + b \qquad (2)$$

The basic choices of M are: 1. M = diagonal part of A (Jacobi's method)
2. M = triangular part of A (Gauss-Seidel method)

Note that the choices of M are 'close' to A. Why they should be 'close' to A has to do with convergence.

The convergence, or divergence, to the solution x depends on M and A. Subtracting (2) from (1), we have the error equation for $e_k = x - x_k$.

$$M e_{k+1} = (M - A)e_k$$

$$\text{or} \quad e_{k+1} = M^{-1}(M - A)e_k$$

$$= Be_k, \text{ where } B = M^{-1}(M - A)$$

$$= I - M^{-1}A$$

The current error is related to the original error, $e_k = B^k e_0$.

Thus, the goal is to make e_k converge to zero, and that will happen only when the powers of B converge to zero.

$$e_k \to 0 \text{ and } x_k \to x \text{ iff } B^k \to 0$$

Recall that $B^k e_0$ splits into terms of the eigenvectors and eigenvalues of B. Then

$$B^k e_0 = c_1(l_1)^k w_1 + \ldots + c_n(l_n)^k w_n \text{ , where l denotes the eigenvalues and w the eigenvectors.}$$

Therefore, the powers B^k converge to zero if and only if every eigenvalue of B satisfies the condition

$$|l_i| < 1.$$

The rate on convergence depends on the largest $|l_i|$, which is called the *spectral radius* of B.

The matrix M should satisfy two criteria:

1. The equation $M x_{k+1} = (M - A)x_k + b$ should be easy to solve. Hence, M should be convenient to use.
2. M should be 'close' to A, so that the eigenvalues of $B = M^{-1}(M - A) = I - M^{-1}A$ are small (less than one).

Jacobi's method takes M as the diagonal part of A. If all a_{ii} are nonzero, then the diagonal matrix, D, is easily invertible. The matrix representaion is

$$D x_{k+1} = (D - A)x_k + b,$$

and by elements

$$a_{11}(x_1)_{k+1} = (-a_{12}x_2 - a_{13}x_3 - \ldots - a_{1n}x_n)_k + b_i$$

$$\vdots$$

$$a_{nn}(x_n)_{k+1} = (-a_{n1}x_1 - a_{n2}x_2 - \ldots - a_{nn-1}x_{n-1})_k + b_n .$$

The Gauss-Seidel method is different in that it starts using each component of the new x_{k+1} as soon as it is computed. Then x_{k+1} replaces x_k an element at a time, and the old vector x_k is replaced as fast as x_{k+1} is created. The first step finds the first component as in Jacobi's method, and the next step operates immediately with that first new component.

$$a_{22}(x_2)_{k+1} = -a_{21}(x_1)_{k+1} + (-a_{23}x_3 - \ldots - a_{2n}x_n)_k + b_2$$

The last equation uses the new values exclusively.

$$a_{nn}(x_n)_{k+1} = (-a_{n1}x_1 - a_{n2}x_2 - \ldots - a_{nn-1}x_{n-1})_{k+1} + b_n$$

M here is the lower triangular part of A, when all the terms x_{k+1} are moved to the left side. On the right side, $M - A$ is a strictly upper triangular matrix.

Improvements of these methods, such as successive overrelaxation and red-black ordering, are also well known.

The problem with the classical iterative methods mentioned above, even with improvements, is that convergence is controlled by the largest eigenvalue of $B = M^{-1}(M - A)$, which usually is associated with errors of lowest frequencies. High frequency errors are quickly eliminated, but the smooth component of error holds back convergence.

As an example of the relationship between error and eigenvalues, let's examine the one dimensional second order differential equation

$$u''(x) = -f(x), \quad 0 < x < 1, \text{ with the boundary conditions } u(0)=u(1)=0$$

The domain of the problem is partitioned into N subintervals by the grid points

$x_j = jh$, where $h = 1/N$ is the constant width of the subintervals. The discretized form of the equation is

$$(u_{j-1} + 2u_j + u_{j+1}) / h^2 = -f(x_j)$$

Recall that the Jacobi method uses the diagonal part of the operator matrix such that

$$B = I - D^{-1}A$$

and written out for our example, the matrix B looks like the following.

$$B = I - \frac{1}{2}\begin{bmatrix} 2 & -1 & & & & & \\ -1 & 2 & -1 & & & & \\ & \cdot & \cdot & \cdot & & & \\ & & \cdot & \cdot & \cdot & & \\ & & & \cdot & \cdot & \cdot & \\ & & & & & -1 & \\ & & & & -1 & 2 & \end{bmatrix}$$

The eigenvalues of B and A are related by

$$l(B) = 1 - l(A) / 2.$$

The eigenvalues of A are found to be

$$l(A) = 4\sin^2(k\pi / 2N), \text{ where } 1 \le k \le N-1,$$

and the eigenvectors, represented as w_{kj}, the jth component of the kth eigenvector,

$$w_{kj} = \sin(jk\pi / N), \quad 1 \le k \le N-1, \quad 0 \le j \le N.$$

Thus, the eigenvalues of B are

$$l_k(B) = 1 - 2\sin^2(k\pi / 2N), \quad 1 \le k \le N-1.$$

Modes in the lower half of the spectrum, where the wave number has the range $1 \le k < N/2$, are said to be the low frequency or smooth modes. The modes in the upper half of the spectrum, with $N/2 \le k \le N-1$, are called high frequency modes.

For the lowest frequency, $k = 1$,

$$l_1 = 1 - 2\sin^2(\pi / 2N) = 1 - 2\sin^2(\pi h / 2) \approx 1 - \pi^2 h^2 / 2,$$

and recalling the relationship,

$$e_k = B^k e_0 = c_1(l_1)^k w_1 + \ldots + c_n(l_n)^k w_n, \text{ here, k is not the wave number}$$

the equations suggests that the eigenvalue associated with the smoothest mode will be very close to one, and therefore convergence to the solution will be slowed down. Notice that the smaller the grid spacing h, the closer

l_1 is to 1. Hence, any attempt to improve the accuracy by decreasing the size of the grid spacing will only worsen the convergence of the smooth components of error.

Multigrid

The multigrid method changes the scale of the problem so that the smooth component of error can be reduced more rapidly. Thus, the idea is to *change the grid.* Smooth errors on a grid of width h can be attacked on a coarser grid, say, of width 2h, where the error is not so smooth. The following is an outline of an elementary multigrid method. Here, Ω^h denotes the grid associated with spacing h, and x^h is the vector associated with Ω^h.

Coarse Grid Correction Scheme, $x^h \leftarrow CG(x^h, b^h)$

Relax μ times on $A^h x^h = b^h$ on Ω^h with any initial guess.
(μ is any arbitrary small number, i.e. 3, 4, or 5)
Compute the residual $r^h = b - A^h x^h$.
Transfer this vector to a coarse grid, $r^{2h} = Cr^h$.
Solve the coarse system $A^{2h}e^{2h} = r^{2h}$ on Ω^{2h}.
Transfer the correction to the fine grid, $e^h = Fe^{2h}$.
Make the correction to x, $(x^h)^{new} = x^h + e^h$.
Relax on $A^h x^h = b^h$ on Ω^h until desired solution is reached.

The coarsening matrix C combines the nine values on the fine grid to give a single value, at their center, on the coarse grid. The weights are shown in the figure and are mutiplied by 1/16. The refining matrix F reverses what C does; each coarse value splits into nine values on the fine grid.

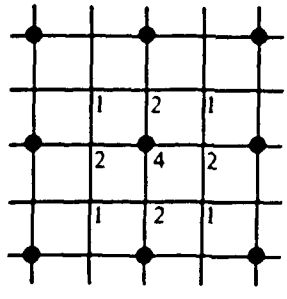

The next trick is evident. Why not nest the CG scheme? The coarse system $A^{2h}e^{2h} = r^{2h}$ can also be coarsened further, 'a correction on the correction,' so to speak. This recursive nesting makes the method possible for asymptotic optimization. The nested scheme is sketched in the following diagram, and by its shape, it is called the V-cycle.

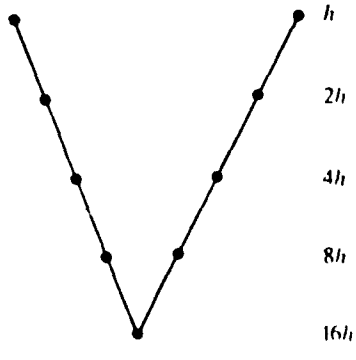

A more sophisticated scheme, called the full multigrid scheme, nests if V-cycles themselves. The scheme begins by initializing b^h, b^{2h}, . . ., and sets x^h, x^{2h}, . . . to zero. The following is the schedule of the full multigrid scheme.

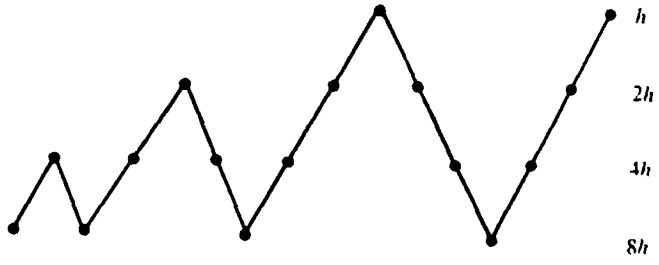

The Poisson Solver

In our case, the discretized del square operator of the Poisson's equation has the form

$$4Ø(1,j)/\Delta r^2 - (4/\Delta r^2 + 2/\Delta z^2)Ø(0,j) + (Ø(0,j+1)+Ø(0,j-1))/\Delta z^2 = -p_{0,j}, \text{ for } r = 0,$$

$$(Ø(i,j+1)+Ø(i,j-1))/\Delta z^2 + \frac{(r+\Delta r/2)Ø(i+1,j)}{r\Delta r^2} + \frac{(r-\Delta r/2)Ø(i-1,j)}{r\Delta r^2} - (2/\Delta r^2 + 2/\Delta z^2)Ø(i,j)$$

$$= -p(i,j), \text{ for } r \neq 0,$$

which determines the operator matrix. The grid that describes the charges p is initially coarsened so that the full multigrid scheme can be used. The operator matrix remains the same (i.e. its elements are not weighted).

The advantage of the iterative methods, even without multigrid, is that the boundary conditions can vary. Say the walls of the cylinder are grounded, or zero, then the Ø matrix will have its appropriate elements fixed to zero. Even these elements of zeros can be fixed to any arbitrary value other than zero. Different geometries can also be easily done with any number of boundary conditions. All that is needed to be done is to fix the correct Ø elements with the proper values.

Included with this report is the early version of my program using the full multigrid scheme, and initial results appear promising. In one test, the time it takes full multigrid to solve a system up to five significant digits is roughly the same as the time it takes for the FST to solve a one-dimensional problem with the same number of grid points (256x256=65536). In another test, the method solves for the 4x4 cylindrical system $p = 4(z^2 - z_1 z)/r_1^2 + 2(r^2/r_1^2 - 1)$, where the solution is $Ø=(r^2/r_1^2-1)(z^2-z_1 z)$. The red-black Gauss-Seidel method takes roughly 90 fine grid iterations to achieve what full multigrid does in only 8 fine grid iterations, along with the much less expensive coarse grid iterations.

A New Approach to Traveling Wave Tube Simulation and Design[1]

E.H. Chao, C.K. Birdsall

September 26, 1991

IBC (Interactive Beam Circuit) is a one-dimensional traveling wave tube simulation that runs on PC'S and UNIX workstations under X. The code uses PIC techniques to model the motion of beam electrons and simple finite-difference methods to model the fields of the coupled slow-wave transmission line.[2] We are currently running simulations at differing values of the Pierce variables QC, C, and b and measuring the power gain at each of these conditions. These measurements are then compared to values calculated by Birdsall and Brewer. [3],[4] The initial comparisons have been encouraging. In addition, changes are being made to the code to make it more valuable to tube designers. These changes include adding new diagnostics (f(E) at collector), modifying old diagnostics, and optimizing the code.

Shown below are some diagnostics for C = 0.096, QC = 0.0799, and b = 0.521.

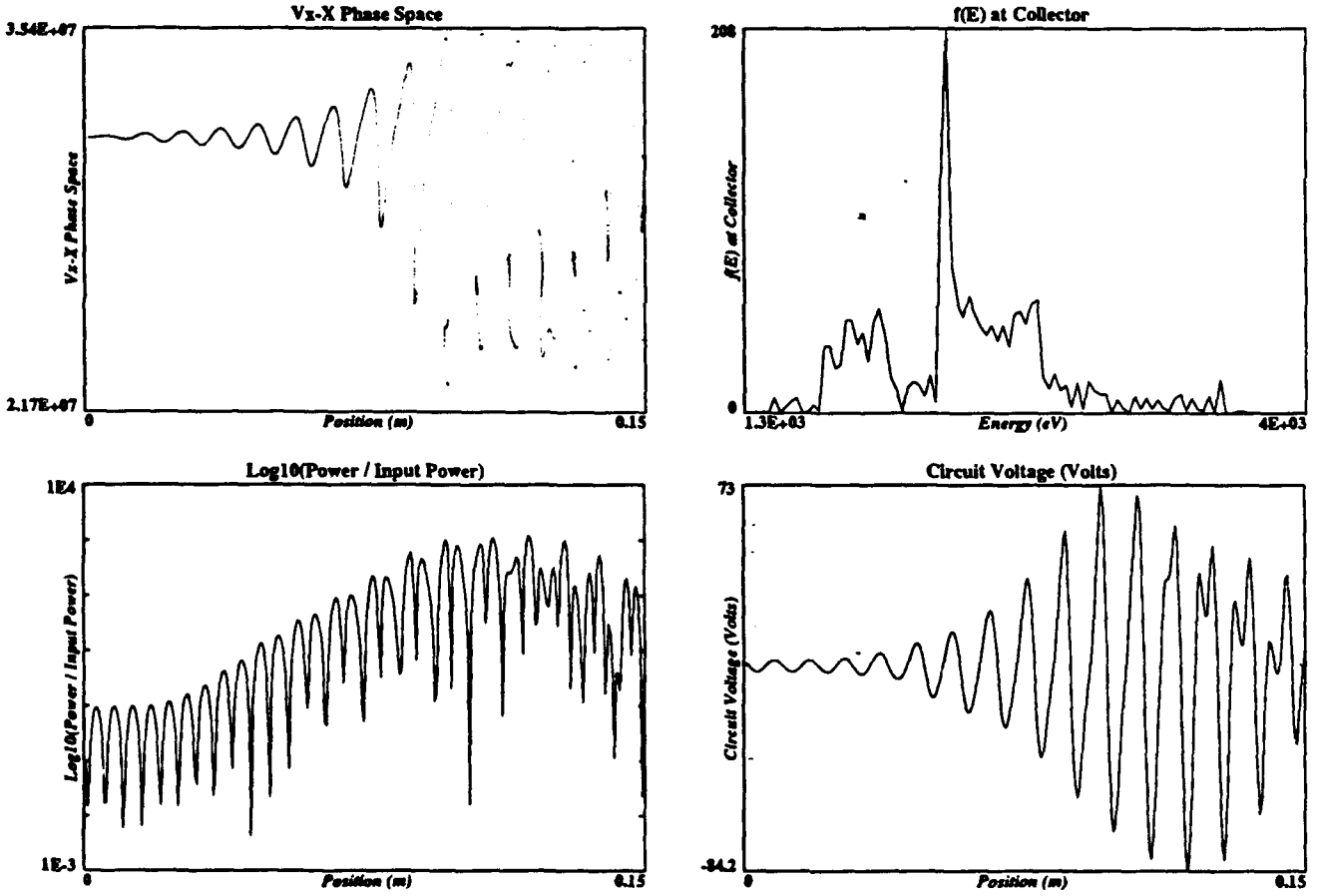

References

[1] Work supported in part by Varian and a MICRO grant.

[2] Morey, I.J. and C.K. Birdsall "Traveling Wave Tube Simulation: The IBC Code", IEEE Trans. on Plasma Science, 18, No.3 June 1990, pp. 482-489

[3] C.K. Birdsall and G.R. Brewer, "Traveling wave tube characteristics for finite values of C," IRE Trans. Electron Devices, vol. ED-1, pp. 1-11, Aug. 1954

[4] G.R. Brewer and C.K. Birdsall, "Traveling-wave tube propagation constants," IRE Trans. Electron Devices, vol. ED-4, pp. 140-144, Apr. 1957

Simulation of Potentials Created by Particulates in RF Discharges: Residence at the Sheath Edges

Frank S. Tsung[1], Jan Trulsen[2],
Vahid Vahedi, C. K. Birdsall

Plasma Theory and Simulation Group,
EECS Department, Univ. Of Calif. Berkeley, CA 94720

Abstract

Heavy particles may play a role in determining the average potentials experienced by ions in RF discharges, hence ion acceleration into targets. Particulates or dust particles also may play a role in many other plasmas. Hence, it is desirable to find where these heavy particles reside (with respect to the edge of the plasma, or sheath) and their effect on the time-average potential which accelerates ions through the sheath.

Using our many-particle PIC-MCC 1d3v simulation code PDP1[5], we have been able to show that the particulates tend to become charged negatively, using cross sections for electron and ion attachment worked out by Trulsen[10], inspired by work of R. Carlile at Univ. Of Arizona[6]. We have placed one heavy particle at various locations in the sheath and found the location where the time average field is a minimum; this is then the residence of the particle, which turns out to be very near the time averaged sheath edge. We are now putting in a large number of particulates and allowing them to reach their respective equilibrium positions. Ion transport is observed only after the addition of a viscous term in the force equation. Without the addition of the ion drag, the dust particles exhibit behaviors similar to those of the negative ions. However, with the viscous term in the force equation, the particulates exhibit behaviors consistent with those observed in the laboratory.

---

1 Current address: Department of Physics, UCLA, Los Angeles, CA 90024.

2 Current Address: Univ. of Tromso, P.O. Box 953, N9001, Tromso, Norway.

Introduction

- A dust particle will tend to charge negatively and therefore acquire an electric potential negative charge. Intuitively, the excess charge is caused by the higher thermal velocity of the electrons.

- Due to its excess negative charge, particulates will create a local potential barrier inside the plasma. This will cause many interesting effects:
  - Scattering of waves with wavelength $\lambda < \lambda_D$
  - Effects the overall charge balance of the system.
  - Creates a potential barrier for positive ions (See Fig. 1).
  - Competes with other collisional processes in a laboratory plasma.

- Our interest in the dusty plasma is related to the presence of sub-micron dust contamination in plasma aided processing. The dust particles are produced by chemical and mechanical means. In some cases, nucleation and growth from plasma negative ions and etch products is the mechanism for particle formation. In other cases, stress-inducing processes may fracture thin films on chamber surfaces thereby injecting particles into the plasma. Laboratory studies show that these particles are suspended near the sheath edge and drop onto the wafer when the rf power is turned off, thereby contaminating critical product surfaces. In the semiconductor industry, it has been claimed that up to 50% of rejection rate is directly caused by the bombardment of dust particles on the wafers[4]. Our main objective is to develop a self-consistent model to simulate dust particles in RF-driven discharges. In addition, we will show that our model agrees with basic probe theories when applied to undriven discharges.

PIC-MCC Scheme

- From optical measurements made by Singh et. al.[6], we have gained some fundamental understanding of the particulates. In the situations which we are interested, it has been observed that the particulates (dust particles) are:
  - Spherical in shape.
  - Located at the sheath edge.

- So, given that the dusty particles are spherical in shape, we can define the capturing cross section as the cross-section for absorption of electrons and ions by the dust particle (*particulate*), i.e.:

$$\sigma_{e,i} = \pi a^2 \left(1 - \frac{q_{e,i} U_{float}}{m v_{e,i}^2}\right) \Theta\left(1 - \frac{q_{e,i} U_{float}}{m v_{e,i}^2}\right)$$

This model has been implemented using a Particle-in-Cell, Monte-Carlo collision (PIC-MCC) scheme. In a Monte-Carlo scheme, the probability for each particle to undergo collision in a time-step Δt is given by:

$$P(\nu_{i,s}) = 1 - e^{(-\nu_{i,s}\sigma_s n_s \Delta t)}$$

In our code, we generate a random number (r) between 0 and 1, then, the random number is compared with the collisional probability(P(v)). If the random number falls within the collisional probability, then a collision is to take place within that time-step. In the case of electron and ion absorptions, two events take place when a collision occurs:

- The charge of the dust particle is incremented by an amount of q_s (charge of the absorbed species.)
- The particle is annihilated. (See Fig. 3)

- The advantages of this algorithm are:
  - Can be easily converted into 2-D and 3-D particle simulations.
  - Can be added into an existing code without changing the structure of the code.
- However, this algorithm also has its flaws:
  - Each dust particle is treated as a separate collisional process, hence, for multiple dust particles, the simulation can be time consuming.
  - The code requires s large number of electrons and ions in order to have good statistics.

Simulation Parameters

The collisional model has been implemented using an one-dimensional, bounded simulation code, PDP1. At $t = 0$, a maxwellianized plasma uniformly fills the space with temperature T_0 and density n_0. A sheet of dust particle is immersed in the plasma at distance L_d. The plasma is allowed to reach equilibrium. The common parameters are:

- Argon Plasma
- Temperature (at t=0) = 1eV to 5eV
- Initial Plasma Density = 10^{14} m^{-3}
- Neutral Density = 0
- Length = 10 cm
- Number of Simulation Particles (t=0) = 8000 per species

In the undriven simulations, we set the neutral pressure to zero in order to suppress all competing collision processes. Therefore, only attachment of electrons and ions is allowed during these runs.

In the RF-driven runs, neutral gas is turned on so electron-neutral, ion-neutral, and dust attachment are present during each simulation. Additionally, a 500-Volt RF source is applied at 13.56MHz. This creates a sheath of 1.70 to 2.60 centimeters, depending on the phase of the RF cycle. The additional parameters are:

- Neutral Pressure = 10 mTorr
- Frequency = 13.56 MHz ($\omega_{RF} = 8.2 \cdot 10^7 sec^{-1}$)
- RF voltage amplitude = 500 Volts

Resuts:

PART I: Undriven Discharges

In order to verify our collision scheme, we have placed a sheet of dust particles in an undriven, maxwellianized plasma, then allow the sheet to reach equilibrium. The floating potential of the dust is then compared with probe theory to verify our algorithm. The floating potential of a probe can be calculated as followed. Let:

- V_s = Velocity of each species.
- T_s = Temperature of each species.

In an unmagnetized plasma, the plasma species have no directional preference, hence, each of the plasma species follows an isotropic Boltzman distribution, i.e.:

$$f_s(\vec{v}) = e^{\left(\frac{-mv_x^2}{2kT_s}\right)} e^{\left(\frac{-mv_y^2}{2kT_s}\right)} e^{\left(\frac{-mv_z^2}{2kT_s}\right)}$$

So, using the distribution above, we can calculate the current for the plasma species:

$$I(V) = \sum_s I_s(V)$$

$$I_s(V) = nqA \int_{-\infty}^{\infty} dv_x \, v_x \, e^{\left(-\frac{mv_x^2}{2kT_s}\right)} \int_{-\infty}^{\infty} dv_y e^{\left(-\frac{mv_y^2}{2kT_s}\right)} \int_{-\infty}^{\infty} dv_x e^{\left(-\frac{mv_z^2}{2kT_s}\right)}$$

Here we assumed the probe is facing the x-direction, hence, only the x-component of the velocity contributes to the current. However, for electrons, the above equations must be modified, because the slow electrons are repelled by the probes. So, if we define:

$$v_{min} = \sqrt{\frac{2q_e V}{m_e}}$$

The quantity v_{min} is the threshold velocity for the electrons and the slow electrons do not contribute to the current. Therefore, the modified equation for electron current becomes:

$$I_e(V) = nqA \int_{vmin}^{\infty} dv_x \, v_x \, e^{\left(-\frac{mv_x^2}{2kT_e}\right)} \int_{-\infty}^{\infty} dv_y e^{\left(-\frac{mv_y^2}{2kT_e}\right)} \int_{-\infty}^{\infty} dv_x e^{\left(-\frac{mv_y^2}{2kT_e}\right)}$$

The above description of electron and ion behavior would yield the familiar curve of the langmuir probe. For our purpose, we can think of the dust particles as floating probes. And the dust particle acquires a negative potential such that the equilibrium electron flux equals to the ion flux.

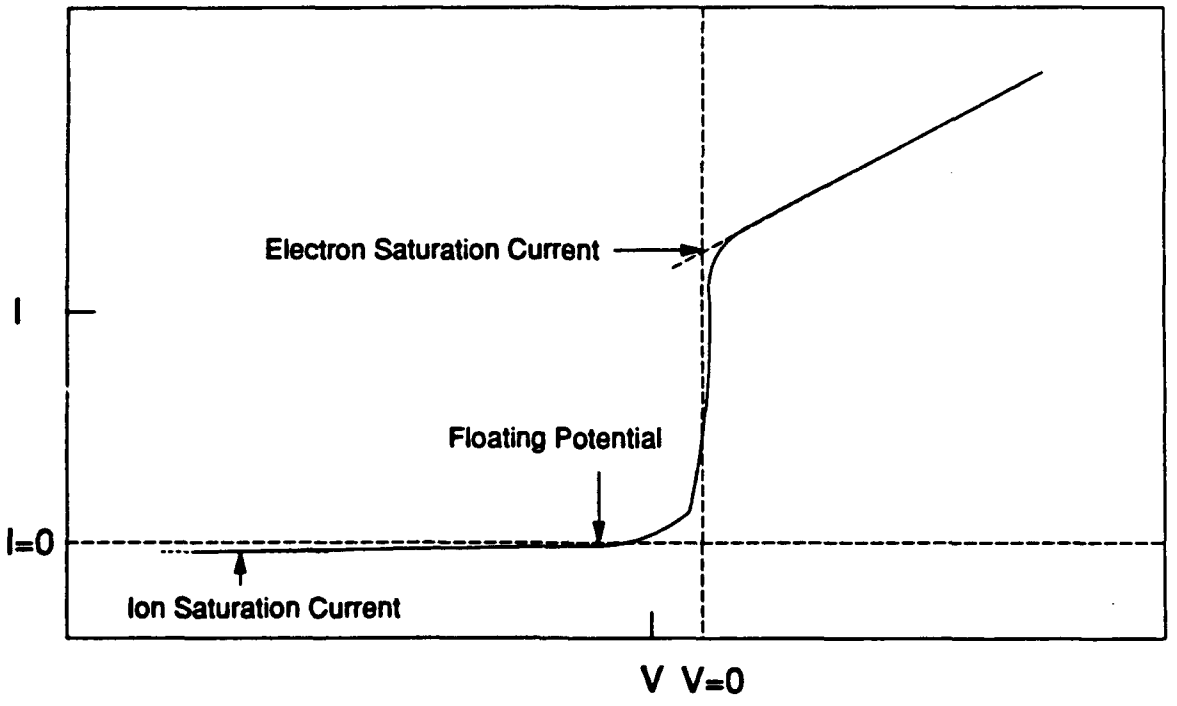

Langmuir Probe I-V Characteristic

So, we can derive the floating potential by setting $I_e = I_i$. This gives the simple and familiar expression for the floating potential, i.e.:

$$V_f = -\frac{T_e}{e} \ln\left(\frac{m_i}{4\pi m_e}\right)^{1/2}$$

We have compared the above results with those obtained by simulation, and we've found our model shows reasonable agreement with theory.

Temperature [eV]	V_f (Theory) [V]	V_f (Simulation) [V]
1	-4.32	-4.18
2	-8.64	-8.23
3	-12.96	-12.21
4	-17.28	-16.59
5	-21.60	-20.85

The discrepancies in the results indicates that there are excess electrons in our model. However, if we taken the spherical geometry of the probe into account and define the enhanced probe area through the following equations:

$$A_{ion}(\vec{v}, V) = \pi a^2 \left(1 + \frac{2eV}{m|\vec{v}|^2}\right)$$

$$A_e(\vec{v}, V) = \pi a^2 \left(1 - \frac{2eV}{m_e|\vec{v}|^2}\right) \Theta\left(1 - \frac{2eV}{m_e|\vec{v}|^2}\right)$$

Hence, using the improved model, we can recalculate the floating potential, once again, by setting $I_i = I_e$, and we have:

Temperature [eV]	V_f (Theory) [V]	V_f (Simulation) [V]
1	-4.18	-4.18
2	-8.25	-8.23

3	-12.35	-12.21
4	-16.95	-16.59
5	-20.90	-20.85

So, taken the geometry of the probe into account, we have shown that our model agrees well with theory. (See below.)

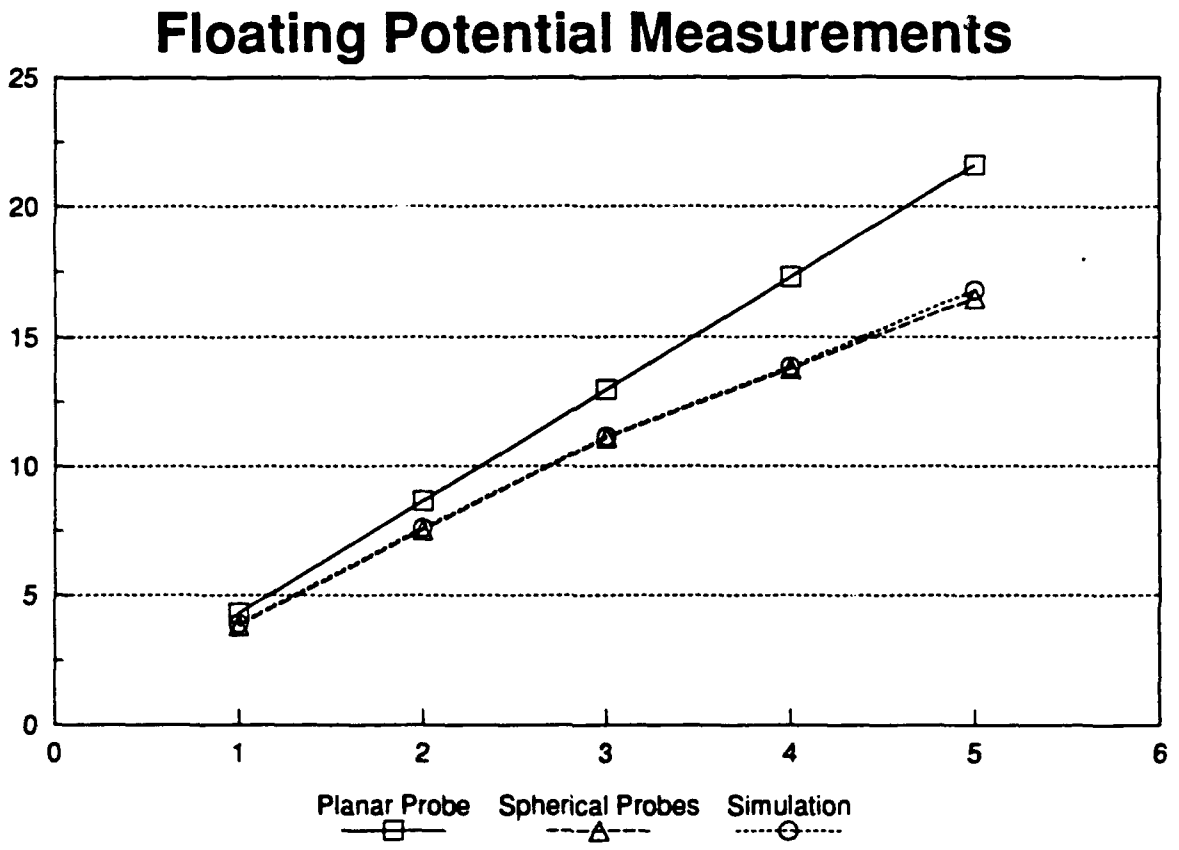

Part II: RF-Driven Plasmas

So, given that our algorithm is consistent with basic probe theories, we now turn our attention to RF-driven discharges. In these runs, we are particularly interested in two aspects of the dust dynamics:

- The position near the sheath-plasma boundary which the local time-averaged field is a minimum.

- The macroscopic dynamics of dust particles inside the bulk.

To understand the equilibrium position of the particulates, we use techniques similar to those used in the undriven plasma. A sheet of immobile dust particle is placed near the sheath of the plasma. Diagnostics are added to measure the peak-to-peak average field at the position of the dust. The parameters are the same to those in the undriven plasma, with the addition of a 500 Volt RF source oscillating at 13.56MHz. This RF source produces a sheath ranging from 1.7 to 2.6 centimeters, depending on the phase of the RF cycle.

In these runs, a large local field is created by the excess negative charges of the dust particles. This field creates a potential barrier hence effects the dynamics of ions near the wall (i.e. wafer). The large field also changes the field configuration around the sheath. So, by placing the dust particles at various positions in the RF sheath, we can find the special position where the average field is at a minimum, and that is the equilibrium position of the particulates. Our measurement yields an equilibrium position of 2.55cm, which is at the sheath-plasma boundary, consistent with observations made in the laboratory.

To study the macroscopic dynamics of the dust particles, we made runs with a large number of dust particles in the bulk. The dust particles are give finite mass, given by the equation:

$$m_p = \rho \cdot r_p^3$$

where ρ is the density of the dust particles (we use water density here), and r_p is the radius of the dust particles. Using optical measurements made in the laboratory, we choose the dust radius to be 0.2 microns. This gives a mass of $8 \cdot 10^{-21}$ grams, which is 10^2 to 10^3 greater than the ion mass. The equilibrium charge of the dust particles are also in the order of 100s of the electrons and the argon ions, hence, the dust charge to mass ratio of the dust particle is in the same order as that of the argon ions. In these runs, the dust particles exhibit behaviors similar to those of the negative ions and they are evenly distributed inside the bulk even after hundreds of RF cycles.

Although we have found the equilibrium position for the particulates near the sheath, the electric field around the equilibrium position is quite large hence it is very difficult for a dust particle of finite mass to maintain its equilibrium position. Therefore, it is necessary to introduce additional forces that would damp the the large time-averaged electric field in the plasma sheath. The work done by Sommerer et. al. suggests that ion drag force (including electrostatic interactions and interactions with the neutral gas) plays a significant role in the transport of dust particles. In the simulation works done by Sommerer et al., the shielded charge of the dust particle Z'_D is modified according to the equation.

$$Z'_D = (1-f)1 + fZ_D$$

Where f = $| E(z,t)/E_m |$, where E_m is the macroscopic electric field at a distance of one Debye length λ from the dust particle of charge Z_D. The shielded charge Z'_D varies according to the local electric field and plasma conditions. In weak field regions such as the bulk plasma, Debye shielding is quite effective, and Z'_D is assumed to be 1. Debye shielding is less effective for particles in the strong RF fields in the sheath because the response times for electrons and ions in the Debye sphere are much longer than the RF period. Particles in the sheaths may therefore respond to the field as though they are less than fully unshielded. The net effect of the modified Z'_D is a strong confining force at the sheath of the plasma, causing the dust particles to stay near the boundary of the sheath.

In our simulations, we modify the expression for the acceleration experienced by the dust particles by adding a viscous term inside the sheath, i.e.:

$$\dot{v} = q/m \cdot E(x,t) - \eta \cdot v$$

Where the viscous term η includes effects such as the interaction of dust particles with the neutral gas, as well as the electrostatic interactions described in Sommerer[8]. Although the interaction of dust with the neutral gas is unknown, it is intuitive that the collision probability increases when the particulate velocity is large. Inside the bulk, the velocity of a dust particle is very small so the particulate is not likely to interact with the neutral gas. Therefore, thermal motion dominates the dust dynamics inside the bulk. When the dust particle passes through the sheath, it is accelerated and picks up momentum very quickly. We expect the viscous term to be significant when the particulate velocity is large, because the dust particle is more likely to interact with the neutral gas; therefore, the drag term is included only inside the sheath.

So, we add the following lines to the mover (**isp** is the species index and **i** is the index for the particles):

```
/* PLASMA_SP is the number of plasma species */
/* LFT_EDGE and RHT_EDGE are measured using
uncontaminated RF discharges */


if((isp<PLASMA_SP) ||
(x[isp][i]>LFT_EDGE && x[isp][i]<RHT_EDGE))
{
      v[isp][i]+=atemp;
}else
{
      v[isp][i]+=atemp-eta*v[isp][i];
}
```

Using η of 0.01 to 0.03, we observe migration of dust particles toward the edge after approximately 100 RF cycles.

Conclusion

In this paper, we presented simulation results for both driven and undriven plasmas. In the situations where there is only one sheet present, it is observed that the particulates acquire a negative potential consistent with basic probe theories. Furthermore, in the RF-driven cases, we observe that the average field is at a minimum near the edge of the plasma sheath, which agrees with experimental observations. Furthermore, using water density, the equilibrium charge-to-mass ratio of the dust particles is similar to those of the ions; therefore, the dust particles would behave like negative ions if Lorentz force is dominant. In the runs where a large number of particulates are used, we believe that ion drag force, including interaction with the neutral gas as well as the electrostatic interaction with the plasma species, is the dominant force in dust transport.

Acknowledgements:

This work is supported in part by Univ. of Arizona Sematech Ctr. for Excellence. The one-dimensional simulation code PDP1 was originally written by Dr. I.J. Morey, Mr. V. Vahedi and Mr. J. Verboncoeur[3,[11]].

3 Codes available from Industrial Liaison Program, EECS Dept., UC Berkeley, CA 94720.

References

[1] Draines, B. T., Salpeter, E. E., "On the Physics of Dust Grains in Hot Gas" *Astrophys. J.*, 231, 77 (1979).

[2] Havnes O., Morfill G. E., "Effects of Electrostatic Forces on the Vertical Structure of Planetary Rings", *Adv. Space Res*, 4, 75 (1984).

[3] Havnes O., de Angelis U., Bingham R., Goertz C. K., Morfill G. E., Tsytovich V., "On the Role of Dust in the Summer Mesopause", *J. Atmos. Terres Phys.* (To appear).

[4] Hoenig, S. A., "Contamination Control for Yield Improvement", *Semiconductor International*, pp. 72-75, Nov. 1987.

[5] Morey, I. J., Vahedi, V., Verboncoeur, J., "Particle Simulation Code for Modeling Processing Plasmas", *Bull. APS*, 34:2028 (1989).

[6] Nowlin, R. N., Carlile, R. N., "Electrostatic Nature of Contaminative Particles in a Semiconductor Processing Plasmas", EECS Dept., Univ. of Arizona. (Submitted for publication)

[7] Selwyn G. S., Singh J., Bennett R. S., "In Situ Laser Diagnostics of Plasma Generated Particulate Contamination", *J. Vac Sci. Tech.* A7, 2758 (1989).

[8] Sommerer, T. J., Barnes, M. S., Keller, J. H., McCaughey, M. J., Kushner, M. J., "Monte Carlo-Fluid Hybrid Model of the Accumulation of Dust Particles at Sheath Edges in RF Discharges", Submitted for Publication.

[9] Spitzer, L., Physical Processes in the Interstellar Medium, Wiley, New York (1978).

[10] Trulsen, J. and PTSG, "Plasma-Charged Particulate Interactions", July 1990.

[11] Vahedi V., Verboncoeur, J. "One Dimensional Monte-Carlos Collisional Model." University of California, May 1990.

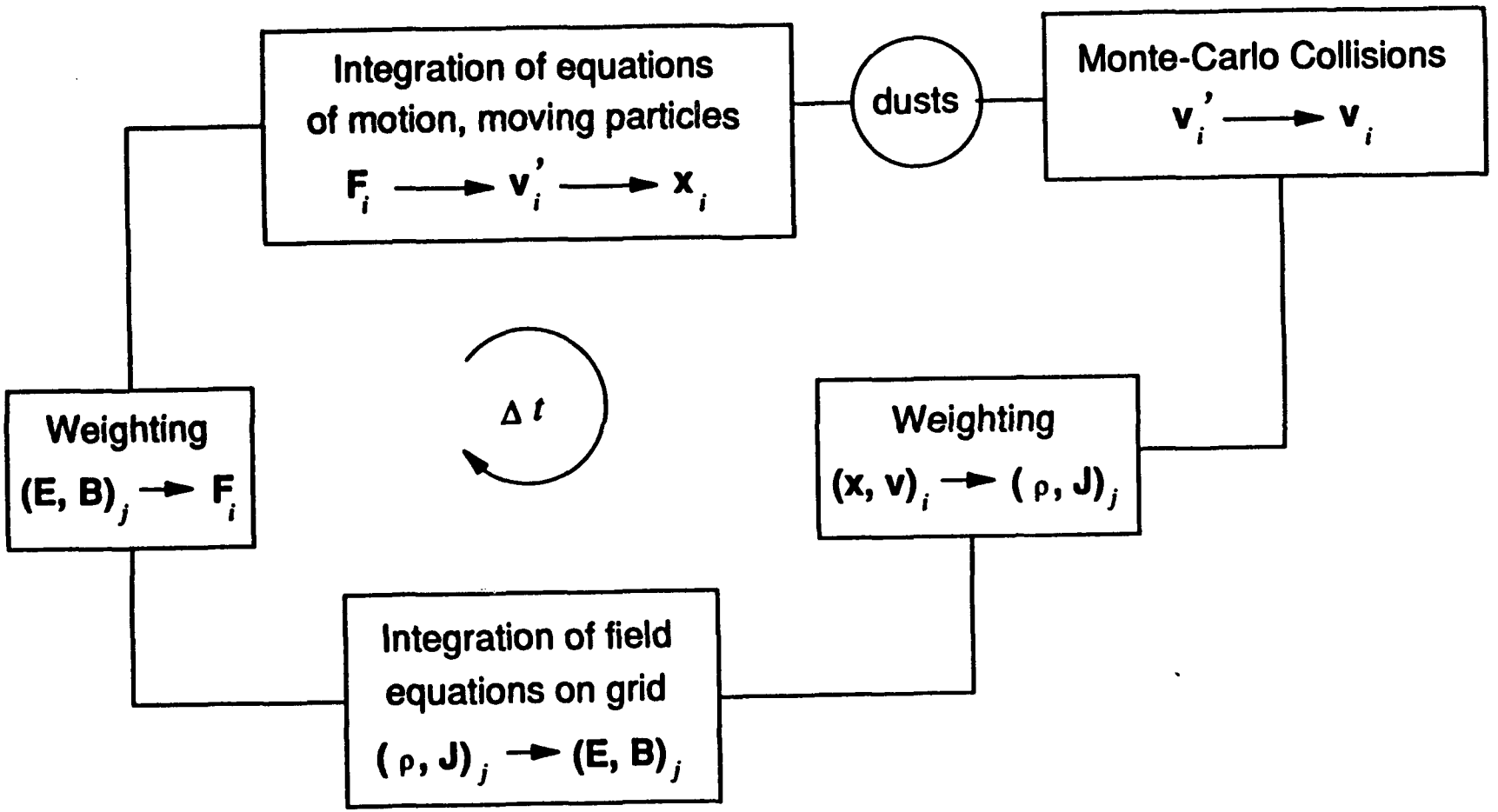

Flowchart of the MCC-PIC scheme with the addition of dust particles

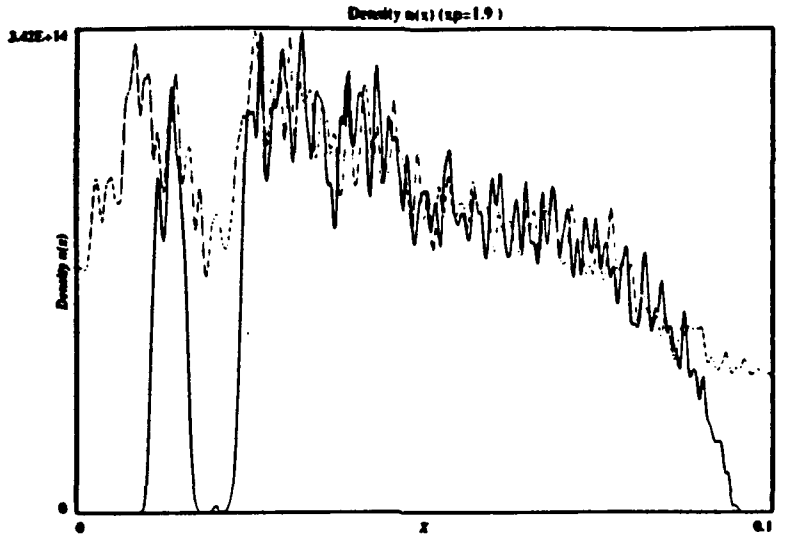

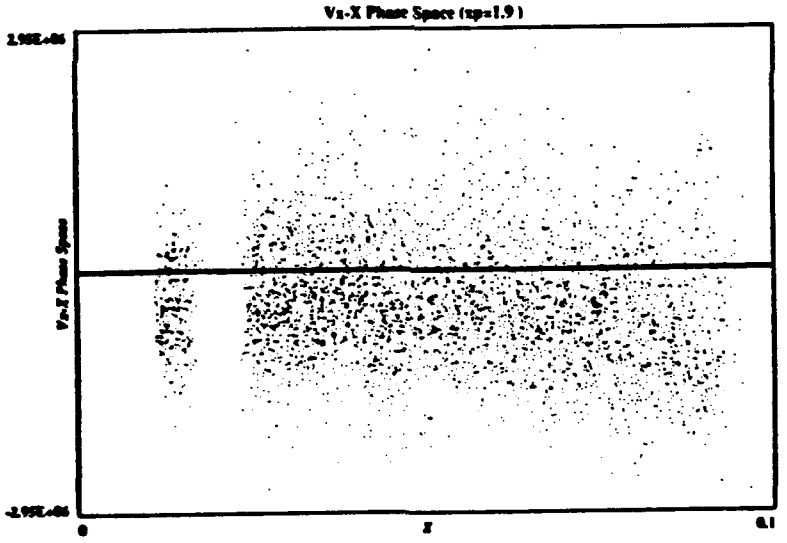

The presence of the dust particles effects the overall charge neutrality, and creates a potential barrier (lower plot). The above plots are made by placing an immobile sheet of dust particle near the sheath of the plasma. In this case, the particulate is placed at $x_p = 1.9cm$.

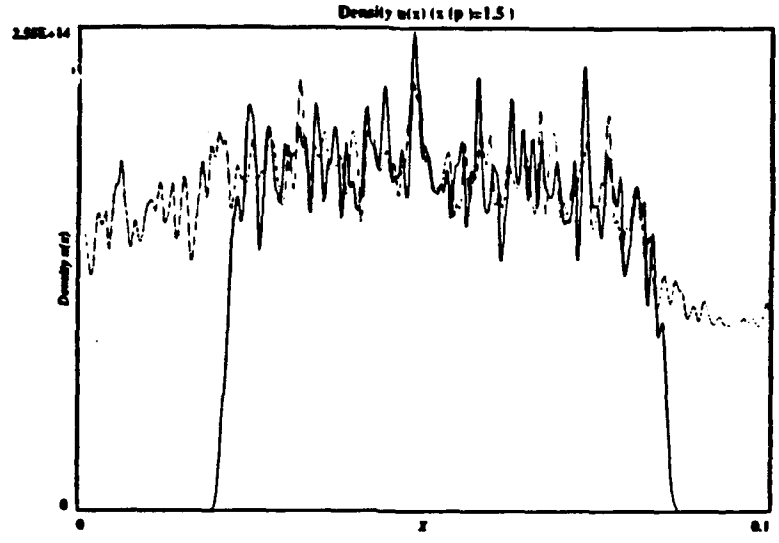

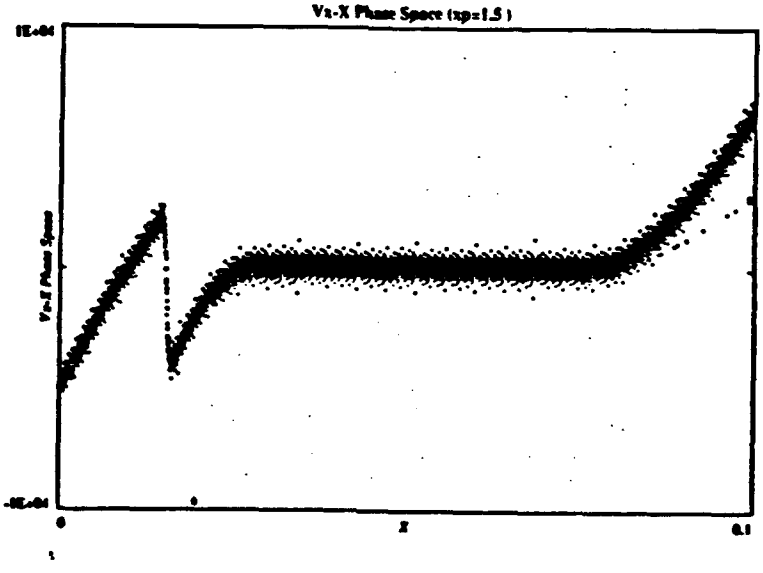

The presence of the dust particles effects the overall charge neutrality, and creates a potential barrier for ions (lower plot). The above plots are made by placing an immobile sheet of dust particle near the sheath of the plasma. In this case, the particulate is placed at $x_p = 1.5cm$.

E Field vs. Particulate Position

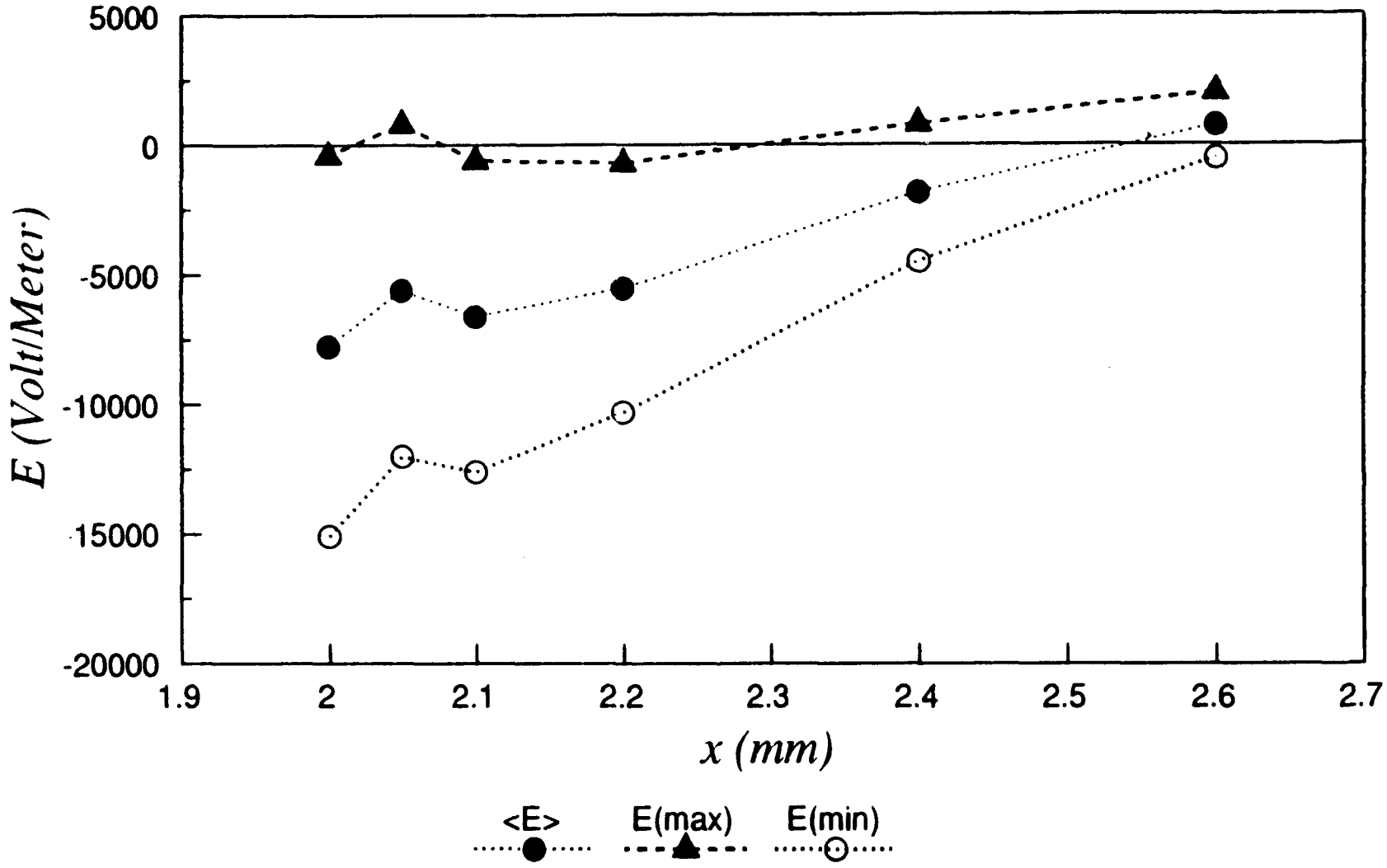

Gas Pressure = 10 mTorr
Frequency = 13.56 MHZ

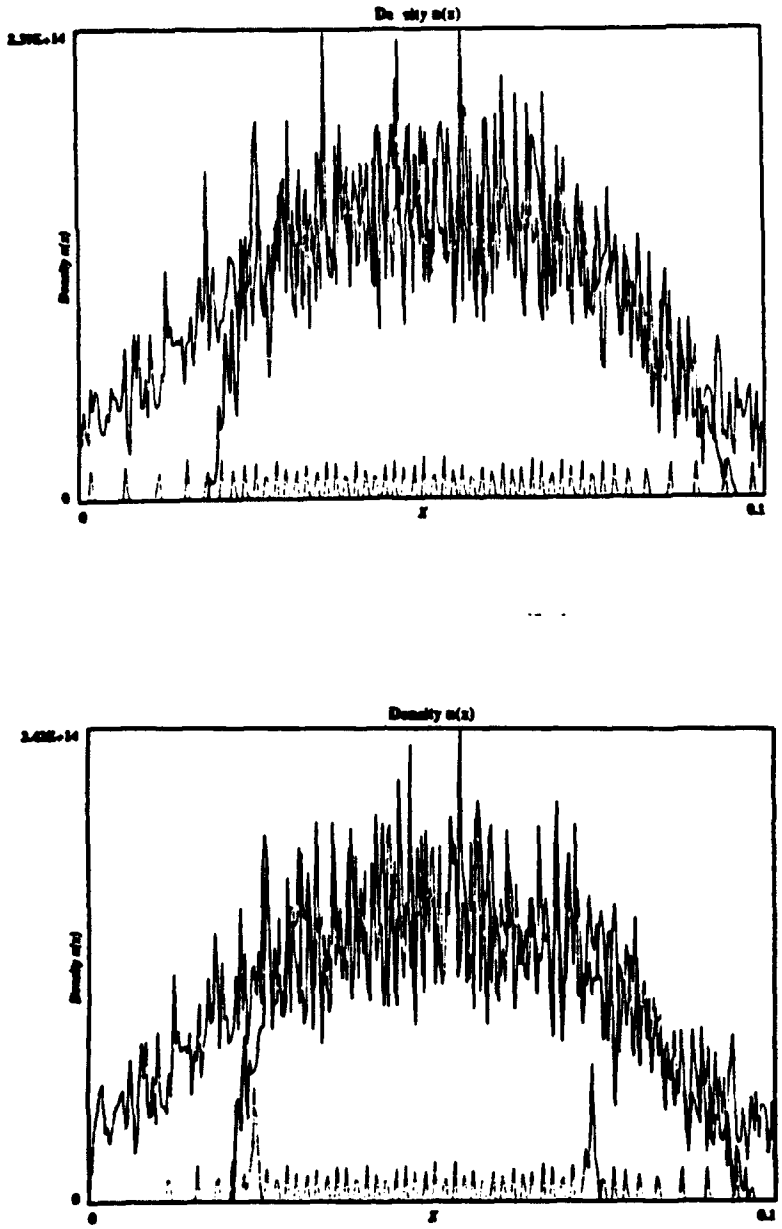

Viscous force plays an important role in the transport of dust particles. The upper plot is made without drag force, and the lower plot is the same simulation, with the addition of a viscous term in the force equation.

V. DISTRIBUTION LIST

Department of Energy
Crandall, Katz, Lankford, Macrusky, Manley, Nelson, Sadowski, Tech. Info. Center

Department of Navy
Condell, Florance, Roberson

Argonne National Laboratory
Brooks

Air Force Weapons Laboratory
Godfrey

Austin Research Associates
Drummond, Moore

Bell Telephone Laboratories
Gottscho

Berkeley Research Assoc.
Brecht, Orens

Cal. Inst. of Technology
Bridges, Gould

Calif. State Polytech. Univ.
Rathmann

Cambridge Research Labs.
Rubin

Columbia University
Chu

Cornell University
Otani

Dartmouth
Hudson, Lotko

E. P. R. I.
Scott

GA Technologies
Bernard, Evans, Helton

Goddard Space Flight Center
Storey

GTE Laboratories
Rogoff, Winsor

Hascomb Air Force Base
Rubin

Hewlett-Packard Laboratories
Gleason, Marcoux

Hughes Aircraft Co., Torrance
Adler, Longo

Hughes Research Lab., Malibu
Harvey, Hyman, Poeschel, Schumacker

Institute of Fusion Studies, Texas
Librarian

JPL
Liewer

Lawrence Berkeley Laboratory
Cooper, Kaufman, Kunkel,

Lawrence Livermore National Lab.
Albritton, Anderson, Brengle, Byers, Chambers, Chen, B.Cohen, R. Cohen, Denavit, Estabrook, Fawley, Friedman, Fuss, Harte, Hewett, Kruer, Langdon, Lasinski, Max, Nevins, Nielsen, Rognlien, Smith, Tull, Ziolkowski

Lockheed
Siambis

Lodestar Research Corp.
D'Ippolito, Myra

Los Alamos Scientific Lab.
Barnes, Borovsky, Forslund, Kwan, Lindemuth, Mason, Nielson, Oliphant, Peratt, Sgro, Thode

M2 Microtek
Phillips, Snyder

Mass. Inst. of Technology
Bers, Lane, Palevsky

Mission Research Corporation
Mostrom

Nasa - Lewis Research Center
Freeman

Naval Research Laboratory
Armstrong, Boris, Craig, Haber, Joyce, Kodis, Orens, Parker, Roberson, Vomvoridis, Zaidman

New York University
Weitzner

Northeastern University
Chan, Silevitch

Oak Ridge National Lab.
Fusion Energy Library, Lebouef, Meier, Mook

Physics International
Woo

Princeton Plasma Physics Lab
Chen, Cheng, Lee, Okuda, Parker, Tang, Librarian

SAIC - Virginia
Drobot, Mankofsky, Smith

Sandia Labs, Albuquerque
Freeman, Poukey, Quintenz, Wright

Sandia Labs, Livermore
Marx, Wilson, Hsu

Stanford University
Buneman

TRW
Wagner

University of Arizona
Carlile

University of California, Berkeley
Arons, Birdsall, Chorin, Graves, Haller, Lawson, Lichtenberg, Lieberman, McKee, Morse, Roth, Vahedi, Verboncoeur

University of California, Davis
DeGroot

University of California, Irvine
Rynn

University of California, Los Angeles
Abdou, Dawson, Decyk, Luhmann, Prinja

University of Illinois
Kushner

University of Iowa
Knorr

University of Maryland
Guillory, Rowland, Winske

University of New Mexico
Anderson, Humphries

University of Southern California
Kuehl

University of Texas
Horton, McMahon, Tajima

University of Washington
Potter

University of Wisconsin
Emmert, Hershkovitz, Intrator, Scheur, Shohet, Wendt

Varian Associates
Anderson, Doniger, Grant, Helmer, Kenyon

Vista Research Inc.
Crystal

Universität Innsbruck
Cap, Kuhn, Schrittwieser

I.N.P.E.
Alves, Bittencourt, Montes

University of Toronto
Stangeby

Riso National Laboratories
Lynov, Pecseli

Culham Laboratory
Eastwood

Imperial College
Burger

Oxford University
Allen, Edgley

Ecole Polytechnique, Palaiseau
Adam

Universite Paris
Raviart

IPP-KFA
Reiter

Max Planck Institute für Plasmaphysik
Biskamp, Chodura, Lackner

University Bayreuth
Schamel

Universität Kaiserslautern
Wick

Israel
Geil

Tel Aviv University
Cuperman

Hiroshima University
Hockney

Kyoto University
Abe, Matsumoto, Jimbo

Nagoya University
Kamimura, Tanaka, Plasma Science Center,
Research Info. Center

Osaka University
Mima, Nishihara

Pohang Institute of Science and Technology
Lee

Ruhr-Universitat, Bochum
Riemann

Shizuoka University
Saeki

Tohoku University
Ishiguro, Sato

University of Tromso
Armstrong, Trulsen

Centro de Electrodinâmica, Lisbon
Brinca

Ecole Polytechnique, Lausanne
Hollenstein